Constitutive Modelling of Elastomers Using the Finite Element Method

By John Hogan

A thesis submitted for the degree of

Doctor of Philosophy of the University of London

and

Diploma of Imperial College

September 1999

Department of Mechanical Engineering,

Imperial College of Science, Technology and Medicine,

London.

Abstract

This thesis presents a new approach to incorporate an important class of constitutive models into finite element software. A method to implement non-Gaussian network models is proposed which involves the exact determination of the inverse Langevin function and its derivative. Non-Gaussian models describe the general deformation behaviour of elastomers correctly using only two material parameters and so offer a distinct advantage over other constitutive theories for these materials. Despite this they have not been widely used in the finite element analysis of elastomeric components because traditional methods of implementation rely on a series approximation for the inverse Langevin function. In the new approach a simple iterative procedure is employed to determine the exact value of the inverse Langevin function. This in turn allows exact expressions for the principal stresses and principal components of the tangent modulus to be derived. These quantities are then transformed to the base directions of the active coordinate system. Using this approach two of the most well known non-Gaussian network models, the three chain model of James and Guth and the eight chain model of Arruda and Boyce have been implemented in the FE code ABAQUS using the user defined material subroutine facility known as UMAT. UMAT routines have been developed to analyse plane stress, plane strain, axisymmetric and three-dimensional problems. To enhance the ability of the non-Gaussian network models to describe the mechanical behaviour of filled elastomers, time dependent effects are introduced into the constitutive formulations by employing a theoretical framework for finite strain viscoelasticity. Strain softening effects are also introduced, using continuum damage mechanics. The ability of these modified network models to reproduce the mechanical behaviour of filled elastomers is determined by comparison with a series of experiments conducted on neoprene and polyurethane.

Acknowledgements

I would like to express my sincere thanks to Dr Noel O'Dowd and Dr John Dear for their guidance throughout the course of this project.

I would also like to thank my colleagues: Adam Bettinson, Farid Biglari, Jonathan Douglas, Richard Dempers, Franck Meissonnier and Philip May for providing a socially and academically fruitful environment.

Finally I wish to express my gratitude to Sarah for her encouragement and unselfish support.

Financial support for this project was provided by the Engineering and Physical Sciences Research Council and the Minnesota Mining and Manufacturing Company.

Table of Contents

1. INTRODUCTION 7

1.1 MOTIVATION AND AIM OF THE STUDY 7
1.2 GENERAL LAYOUT OF THIS THESIS 8

2. FINITE DEFORMATION KINEMATICS 11

2.1 INTRODUCTION 11
2.2 CONFIGURATIONS AND DISPLACEMENTS 12
2.3 DEFORMATION GRADIENT 13
2.4 VELOCITY GRADIENT AND RATE OF DEFORMATION 14
2.5 MEASURES OF FINITE DEFORMATION 16
2.6 DECOMPOSITION OF THE DEFORMATION GRADIENT 17
2.7 STRESS MEASURES & STRAIN ENERGY FUNCTION 19
2.8 STRESS RATES 20

3. MOLECULAR AND PHENOMENOLOGICAL BASIS OF RUBBER ELASTICITY 25

3.1 INTRODUCTION 25
3.2 CONSTITUTIVE THEORIES FOR THE EQUILIBRIUM RESPONSE OF ELASTOMERS 27
3.2.1 Phenomenological Theories 28
3.2.1.1 Mooney's Theory 28
3.2.1.2 Rivlin's Theory 29
3.2.1.3 Valanis-Landel Hypothesis 30
3.2.1.4 Ogden's Theory 30
3.2.2 Physically Based Theories 31
3.2.2.1 Gaussian Theory of Rubber Elasticity 32
3.2.2.1.1 Entropy of a Single Gaussian Chain 34
3.2.2.1.2 Work of Extension of a Single Gaussian Chain 35
3.2.2.1.3 Gaussian Chain Networks 36
3.2.2.1.4 Work of Deformation for a Network of Gaussian Chains 39
3.2.2.2 Non Gaussian Theory of Rubber Elasticity 41
3.2.2.2.1 Entropy of a Single non-Gaussian Chain 43
3.2.2.2.2 Work of Extension of a Single non-Gaussian Chain 43
3.2.2.2.3 Non-Gaussian Chain Networks 45
3.2.2.2.4 Three Chain Model 46
3.2.2.2.5 Eight Chain Model 49
3.3 FINAL REMARKS 51

4. IMPLEMENTATION OF INCOMPRESSIBLE FORMS OF THE NON-GAUSSIAN NETWORK MODELS INTO FE SOFTWARE 53

4.1 INTRODUCTION 53
4.2 DETERMINATION OF THE INVERSE LANGEVIN FUNCTION 54
4.3 THE PRINCIPAL AXES TECHNIQUE 57
4.4 MODELLING HOMOGENEOUS DEFORMATIONS 64
4.4.1 Homogenous Uniaxial Extension 65
4.4.2 Homogeneous Equi-biaxial Extension 66
4.4.3 Homogeneous Pure Shear 67
4.5 ABAQUS USER DEFINED MATERIAL INTERFACE 68
4.6 MODELLING NON-HOMOGENEOUS DEFORMATIONS 69
4.6.1 Constitutive Equations (2-D plane stress formulation) 69
4.6.2 Constitutive Equations (general 2-D plane stress formulation) 73
4.7 NUMERICAL TESTS 76
4.7.1 Homogeneous Deformation Tests 76
4.7.2 Stretching of a square sheet with a central circular hole 78
4.7.3 Inflation of a balloon 80
4.7.4 Inflation of a shallow spherical cap 81
4.8 FINAL REMARKS 83

5. IMPLEMENTATION OF COMPRESSIBLE FORMS OF THE NON-GAUSSIAN NETWORK MODELS INTO FE SOFTWARE 84

5.1 INTRODUCTION 84
5.1.1 Deviatoric-volumetric multiplicative split 85
5.1.2 Uncoupled forms of the non-Gaussian network models 86
5.1.3 Constitutive Equations (axisymmetric and plane strain formulations) 88
5.1.4 Constitutive Equations (3-D formulation) 94
5.2 NUMERICAL TESTS 97
5.2.1 Homogeneous Deformation Tests 97
5.2.2 Compression of a bonded cylindrical block 99
5.2.3 Cook's membrane problem 101
5.3 FINAL REMARKS 102

6. STRAIN INDUCED SOFTENING 103

6.1 INTRODUCTION 103
6.2 MECHANISMS OF REINFORCEMENT AND MULLINS EFFECT 105
6.2.1 Hydrodynamic Theories of Smallwood and Guth 105
6.2.2 Strain-amplification theory of Mullins et al 107
6.2.3 Blanchard and Parkinson mechanisms 107
6.2.4 Bueche's Interparticle Chain Breakage Mechanism 108
6.2.5 Molecular Slippage Mechanism 108
6.3 CONTINUUM MODELS 109
6.3.1 Gurtin and Francis 1-D Phenomenological Damage Model 109
6.3.2 Simo's 3-D Finite Strain Isotropic Damage Model 110
6.3.3 Govindjee and Simo Phenomenological/Micromechanical Model 112
6.4 EXTENSION OF NON-GAUSSIAN NETWORK MODELS TO ACCOUNT FOR THE MULLINS EFFECT 113
6.4.1 Constitutive Equations (2-D general plane stress formulation) 113
6.4.1.1 Damage Force 114
6.4.1.2 Damage Evolution 115
6.4.2 Constitutive Equations (3-D formulation) 117
6.5 NUMERICAL EXAMPLES 119
6.5.1 Cyclic Tension Tests 119
6.5.2 Stretching of a square sheet with a central circular hole 120
6.6 FINAL REMARKS 121

7. VISCOELASTICITY 122

7.1 INTRODUCTION 122
7.2 STRESS RELAXATION AND CREEP 123
7.3 LINEAR VISCOELASTICITY AND THE SUPERPOSITION PRINCIPAL 123
7.4 FINITE STRAIN VISCOELASTICITY 124
7.5 INCORPORATION OF TIME DEPENDENT EFFECTS IN NON-GAUSSIAN NETWORK MODELS 126
7.5.1 Constitutive Equations (2-D general plane stress formulation) 127
7.5.2 Constitutive Equations (3-D formulation) 131
7.6 NUMERICAL EXAMPLES 133
7.6.1 Stress Relaxation 133
7.7 FINAL REMARKS 137

8. EXPERIMENTAL STUDIES 138

8.1 INTRODUCTION 138
8.1.1 Materials Studied 139
8.1.2 Interrupted Uniaxial Tensile Tests 139
8.1.3 Interrupted Uniaxial Compression Tests 142
8.1.4 Tensile and Compressive Stress Relaxation Tests 144
8.1.5 Constant Velocity Uniaxial Tensile Tests 152
8.2 FINAL REMARKS 156

9. COMPARISON WITH EXPERIMENTAL DATA 157

9.1 INTRODUCTION 157
9.1.1 Determination of the Time Independent Material Constants 158
9.1.2 Determination of the Time Dependent Material Constants 161

9.1.3 Comparison with Constant Velocity Uniaxial Tensile tests *169*
9.2 FINAL REMARKS 172

10. CONCLUSIONS AND FUTURE WORK 173

10.1 CONCLUSIONS 173
10.2 FUTURE WORK 174

REFERENCES 176

Chapter 1

1. Introduction

1.1 Motivation and aim of the study

As use of rubber and other elastomeric materials in engineering applications has grown so has the demand for tools to assist in the design of components made from these materials. Because the non-linear characteristics of elastomers do not lend themselves readily to generalisations or simplifications, the design of elastomeric components has traditionally been driven by a process of trial and error, Charlton and Yang (1994). More recently the introduction of digital computers and the development of computer aided engineering (CAE) methods, in particular the finite element method, have provided a powerful means to further the study, understanding and optimisation of elastomers in engineering applications. However the effectiveness of an approach like the finite element method is heavily dependent upon the accuracy with which the constitutive response of the materials concerned can be reproduced. Currently constitutive models for the non-linear analysis of elastomeric materials are only available in a limited form in most commercial finite element packages. The most widely offered models are those based on the theories of Rivlin (1948a) and Ogden (1972a), which being phenomenological in origin lack any direct link to the underlying mechanism of deformation.

The aim of this work is to examine the use of a class of physically based constitutive models in the finite element analysis of elastomeric materials. The non-Gaussian network models of James and Guth (1943) and Arruda and Boyce (1993), based on the kinetic theory of rubber elasticity, offer an advantage over other constitutive models in that they are capable of describing the general mechanical behaviour of elastomers using only two material parameters. Despite this advantage they are not widely used in the FEA of elastomeric materials, since exact constitutive equations suitable for implementation in FE codes have not been available. In a significant step to permit the wider use of these models, the development of a set of exact constitutive equations for the 3 and 8 chain non-Gaussian network models is examined in detail. The extension of these models to provide a realistic description of the time dependent response of filled elastomers is also considered.

1.2 General Layout of this thesis

This section briefly describes the contents of each part of the thesis.

Chapter 2 presents some essential kinematics concepts and basic definitions employed in the field of continuum mechanics. The chapter also includes a discussion of the objective stress rates most commonly used in connection with hyperelastic material models, namely the Truesdell and Jaumann stress rates, and demonstrates how the tangent of one rate may be related to that of another.

Chapter 3 reviews some of the constitutive models that have been developed to describe mechanical behaviour of rubber-like materials at large strains. In addition the section on physically based models introduces the 3 and 8 chain non-Gaussian network theories of James and Guth (1943) and Arruda and Boyce (1993), which are used to describe the long-term or equilibrium response of the viscoelastic damage models developed in chapter 7.

Chapter 4 presents a new approach to implement the 3 and 8 chain non-Gaussian network models into a commercial finite element program ABAQUS. The chapter commences with a discussion of the iterative technique used to determine the exact value of the inverse Langevin function and its derivative. The derivation of analytical solutions for the response of the 3 and 8 chain models in the homogeneous deformation states of uniaxial extension, equi-biaxial extension and pure shear is also

discussed. This in turn leads to the development of the constitutive relations necessary for the analysis of non-homogeneous deformations using the finite element method. Constitutive equations suitable for the analysis of plane-stress problems are derived and given in full. The chapter concludes with a number of test cases to examine the response of the 3 and 8 chain models, implemented into ABAQUS using the user defined material subroutine facility UMAT.

Following a similar approach to that proposed by Flory (1961) the 3 and 8 chain models are modified to allow for material compressibility in Chapter 5. Constitutive relations for the analysis of plane strain, axisymmetric and three-dimensional problems are also developed. The chapter concludes with a number of test cases to examine the response of UMAT subroutines developed for the compressible forms of the 3 and 8 chain models.

Chapter 6 commences with a discussion of filler reinforcement and the Mullins effect and goes on to review the various theories that have been put forward for their origin. Later in the chapter, the 3 and 8 chain models are extended to account for the Mullins effect, using continuum damage mechanics.

In Chapter 7 viscoelastic damage models based on the 3 and 8 chain models are developed to describe the time dependent response of filled elastomers. A Prony series is used to represent the time dependent effects, which are introduced into the constitutive formulations by employing a theoretical framework for finite strain viscoelasticity.

In order to calibrate the viscoelastic damage models developed in the previous chapter, and assess their ability to describe the mechanical behaviour of filled elastomers, experimental data from a wider set tests is required than is available in published literature. To this end a series of experiments have been performed to investigate the mechanical behaviour of several filled elastomers. A discussion of these tests together with the experimental results is given in Chapter 8

A comparison of the response of the viscoelastic damage models and the experimental results is given in Chapter 9. The equilibrium response is compared with results from interrupted loading tests, while the time dependent response is compared with results from stress relaxation tests and constant velocity uniaxial tensile tests. A new

approach is also presented in this chapter to determine the values of the Prony series that accounts for the stress relaxation that occurs during the loading-up phase of a typical stress relaxation test. The approach leads to a more accurate description of the viscoelastic behaviour, and may be used to determine the time dependent constants for any viscoelastic model that employs the Prony series.

The final chapter gives a summary of the conclusions and some suggestions for future work.

Chapter 2

2. Finite Deformation Kinematics

2.1 Introduction

Elastomeric structures are often subject to large deformations and it is therefore necessary to account for both geometrical and material non-linearities. Treatment of the former within the finite element method can be achieved using Lagrangian kinematics, whereby the progress of material particles is traced during the deformation process. This chapter commences with a review of the fundamentals of such an approach, introducing the concept of initial and current configurations. This leads to a discussion of the relationship between geometrical elements in the initial and current configurations, and in turn to the deformation gradient, relating line elements in these configurations. The velocity gradient and rate of deformation tensors are also defined, along with convenient measures of finite strain based on the deformation gradient. The derivation of the second Piola-Kirchhoff stress tensor for a hyperelastic material is discussed, together with its relationship to equivalent spatial stress measures. The chapter concludes with a discussion of the objective stress rates most commonly employed in connection with hyperelastic material models, namely the Truesdell and Jaumann stress rates, and demonstrates how the tangent tensor of one rate may be transformed to that of another.

2.2 Configurations and Displacements

The physics of deformation of a continuum material has been established by way of the concept of a body whose elements can be defined through a one-to-one relationship with the points of a Euclidean space. At a given reference time $t = t_0$, a material body, B, occupies a region of space denoted by R_0, as shown in Figure 2.1. The particles of the body are continuously distributed over the region R_0. The position of a particle P in the region R_0 is given by the vector **X**. At some subsequent time t the body moves to (and occupies) another region R in space. All particles in B are now continuously distributed over the region R and there is a one-to-one correspondence between the material particles of B and the points in R. The particle P in the reference position **X**, now occupies the position Q in the region R given by the vector **x**. The motion can be mathematically described as

$$\mathbf{x} = \mathbf{x}(\mathbf{X}, t) \tag{2.1}$$

A typical particle that moves in space according to Equation (2.1) must have a reference position **X** in the region R_0; hence the point **X** is its starting point, or reference point. At any subsequent time t, this particle may be found by identifying its starting or reference point. Regardless of how it moves and the distance it travels, it can only change its current position and will always have the same original reference position. Hence the coordinates of **X** can be thought of as a fixed label for a typical particle and will not change for a given particle. These coordinates are therefore generally called material or reference coordinates though they are sometimes also referred as Lagrangian coordinates. The position vector **x** on the other hand, specifies a spatial point that can be occupied by different particles at different times. The coordinates of **x** are usually called spatial coordinates though they are also sometimes referred to as Eulerian coordinates. For a particle P with position **X** at $t = t_0$ that moves to position **x** denoted by Q, Figure 2.1 illustrates that the particle motion can be described by introducing a displacement vector **u** that relates **X** to **x** by

$$\mathbf{x} = \mathbf{X} + \mathbf{u} \tag{2.2}$$

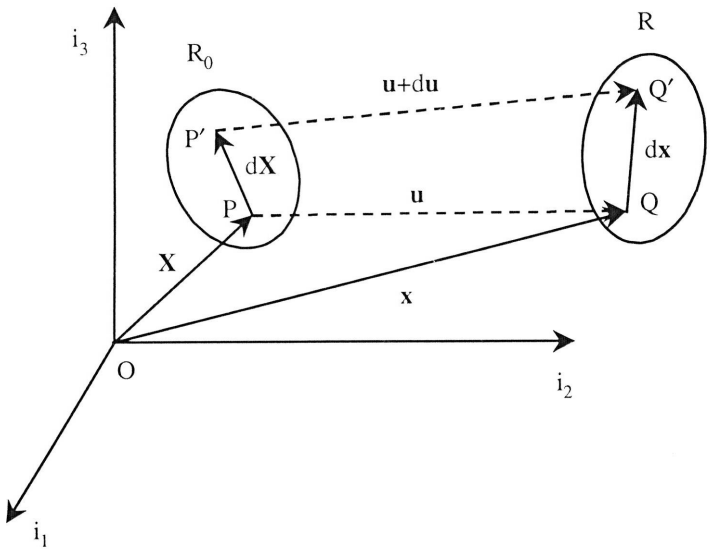


Figure 2.1 : Body and Configuration.

Using a material description, the displacement $\mathbf{u}$ may be expressed as a function of $\mathbf{X}$ and t:

$$\mathbf{u}(\mathbf{X},t) = \mathbf{x}(\mathbf{X},t) - \mathbf{X} \tag{2.3}$$

Alternatively a spatial description may be employed by writing the displacement as a function of $\mathbf{x}$ and t:

$$\mathbf{u}(\mathbf{x},t) = \mathbf{x} - \mathbf{X}(\mathbf{x},t) \tag{2.4}$$

2.3 Deformation Gradient

One of the main purposes of kinematic analysis is to determine the relationship between geometrical elements such as points, lines, areas and volumes in R_0 and R. At any given time t the relationship between points in R_0 and R is given by Equation (2.1). To determine the transformation equation between infinitesimal line elements consider two particles, located at $\mathbf{X}$ and $\mathbf{X} + d\mathbf{X}$ in the initial configuration. In the current configuration the particles are located at $\mathbf{x}$ and $\mathbf{x} + d\mathbf{x}$. Using the mapping Equation (2.1), $d\mathbf{x}$ may be related to $d\mathbf{X}$ via

$$d\mathbf{x} = \frac{\partial \mathbf{x}}{\partial \mathbf{X}} \cdot d\mathbf{X} = \mathbf{F} \cdot d\mathbf{X} \tag{2.5}$$

where

$$\mathbf{F} = \frac{\partial \mathbf{x}}{\partial \mathbf{X}} \tag{2.6}$$

is called the deformation gradient. In component form the deformation gradient is defined as

$$F_{iK} = \frac{\partial x_i}{\partial X_K} \tag{2.7}$$

The deformation gradient tensor $\mathbf{F}$ is a linear operator which relates every material line element $d\mathbf{X}$ in R_0 to the corresponding $d\mathbf{x}$ in R. Equation (2.5) may be inverted to give

$$d\mathbf{X} = \frac{\partial \mathbf{X}}{\partial \mathbf{x}} \cdot d\mathbf{x} = \mathbf{F}^{-1} \cdot d\mathbf{x} \tag{2.8}$$

2.4 Velocity Gradient and Rate of Deformation

In kinematic theory many problems are related not to changes in the shape of a body but the rate at which those changes take place. This requires a definition of the rate of deformation. The velocity of a material particle can be defined as

$$\mathbf{v} = \frac{\partial \mathbf{x}}{\partial t} \tag{2.9}$$

where the partial differentiation with respect to time, t, means the rate of change of the spatial position, **x**, of a material particle. In general **v** varies with time but for a fixed time t, varies only with the spatial coordinate **x**. The velocity difference between two neighbouring particles in the current configuration is given by

$$d\mathbf{v} = \frac{\partial \mathbf{v}}{\partial \mathbf{x}} \cdot d\mathbf{x} = \mathbf{L} \cdot d\mathbf{x} \tag{2.10}$$

where

$$\mathbf{L} = \frac{\partial \mathbf{v}}{\partial \mathbf{x}} \tag{2.11}$$

is the velocity gradient in the current configuration. Using the definition of the deformation gradient given in Equation (2.6), the velocity difference may written as

$$d\mathbf{v} = \mathbf{L} \cdot \mathbf{F} \cdot d\mathbf{X} \tag{2.12}$$

Alternatively, velocity difference may be obtained directly by

$$d\mathbf{v} = \frac{\partial}{\partial t}(\mathbf{F} \cdot d\mathbf{X}) = \dot{\mathbf{F}} \cdot d\mathbf{X} \tag{2.13}$$

where

$$\dot{\mathbf{F}} = \frac{\partial \mathbf{F}}{\partial t}. \tag{2.14}$$

Because $d\mathbf{v}$ is defined as the velocity difference between two neighbouring material particles and, having chosen these particles, the gauge length between them in the reference configuration, $d\mathbf{X}$ is the same throughout the motion, and so has no time derivative. Comparing the two expressions for $d\mathbf{v}$ in terms of the reference configuration gauge length $d\mathbf{X}$, it is observed that

$$\mathbf{L} \cdot \mathbf{F} = \dot{\mathbf{F}} \tag{2.15}$$

or

$$\mathbf{L} = \dot{\mathbf{F}} \cdot \mathbf{F}^{-1} \tag{2.16}$$

The velocity gradient **L**, can be decomposed into a symmetric strain rate matrix and anti-symmetric rotation matrix, as follows:

$$\mathbf{L} = \dot{\varepsilon} + \dot{\Omega} \tag{2.17}$$

The symmetric part of the decomposition is deformation rate tensor,

$$\dot{\boldsymbol{\varepsilon}} = \frac{1}{2}\left(\mathbf{L} + \mathbf{L}^T\right) \tag{2.18}$$

The anti-symmetric part of the decomposition is the spin tensor,

$$\dot{\boldsymbol{\Omega}} = \frac{1}{2}\left(\mathbf{L} - \mathbf{L}^T\right) \tag{2.19}$$

2.5 Measures of Finite Deformation

The square length of any line element in R_0 and R is given by

$$dS^2 = d\mathbf{X} \cdot d\mathbf{X} \tag{2.20}$$

$$ds^2 = d\mathbf{x} \cdot d\mathbf{x} \tag{2.21}$$

Using the deformation gradient, dS^2 can be written as follows:

$$dS^2 = (\mathbf{F}^{-1} \cdot d\mathbf{x}) \cdot (\mathbf{F}^{-1} \cdot d\mathbf{x}) = d\mathbf{x} \cdot (\mathbf{F}^{-1})^T \cdot (\mathbf{F}^{-1}) \cdot d\mathbf{x} \tag{2.22}$$

Similarly

$$ds^2 = (\mathbf{F} \cdot d\mathbf{x}) \cdot (\mathbf{F} \cdot d\mathbf{x}) = d\mathbf{X} \cdot \mathbf{F}^T \cdot \mathbf{F} \cdot d\mathbf{X} \tag{2.23}$$

Inspection of Equation (2.22) and (2.23) has led to the introduction of the following tensors to describe finite deformation:

$$\mathbf{B}^{-1} = (\mathbf{F}^{-1})^T \cdot \mathbf{F}^{-1} \tag{2.24}$$

and

$$\mathbf{C} = \mathbf{F}^T \cdot \mathbf{F} \tag{2.25}$$

where $\mathbf{B}^{-1}$ in Equation (2.24) is inverse of $\mathbf{B}$ the left Cauchy-Green tensor and $\mathbf{C}$ in Equation (2.25) is the right Cauchy-Green tensor. The basic requirement for a strain tensor is that it should completely determine the deformation state at any material point, both $\mathbf{B}^{-1}$ and $\mathbf{C}$ are known to be sufficient for this purpose. It should be noted that for a rigid body motion,

$$\mathbf{C} = \mathbf{I} \tag{2.26}$$

$$\mathbf{B}^{-1} = \mathbf{I} \tag{2.27}$$

Usually the deformation measure is expected to be a zero tensor for a rigid body motion. This leads to the introduction of the Lagrangian strain tensor **E,** also known and the Green strain, and the Eulerian strain tensor **e**, defined as

$$\mathbf{E} = \frac{1}{2}(\mathbf{C} - \mathbf{I}) \tag{2.28}$$

$$\mathbf{e} = \frac{1}{2}(\mathbf{I} - \mathbf{B}^{-1}) \tag{2.29}$$

It can be easily seen from Equation (2.28) and (2.29) for rigid body motion $\mathbf{E} = \mathbf{e} = 0$. The tensors $\mathbf{E}$ and $\mathbf{e}$ are convenient measures of strain because they may be calculated directly from the deformation gradient.

2.6 Decomposition of the Deformation Gradient

Using the theory of polar decomposition, as described by Khan and Huang (1995), it can be shown that the deformation gradient can be decomposed into either of the following products:

$$\mathbf{F} = \mathbf{R} \cdot \mathbf{U} = \mathbf{V} \cdot \mathbf{R} \tag{2.30}$$

where $\mathbf{R}$ is an orthogonal rotation tensor, and $\mathbf{V}$ and $\mathbf{U}$ are the left and right stretch tensors.

From the definition of **B** and **C** and the decomposition of **F**, it can be seen that

$$\mathbf{B} = \mathbf{F} \cdot \mathbf{F}^T = \mathbf{V} \cdot \mathbf{R} \cdot \mathbf{R}^T \cdot \mathbf{V} = \mathbf{V}^2 \tag{2.31}$$

$$\mathbf{C} = \mathbf{F}^T \cdot \mathbf{F} = \mathbf{U} \cdot \mathbf{R} \cdot \mathbf{R} \cdot \mathbf{U} = \mathbf{U}^2 \tag{2.32}$$

Equation (2.5) may then be rewritten in either of the following forms

$$d\mathbf{x} = \mathbf{F} \cdot d\mathbf{X} = \mathbf{R} \cdot \mathbf{U} \cdot d\mathbf{X} = \mathbf{V} \cdot \mathbf{R} \cdot d\mathbf{X} \tag{2.33}$$

Thus the deformation of any material particle may be decomposed into a rigid body rotation, **R**, and a pure stretch, the sequence of these is arbitrary. The deformation given by **F** may be produced by first stretching the material in R_0 in three mutually orthogonal directions $\mathbf{N}_1$, $\mathbf{N}_2$ and $\mathbf{N}_3$ known as the material triad by amounts $\lambda_I (I = 1,2,3)$, followed by a rigid body rotation of these directions. The deformation could also be produced by performing the same rigid body rotation, then stretching in the three mutually orthogonal directions $\mathbf{n}_1$, $\mathbf{n}_2$ and $\mathbf{n}_3$ in R, known as the spatial triad, by the amount $\lambda_i (i = 1,2,3)$. The quantities $\lambda_i (= \lambda_I)$ are the principal stretch ratios (or simply the principal stretches) along the principal axes of **U** and **V** in R_0 and R respectively. Mathematically the principal stretches represent the eigenvalues of stretch tensors and their principal directions the eigenvectors. The stretch tensors **V** and **U** may be expressed in terms of the principal stretches and directions as:

$$\mathbf{V} = \mathbf{Q}(\mathbf{n})[\mathbf{diag}\lambda\,]\mathbf{Q}^{\mathrm{T}}(\mathbf{n}) \tag{2.34}$$

$$\mathbf{U} = \mathbf{Q}(\mathbf{N})[\mathbf{diag}\lambda\,]\mathbf{Q}^{\mathrm{T}}(\mathbf{N}) \tag{2.35}$$

where $\mathbf{Q}(\mathbf{n}) = [\mathbf{n}_1 \mathbf{n}_2 \mathbf{n}_3]$ is the matrix containing the principal direction vectors $\mathbf{n}_1$, $\mathbf{n}_2$ and $\mathbf{n}_3$, $\mathbf{Q}(\mathbf{N}) = [\mathbf{N}_1 \mathbf{N}_2 \mathbf{N}_3]$ is the matrix containing the principal direction vectors $\mathbf{N}_1$, $\mathbf{N}_2$ and $\mathbf{N}_3$ and $[\mathbf{diag}\lambda]$ is the diagonal matrix containing the principal stretches λ_1, λ_2 and λ_3.

The rotation tensor in Equation (2.30) defines the movement from $\mathbf{N}_i$ to $\mathbf{n}_i$ and may be written as

$$\mathbf{R} = \mathbf{Q}(\mathbf{n})\mathbf{Q}(\mathbf{N})^T \tag{2.36}$$

Using the expressions for **V** and **U** from Equation (2.34) and (2.35), the deformation tensors **B** and **C** may be expressed as

$$\mathbf{B} = \mathbf{Q}(\mathbf{n})[\mathbf{diag}\lambda^2]\mathbf{Q}^{\mathrm{T}}(\mathbf{n}) \tag{2.37}$$

$$\mathbf{C} = \mathbf{Q}(\mathbf{N})[\mathbf{diag}\lambda^2]\mathbf{Q}^{\mathrm{T}}(\mathbf{N}) \tag{2.38}$$

where $[\mathbf{diag}\lambda^2]$ is the diagonal matrix containing the squares of the principal stretches.

2.7 Stress Measures & Strain Energy Function

In continuum mechanics a number of strain measures may be employed. When deformations are large it is often convenient to use the Green strain tensor, **E**. The stress measure used in conjunction with Green strain is the second Piola-Kirchhoff stress tensor, here termed **S**. This stress measure is the work conjugate of **E**, i.e., the virtual work expression is given by

$$V = V_i - V_e = \int_{V_o} \mathbf{S} : \delta\mathbf{E}_v \, dV_o - V_e \tag{2.39}$$

where V_i and V_e are the internal and external virtual works, respectively. Another relevant stress measure that should be mentioned here is the Cauchy or true stress. The use of the Cauchy stress $\boldsymbol{\sigma}$ instead of the second Piola-Kirchhoff, **S**, stress eases the interpretation of the final results. The former relates the forces to the final area where they have been applied whereas the later relates them to the original area and the original configuration. The Cauchy stress is related to the second Piola-Kirchhoff stress via

$$\boldsymbol{\sigma} = \frac{1}{J}\mathbf{F}\mathbf{S}\mathbf{F}^T \tag{2.40}$$

where $J = \det(\mathbf{F})$. It is also possible to define an equivalent stress to the Cauchy stress but defined on the original volume, known as the Kirchhoff stress it is defined as

$$\boldsymbol{\tau} = J\boldsymbol{\sigma} = \mathbf{F}\,\mathbf{S}\,\mathbf{F}^T \tag{2.41}$$

The strain energy function W is the strain energy per unit initial volume under deformation. The change of W may be expressed as

$$\delta W = \mathbf{S} : \delta\mathbf{E} \tag{2.42}$$

hence

$$\mathbf{S} = \frac{\partial W}{\partial \mathbf{E}} \tag{2.43}$$

A second variation with respect to strain yields the tangent relationship, i.e., $\mathscr{D}^{K2}$ (with the subscript K2 for the second Piola-Kirchhoff).

$$\delta\mathbf{S} = \mathscr{D}^{K2} : \delta\mathbf{E} \tag{2.44}$$

and

$$\mathscr{D}^{K2} = \frac{\partial \mathbf{S}}{\partial \mathbf{E}} \tag{2.45}$$

Equation (2.45) illustrates that the tangent tensor is not a constant for hyperelastic materials but rather is dependent upon the current strain.

2.8 Stress Rates

For materials which exhibit history dependence it is common for their constitutive relations to appear in rate form. In finite deformation problems this requires the use of an objective stress rate, in order that the stresses associated with the constitutive response of the material are independent of rigid body motion. Several objective stress rates have been proposed, a number of which have been discussed by Crisfield (1997). The Truesdell rate of Kirchhoff stress is frequently employed in conjunction with

hyperelastic material models, and may be obtained by taking the time derivative of the Kirchhoff stress defined in Equation (2.41), yielding

$$\dot{\boldsymbol{\tau}} = \mathbf{F}\cdot\dot{\mathbf{S}}\cdot\mathbf{F}^T + \dot{\mathbf{F}}\cdot\mathbf{S}\cdot\mathbf{F}^T + \mathbf{F}\cdot\mathbf{S}\cdot\dot{\mathbf{F}}^T \tag{2.46}$$

where $\dot{\mathbf{S}}$ indicates rate of the second Piola-Kirchhoff stress, given by

$$\dot{\mathbf{S}} = \mathscr{D}^{K2} : \dot{\mathbf{E}} \quad \text{or} \quad \dot{S}_{ab} = \mathscr{D}^{K2}_{abcd}\,\dot{E}_{cd} \tag{2.47}$$

Substituting for $\mathbf{S}$ in Equation (2.46), in terms of $\boldsymbol{\tau}$ leads to

$$\dot{\boldsymbol{\tau}} = \mathbf{F}\cdot\dot{\mathbf{S}}\cdot\mathbf{F}^T + \dot{\mathbf{F}}\cdot\mathbf{F}^{-1}\cdot\boldsymbol{\tau} + \boldsymbol{\tau}\cdot\mathbf{F}^{-T}\cdot\dot{\mathbf{F}}^T \tag{2.48}$$

From the definition of the velocity gradient given in Equation (2.16), it follows

$$\dot{\boldsymbol{\tau}} = \mathbf{F}\cdot\dot{\mathbf{S}}\cdot\mathbf{F}^T + \mathbf{L}\cdot\boldsymbol{\tau} + \boldsymbol{\tau}\cdot\mathbf{L}^T \equiv \boldsymbol{\tau}_T + \mathbf{L}\cdot\boldsymbol{\tau} + \boldsymbol{\tau}\cdot\mathbf{L}^T. \tag{2.49}$$

Here, $\boldsymbol{\tau}_T$, known as the Truesdell rate of Kirchhoff stress represents that part of the rate of Kirchhoff stress associated with the constitutive response of a material. To further explore the relationship between (2.47) and (2.49), it is necessary to adopt index notation coupled with the relationship between $\dot{\mathbf{E}}$ and $\dot{\boldsymbol{\varepsilon}}$ whereby:

$$\dot{\mathbf{E}} = \mathbf{F}^T\cdot\dot{\boldsymbol{\varepsilon}}\cdot\mathbf{F} \quad \text{or} \quad \dot{E}_{cd} = F_{kc}\dot{\varepsilon}_{kl}F_{ld} \tag{2.50}$$

Substituting from Equation (2.47) and (2.50) into Equation (2.49) leads to

$$\dot{\boldsymbol{\tau}} = \mathscr{D}^{TK} : \dot{\boldsymbol{\varepsilon}} + \mathbf{L}\cdot\boldsymbol{\tau} + \boldsymbol{\tau}\cdot\mathbf{L}^T \tag{2.51}$$

where

$$\mathscr{D}^{TK}_{ijkl} = F_{ia}F_{jb}F_{kc}F_{ld}\mathscr{D}^{K2}_{abcd} \tag{2.52}$$

Equation (2.52) gives the relationship between the tangent ($\mathscr{D}^{TK}$) of the Truesdell rate of Kirchhoff stress, and the tangent tensor ($\mathscr{D}^{K2}$) relating the rates of the second Piola-Kirchhoff stress and Green strain. The tangent of the Truesdell rate may be calculated directly from Equation (2.52), if the tangent tensor $\mathscr{D}^{K2}$ is known. Alternatively it may be found indirectly from the relationship above, using the principal axes method of Chadwick and Ogden (1971a,b) described by Crisfield (1997).

The constitutive relations presented in later chapters, based on the material models of James and Guth (1943) and Arruda and Boyce (1993) have been implemented into the finite element package ABAQUS (see the ABAQUS theory manual (1996) for details) using the user defined material facility known as UMAT. In finite deformation problems, ABAQUS requires the UMAT subroutine to define the tangent of the Jaumann rate of Cauchy stress, so as to remain consistent with the solid element formulation based on this stress rate. Determination of the tangent tensor for the Jaumann rate of Cauchy stress requires examination of the relationship between the Jaumann and Truesdell rates. Consider first the Jaumann rate of Kirchhoff stress, defined via the expression

$$\dot{\boldsymbol{\tau}} \equiv \boldsymbol{\tau}_J + \dot{\boldsymbol{\Omega}} \cdot \boldsymbol{\tau} + \boldsymbol{\tau} \cdot \dot{\boldsymbol{\Omega}}^T = \mathscr{D}^{JK} : \dot{\boldsymbol{\varepsilon}} + \dot{\boldsymbol{\Omega}} \cdot \boldsymbol{\tau} + \boldsymbol{\tau} \cdot \dot{\boldsymbol{\Omega}}^T \tag{2.53}$$

Here, $\boldsymbol{\tau}_J$, is the Jaumann rate of Kirchhoff stress and, $\mathscr{D}^{JK}$, is the tangent of the Jaumann rate of Kirchhoff stress. Like $\boldsymbol{\tau}_T$, $\boldsymbol{\tau}_J$ is an objective stress rate. The tangent of the Jaumann rate of Kirchhoff stress, $\mathscr{D}^{JK}$, may be obtained by equating $\dot{\boldsymbol{\tau}}$ from Equation (2.51) and (2.53)

$$\boldsymbol{\tau}_T + \mathbf{L} \cdot \boldsymbol{\tau} + \boldsymbol{\tau} \cdot \mathbf{L}^T = \boldsymbol{\tau}_J + \dot{\boldsymbol{\Omega}} \cdot \boldsymbol{\tau} + \boldsymbol{\tau} \cdot \dot{\boldsymbol{\Omega}}^T \tag{2.54}$$

Allowing for the fact that $\mathbf{L} = \dot{\boldsymbol{\varepsilon}} + \dot{\boldsymbol{\Omega}}$ and noting the symmetry of $\dot{\boldsymbol{\varepsilon}}$

$$\boldsymbol{\tau}_T = \mathscr{D}^{TK} : \dot{\boldsymbol{\varepsilon}} = \boldsymbol{\tau}_J - \dot{\boldsymbol{\varepsilon}} \cdot \boldsymbol{\tau} - \boldsymbol{\tau} \cdot \dot{\boldsymbol{\varepsilon}} = \mathscr{D}^{JK} : \dot{\boldsymbol{\varepsilon}} - \dot{\boldsymbol{\varepsilon}} \cdot \boldsymbol{\tau} - \boldsymbol{\tau} \cdot \dot{\boldsymbol{\varepsilon}} \tag{2.55}$$

Using index notation the tangent of the Jaumann rate of Kirchhoff stress may be expressed as

$$\mathscr{D}^{JK}_{ijkl} = \mathscr{D}^{TK}_{ijkl} + \frac{1}{2}(\tau_{il}\delta_{jk} + \tau_{jl}\delta_{ik} + \tau_{ik}\delta_{jl} + \tau_{jk}\delta_{il}) \tag{2.56}$$

This is an important result, relating the tangents of the Jaumann and Truesdell rates of Kirchhoff stress. With the aid of Equation (2.56), the tangent of the Jaumann rate of Cauchy stress may be determined by considering the relationship between the Jaumann rates of the Cauchy and Kirchhoff stress tensors. The Jaumann rate of Cauchy stress is defined via

$$\dot{\boldsymbol{\sigma}} = \boldsymbol{\sigma}_J + \dot{\boldsymbol{\Omega}}\cdot\boldsymbol{\sigma} + \boldsymbol{\sigma}\cdot\dot{\boldsymbol{\Omega}}^T = \mathscr{D}^{JC} : \dot{\boldsymbol{\varepsilon}} + \dot{\boldsymbol{\Omega}}\cdot\boldsymbol{\sigma} + \boldsymbol{\sigma}\cdot\dot{\boldsymbol{\Omega}}^T \tag{2.57}$$

where $\boldsymbol{\sigma}_J$ is the Jaumann rate of Cauchy stress and $\mathscr{D}^{JC}$ is the tangent of the Jaumann rate of Cauchy stress. The tangent tensor $\mathscr{D}^{JC}$, relating the Jaumann rate of Cauchy stress to the rate of deformation tensor may be found by taking the time derivative of Equation (2.41), to give

$$\dot{\boldsymbol{\tau}} = \dot{J}\boldsymbol{\sigma} + J\dot{\boldsymbol{\sigma}} \tag{2.58}$$

where

$$\dot{J} = J\, tr(\dot{\boldsymbol{\varepsilon}}) \tag{2.59}$$

Equation (2.58) may be rewritten by substituting for $\dot{\boldsymbol{\sigma}}$ from Equation (2.57), to yield

$$\dot{\boldsymbol{\tau}} = \mathscr{D}^{JK} : \dot{\boldsymbol{\varepsilon}} + \dot{\boldsymbol{\Omega}}\cdot\boldsymbol{\tau} + \boldsymbol{\tau}\cdot\dot{\boldsymbol{\Omega}}^T = J(\dot{\boldsymbol{\sigma}} + \boldsymbol{\sigma}\, tr(\dot{\boldsymbol{\varepsilon}})) = J\,\mathscr{D}^{JC} : \dot{\boldsymbol{\varepsilon}} + \dot{\boldsymbol{\Omega}}\cdot\boldsymbol{\tau} + \boldsymbol{\tau}\cdot\dot{\boldsymbol{\Omega}}^T + \boldsymbol{\tau}\, tr(\dot{\boldsymbol{\varepsilon}}) \tag{2.60}$$

So that:

$$\mathscr{D}^{JC} : \dot{\boldsymbol{\varepsilon}} = \frac{1}{J}\mathscr{D}^{JK} : \dot{\boldsymbol{\varepsilon}} - \boldsymbol{\sigma}\, tr(\dot{\boldsymbol{\varepsilon}}) \tag{2.61}$$

Adopting index notation, it follows that:

$$\mathscr{D}_{ijkl}^{JC} = \frac{1}{J}\mathscr{D}_{ijkl}^{JK} - \boldsymbol{\sigma}_{ij}\,\delta_{kl} \tag{2.62}$$

The relationship above, coupled with that given in Equation (2.56) is sufficient to express the tangent of the Jaumann rate of Cauchy stress as a function of the tangent of the Truesdell rate of Kirchhoff stress.

Chapter 3

3. Molecular and Phenomenological Basis of Rubber Elasticity

3.1 Introduction

Elastomers distinguish themselves from other more common engineering materials in several important ways, the best known of which is the ability to undergo large elastic or instantaneously reversible strains. Elastic strains of up to 700% have been observed by Treloar (1944) in studies of the mechanical behaviour natural rubber. In contrast, ordinary hard solids (e.g. crystalline or glassy in nature) are seldom capable of elastic strains greater than 1%. Elastomers also possess a much lower stiffness the Young's modulus of a typical elastomer is of the order 10 MPa while that for a hard solid is 10^5 MPa. The thermomechanical properties of elastomeric materials are also quite unusual compared to that of ordinary hard solids. The tension in a piece of an elastomer stretched between two rigid supports is observed to vary in proportion to the absolute temperature while for a hard solid the inverse is true.

Elastomers possess an amorphous structure consisting of a highly entangled network of long chain-like molecules and as such are classified as lying within a group of materials referred to as polymers. Elastomeric materials are generally categorised

according to whether they are natural or synthetic in origin. Elastomers derived from natural sources are commonly referred to as rubbers whilst man-made products are known as synthetic elastomers. As a class of materials elastomers achieved industrial importance in the first half of the 19th century with the introduction of products manufactured from natural rubber (NR). The commercial exploitation of NR at this time was made possible by the twin developments of mastication by Thomas Hancock in 1820 and vulcanisation by Charles Goodyear in 1839. Raw or unvulcanised NR despite displaying a considerable degree of elasticity, will exhibit plastic flow *i.e.* permanent deformation when subjected to prolonged stressing. In the vulcanisation process developed by Goodyear, chemical bonds termed 'crosslinks' are formed between the chain-like molecules. The introduction of crosslinks has the effect of inhibiting plastic flow and leads to a marked increase in elasticity. Although the performance of vulcanised NR is satisfactory in many applications, a variety of synthetic elastomers have been developed in the 20th century which are less prone to degradation by ozone and offer greater resistance to solvents. These materials demonstrate similar elastic properties to NR but differ significantly in chemical structure. Synthetic elastomers imitate the long chain molecular structure of NR and are usually copolymerised from smaller synthetic molecular units such as butadiene and styrene.

The first systematic series of experiments performed to study the elastic behaviour of rubber-like materials are widely regarded to be those of Treloar (1944). Treloar investigated the behaviour of NR in uniaxial tension, equi-biaxial tension and pure shear, and demonstrated that the elastic or long term behaviour could be described by a scalar function of strain referred to as a strain energy function. The experimental data for one of the compounds of NR studied by Treloar is given in Figure 3.1. The stress-stretch curve for each deformation state is seen to display a characteristic S-shape. Upon extension from the unstrained state there is a continuous reduction in stiffness until it reaches around one third of its initial value. As the strain is increased above this level there is a progressive increase in stiffness. At higher strains, an asymptote is approached which is known as the limiting extensibility. While there is much similarity in the extensibility in pure shear and uniaxial tension the limiting extension in equi-biaxial tension is observed to be much smaller.

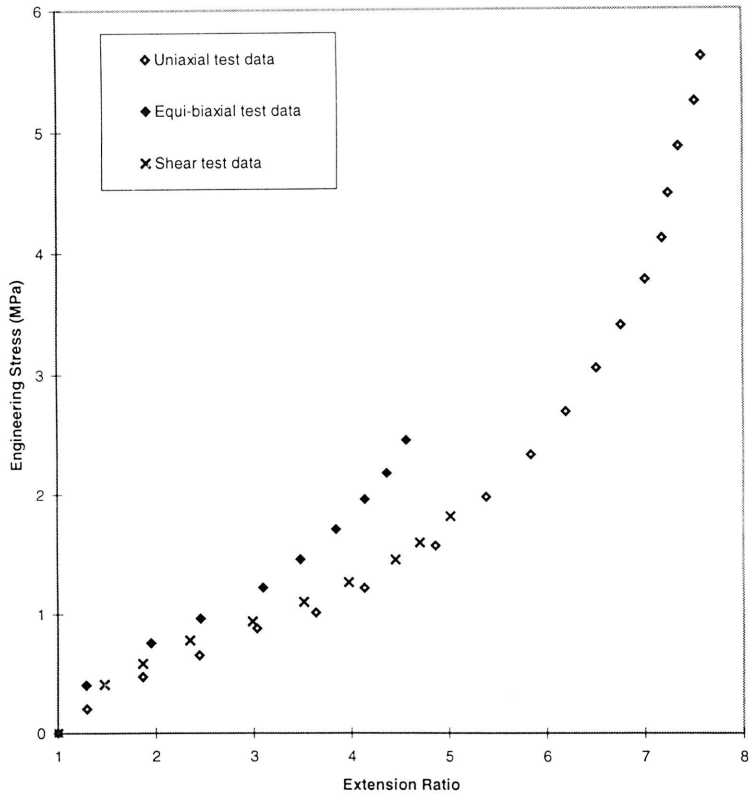


Figure 3.1 : Data from Treloar (1944), plotted as load per unit unstrained area versus extension ratio.

3.2 Constitutive Theories for the Equilibrium Response of Elastomers

Theories to account for the large elastic deformability of rubber-like materials can be divided into one of two categories, depending on whether they have a phenomenological or physical basis. Although phenomenologically and physically based theories are constructed using very different arguments, both consider the material to be isotropic in the unstrained state and seek to describe equilibrium or long-term behaviour by the means of a strain energy function, that is, a scalar function of strain independent of the time scale and loading history. This is a fair approximation for elastomeric materials which at a fixed temperature are very nearly perfectly elastic for quite large quasi-static deformations. Theories to describe the equilibrium response of rubber-like materials may also be divided into two additional classes: the first in which constitutive relations are phrased in terms of the invariants of the Cauchy Green deformation tensors and the second where relations are phrased in terms of the principal stretches (both satisfying objectivity requirements). It is also

observed that theories with a phenomenological basis usually fall into the first category while theories based on physical arguments fall into the second.

3.2.1 Phenomenological Theories

Phenomenological theories for rubber-like elasticity are concerned only with observed behaviour and as such possess no direct physical connection to the underlying mechanism of deformation responsible for that behaviour. The primary aim of a theory of this type is to find a general way of describing the relationship between the state of strain in a deformed body and the applied forces. Although constitutive developments presented in later chapters are solely confined to physically based strain energy functions, a review of phenomenological theories is merited because of their widespread application in the finite element analysis of elastomeric structures.

3.2.1.1 Mooney's Theory

Among the numerous phenomenological theories which have been proposed, that of Mooney (1940) is widely regarded as the earliest significant theoretical development. By applying purely mathematical arguments and assuming that rubber-like materials may be regarded as incompressible and isotropic in the undeformed state, Mooney derived the strain energy function which may be expressed in the form

$$W = C_1(\lambda_1^2 + \lambda_2^2 + \lambda_3^2 - 3) + C_2(\lambda_1^{-2} + \lambda_2^{-2} + \lambda_3^{-2} - 3) \tag{3.1}$$

where C_1 and C_2 are constants and λ_1, λ_2 and λ_3 represent the principal extension ratios. Equation (3.1) is commonly referred to as the Mooney-Rivlin function as it is also a special case of the general theory for isotropic elasticity of Rivlin, which is discussed in the next section. The Mooney-Rivlin strain energy function agrees with the uniaxial data of Treloar up to a strain of around 200%. Agreement with the shear data is however much poorer, the shear stresses predicted from Equation (3.1) deviate from the experimentally determined values at a shear strain of 25%. Despite the limitations of the Mooney-Rivlin function it has been pointed out by Gent (1992) that it still remains one the most widely used constitutive relationship for the non-linear stress analysis of elastomers.

3.2.1.2 Rivlin's Theory

The phenomenological treatment of isotropic elasticity was further advanced by the work of Rivlin (1948 a-d, 1949 a-c). Rivlin argued that the strain energy function for an isotropic solid must be expressible in the form

$$W = f(I_1, I_2, I_3) \tag{3.2}$$

where I_1, I_2 and I_3 are the three strain invariants of the Cauchy Green deformation tensors, given in terms of the principal extension ratios by

$$I_1 = \lambda_1^2 + \lambda_2^2 + \lambda_3^2 \tag{3.3}$$

$$I_2 = \lambda_1^2\lambda_2^2 + \lambda_2^2\lambda_3^2 + \lambda_3^2\lambda_1^2 \tag{3.4}$$

$$I_3 = \lambda_1^2\lambda_2^2\lambda_3^2 \tag{3.5}$$

Rivlin proposed that Equation (3.2) may be approximated by a power series.

$$W = \sum_{i+j+k=1}^{\infty} C_{ijk}(I_1 - 3)^i (I_2 - 3)^j (I_3 - 3)^k \tag{3.6}$$

For incompressible materials, $I_3 = 1$ and Equation (3.6) reduces to

$$W = \sum_{i+j=1}^{\infty} C_{ij}(I_1 - 3)^i (I_2 - 3)^j \tag{3.7}$$

which is similar to the general theory proposed by Mooney (1940). Equation (3.7) is widely referred to as the Rivlin strain energy function. The experimental study of James *et al* (1975) indicates that a third order expansion of Equation (3.7) is sufficient to obtain a good fit to general homogeneous strain data, this is also confirmed by the work of Johnson *et al* (1994) who demonstrated that the experimental work of Treloar can be reproduced using a third order expansion.

3.2.1.3 Valanis-Landel Hypothesis

The hypothesis of Valanis and Landel (1967) is also regarded as an important development. Valanis and Landel argued that from considerations of symmetry, the strain energy function W should be separable into independent functions of the principal extension ratios. This leads to a strain energy function of the form

$$W = w(\lambda_1) + w(\lambda_2) + w(\lambda_3) \tag{3.8}$$

where the functions $w(\lambda_i)$ are identical. Though there is no physical basis for this hypothesis, the experimental studies of Obata *et al* (1970), Jones and Treloar (1975) and Vangerko and Treloar (1978) have demonstrated its validity. However only a few forms for the function $w(\lambda_1)$ have been widely discussed like those of Ogden (1972a).

3.2.1.4 Ogden's Theory

In common with the theories of Mooney and Rivlin, Ogden (1972a) assumes that under isothermal conditions rubber-like materials in the undeformed state may be considered as isotropic and incompressible. The strain energy function proposed by Ogden obeys the Valanis-Landel hypothesis and is usually presented in the form

$$W = \sum_n \frac{\mu_n}{\alpha_n}(\lambda_1^{\alpha_n} + \lambda_2^{\alpha_n} + \lambda_3^{\alpha_n} - 3) \tag{3.9}$$

where μ_n and α_n are constants. It has been suggested by Ogden that a strain energy function of this form has the advantage of mathematical simplicity compared with the Rivlin function. However Rivlin and Sawyers (1976) have argued that functions which satisfy the Valanis-Landel hypothesis and hence that of Ogden are of a particular form of the Rivlin strain energy function and are therefore of an equivalent complexity. Despite this, the strain energy function of Ogden does have simplicity in the context of finite element formulations, since the terms in Equation (3.9) are identical in form, which is not so for the Rivlin function. It has also been demonstrated by Ogden that a three term function is sufficient to reproduce the experimental data of Treloar (1944) without significant deviation. The major drawback of both the Rivlin and Ogden

models is their dependence on the availability of experimental data from more than one deformation state. For these models experimental data from at least three deformation states is usually required to determine a set of constants capable of accurately reproducing the multiaxial behaviour. However in many circumstances such experimental data is unavailable.

3.2.2 Physically Based Theories

In contrast to the phenomenological approach, physically based theories attempt to derive a strain energy function by pursuing a connection between the material's molecular structure and its mechanical behaviour. Theories of this type have their origin in the kinetic or statistical mechanics theory of rubber elasticity, see Treloar (1975) for details. Kinetic theory is based on the assumption that the phenomenon of rubber-like elasticity is associated with the Brownian motion of individual elements of the chain-like molecules. This type of motion is similar to the thermal motion of molecules in an ideal gas, with the exception that the moving units instead of being entirely independent, are connected together in the form of a chain. This ultimately leads to the conclusion that the elastic properties of rubber-like materials are primarily related to changes in entropy. Kinetic theory stems from the observation that the intramolecular forces along a polymer chain are much larger than the intermolecular forces in the lateral direction. The thermally induced motions of the chain are therefore greater in the lateral direction, and so give rise to a repulsive pressure between parallel chains. The repulsive pressure which is produced tends to draw the ends of a chain together, so that the end-to-end separation of a long and flexible polymer chain in the unstrained state is much less than the fully extended chain length. Thus the highly extensible nature of elastomeric materials may be explained by the ability of these chains to undergo large increases in their end-to-end separation.

The development of a constitutive model using statistical mechanics may be thought of as taking place in two stages. In the first stage the statistical properties of a single long chain polymer molecule are treated in a quantitative manner, leading to expressions for the probability and entropy of a chain as a function of the distance between its ends. The second stage involves the statistical treatment of a network of such chains and so provides a description of the bulk properties of the elastomer.

Within kinetic theory individual polymer chains are considered to be randomly jointed, consisting of n rigid links of fixed, *i.e.* inextensible length l.

3.2.2.1 Gaussian Theory of Rubber Elasticity

Solution of the randomly jointed chain problem consists essentially of determining the probability of a particular chain end separation by evaluating the relative number of conformations available to a chain as a function of the end-to-end separation. Consider a polymer chain with one end A, fixed at the origin of the Cartesian coordinate system OX,OY,OZ (see Figure 3.2). The probability that the end B will be found at any instant in a small element of volume dv in the neighbourhood of point P will be proportional to the volume of this element, and some function $p(x,y,z)$ representing probability density at the point P.

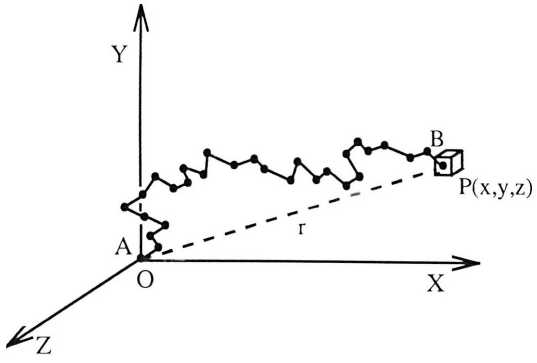


Figure 3.2 : The randomly jointed chain. Specification of probability that the end should fall in the volume $dv = dxdydz$

The approximate solution to this problem given in the text of Treloar (1975) takes the form

$$p(x,y,z)\,dxdydz = (b^3 / \pi^{3/2})\; e^{-b^2(x^2+y^2+z^2)} dxdydz \tag{3.10}$$

where $b^2 = 3/2nl^2$, and n and l represent the number of rigid links per chain and the length of each link. In Equation (3.10), $p(x,y,z)$ represents the density of the probability and $dxdydz$ is the size of the volume element considered, so that $p(x,y,z)\,dxdydz$ represents the probability that the components of the vector r should

be between x and $x+dx$, y and $y+dy$, z and $z+dz$ respectively. The derivation of this equation is based on approximations that are valid only so long as the distance between the ends of the chain is not comparable with the maximum possible extension and as such is not applicable when the chain is nearly fully extended. The probability density may also be expressed in terms of r, the distance of the P from the origin O, since $x^2 + y^2 + z^2 = r^2$

$$p(r) = (b^3 / \pi^{3/2}) e^{-b^2(x^2+y^2+z^2)} = (b^3 / \pi^{3/2})\, e^{-b^2 r^2}, \tag{3.11}$$

indicating that $p(r)$ is a maximum when $r = 0$, that is when the two ends are coincident. However it is not the case that the most probable end-to-end length is zero. To determine the probability of an end-to-end length between r and $r+dr$, the free end must be allowed to fall anywhere between two concentric circles of radii r and $r+dr$. The volume enclosed between these spherical surfaces is $4\pi r^2 dr$. The required probability is thus obtained by multiplying Equation (3.11) by $4\pi r^2 dr$ to give

$$P(r)dr = (b^3 / \pi^{3/2}) e^{-b^2 r^2}\, 4\pi r^2 dr \tag{3.12}$$

The most probable value of r may be determined by setting the derivative of Equation (3.12) equal to zero, to give

$$r = \frac{1}{b} = \sqrt{\left(\frac{2n}{3}\right)} l \tag{3.13}$$

Thus the most probable chain length is proportional to the square root of the number of rigid links. The root mean square value of r may also be obtained from Equation (3.12) by taking the average,

$$\overline{r^2} = \int_0^\infty r^2 P(r)\, dr \Big/ \int_0^\infty P(r)\, dr \tag{3.14}$$

where the denominator in Equation (3.14) is equal to unity. The mean square value of r is thus

$$\overline{r^2} = \frac{3}{2b^2} = nl^2 \tag{3.15}$$

The root mean square value of r can therefore be determined by taking the square root of Equation (3.15), to give

$$\sqrt{\left(\overline{r^2}\right)} = \sqrt{n}\, l \tag{3.16}$$

Thereby demonstrating that the root mean square length is also proportional to the number of rigid links per chain.

3.2.2.1.1 Entropy of a Single Gaussian Chain

The entropy of a single Gaussian chain may be obtained using the Boltzmann's relation, where the entropy is taken as proportional to the logarithm of the probability density, to give

$$s = k \ln\left[p(r)\right] = k\left[c - \frac{3r^2}{2nl^2}\right] \tag{3.17}$$

where k is the Boltzmann constant and c is an constant. It can be seen from Equation (3.17) that the entropy has a maximum value when the chain ends are coincident, $r = 0$, and decreases continuously as the distance between the chain ends is increased. This follows from the structure of the unstrained polymer chain being random or disordered and hence of high entropy. As the chain end separation is increased the number of available conformations is reduced and hence the entropy is decreased. Thus it is observed from kinetic theory that it is the reduction in entropy upon extension of the chain that provides the restoring force to return the chain to the unstrained state.

3.2.2.1.2 Work of Extension of a Single Gaussian Chain

The work required to extend a single Gaussian chain may be determined from consideration of the first and second laws of thermodynamics. For an isothermal reversible process the work done on a system by external forces, ΔW, is equal to the change in Helmholtz free energy, ΔG, provided there is no change in internal energy. This result may be expressed by a relation of the form

$$\Delta W = \Delta G = -T\Delta S \tag{3.18}$$

If Equation (3.17) is substituted into the expression above, the work required to extend a single Gaussian chain from the unstrained state, ΔW, may be written as

$$\Delta W = kT\left[\frac{3r^2}{2nl^2} - c\right] \tag{3.19}$$

For a chain whose ends are located at specified points separated by a distance r, the work required to move one end from a distance r to a distance $r+dr$ is by definition equal to the change in the Helmholtz free energy, and therefore

$$\frac{dG}{dr} = \frac{dW}{dr} = -T\frac{ds}{dr} \tag{3.20}$$

From (3.19),

$$\frac{dW}{dr} = \frac{3kT}{l}\left(\frac{r}{nl}\right) \tag{3.21}$$

Since work is required to extend the chain it follows that a tensile force f must act along the direction r. The work done by this force in a virtual displacement dr is $f\,dr$, i.e

$$dW = f\,dr \tag{3.22}$$

Comparing Equation (3.21) and (3.22)

$$f = \frac{3kT}{l}\left(\frac{r}{nl}\right) \tag{3.23}$$

Thus, a molecule with its ends fixed at specified points is acted on by a tensile force in the direction of a line joining its ends and proportional to the length of that line. Since the tension in the chain is proportional to its length, the molecule may be regarded as possessing an elasticity governed by Hooke's law. However it must be remembered that the linear-force extension relation given in Equation (3.23) is subject to the same limitations as the Gaussian distribution function from which it is derived. It is therefore only valid as long as the distance between the ends of the chain is small compared with the fully extended length. In practice this corresponds to values of r less than one-third the fully extended length.

3.2.2.1.3 Gaussian Chain Networks

As discussed in the introduction to this chapter elastomers are polymeric materials, made up of long chain-like molecules. During vulcanisation permanent chemical bonds are created between chains, leading to the formation of irregular three-dimensional network structures. The statistical mechanics approach has been extended to treat the properties of such networks by several authors. In the approach of Treloar (1975), who considered a random network containing a total of N chains per unit volume, of varying contour length characterised by different values of the parameter b, chains are assumed to deform affinely. The assembly of chains is divided into in number of groups, such that the contour length and hence the value of b is the same for all the members of a particular group. The total entropy of deformation is calculated by determining the sum of the entropies for all the chains in any one group and then summing over all the groups. Consider an individual chain in such a network Figure 3.3, having a end-to-end separation represented by the vector r in the undeformed state, with components (x, y, z).

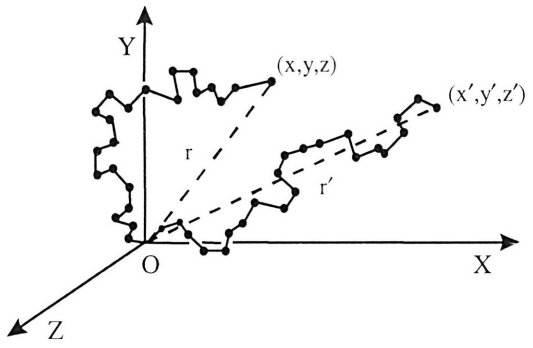


Figure 3.3 : The 'affine' deformation of randomly jointed chains.

In the deformed state the assumption of affine deformation permits the chain to be represented by the vector r', having components (x', y', z') given by

$$x' = \lambda_1 x \quad , \quad y' = \lambda_2 y \quad , \quad z' = \lambda_3 z \tag{3.24}$$

with the coordinate frame being chosen so as to coincide with the principal axes of strain. The entropy of the chain before deformation may be determined from Equation (3.11) using Boltzmann's relation, to give

$$s = c - kb^2(x^2 + y^2 + z^2) \tag{3.25}$$

The corresponding entropy after deformation is given by

$$s' = c - kb^2(\lambda_1^2 x^2 + \lambda_2^2 y^2 + \lambda_3^2 z^2) \tag{3.26}$$

The contribution to the total change in entropy as a result of deformation of this chain is therefore

$$\Delta s = s' - s = -kb^2[(\lambda_1^2 - 1)x^2 + (\lambda_2^2 - 1)y^2 + (\lambda_3^2 - 1)z^2] \tag{3.27}$$

Consider the contribution of the chains (N_p in number) in a single group, characterised by a chain length and corresponding value of the parameter b, namely b_p. The total entropy of deformation ΔS_p for this group is determined by summation

of the individual contributions made by each chain, represented by Equation (3.27). This summation takes the form

$$\Delta S_p = \sum_{i=1}^{N_p} \Delta s_{ip} = -kb_p^2 \left[(\lambda_1^2 - 1) \sum_{i=1}^{N_p} x_{ip}^2 + (\lambda_2^2 - 1) \sum_{i=1}^{N_p} y_{ip}^2 + (\lambda_3^2 - 1) \sum_{i=1}^{N_p} z_{ip}^2 \right] \tag{3.28}$$

where the subscript ip represents the ith chain of the pth group. In Equation (3.28) the term $\sum x_{ip}^2$ is the sum of the squares of the x-components, in the unstrained state, for all the chains in the group. From consideration of a single chain, Figure 3.2, it follows that for an individual group of chains

$$\sum_{i=1}^{N_p} x_{ip}^2 + \sum_{i=1}^{N_p} y_{ip}^2 + \sum_{i=1}^{N_p} z_{ip}^2 = \sum_{i=1}^{N_p} r_{ip}^2 \tag{3.29}$$

For a random isotropic network all directions of the vector r are considered equally probable thus

$$\sum_{i=1}^{N_p} x_{ip}^2 = \sum_{i=1}^{N_p} y_{ip}^2 = \sum_{i=1}^{N_p} z_{ip}^2 = \frac{1}{3} \sum_{i=1}^{N_p} r_{ip}^2 \tag{3.30}$$

The mean-square vector length of chains in the same group $\overline{r_{ip}^2}$ is defined via Equation (3.31).

$$\sum_{i=1}^{N_p} r_{ip}^2 = N_p \overline{r_{ip}^2} \tag{3.31}$$

Using Equations (3.28),(3.30) and (3.31) the entropy of deformation for a given group reduces to

$$\Delta S_p = -\frac{1}{3} k N_p b_p^2 \overline{r_{ip}^2} (\lambda_1^2 + \lambda_2^2 + \lambda_3^2 - 3) \tag{3.32}$$

This may be further simplified by assuming that the mean-square vector length for this group of chains is the same as the mean square vector length of a free chain with the same contour length, Equation (3.15), such that

$$\overline{r_{ip}^2} = \frac{3}{2b_p^2} \tag{3.33}$$

Introducing this assumption leads to Equation (3.34)

$$\Delta S_p = -\frac{1}{2} k N_p (\lambda_1^2 + \lambda_2^2 + \lambda_3^2 - 3) \tag{3.34}$$

Summation over the p groups of chains finally yields the total entropy of deformation for the whole assembly.

$$\Delta S = \sum_p \Delta S_p = -\frac{1}{2} N k (\lambda_1^2 + \lambda_2^2 + \lambda_3^2 - 3) \tag{3.35}$$

Since the total number of chains per unit volume is equal to the summation of the number of chains in each group

$$\sum_p N_p = N . \tag{3.36}$$

3.2.2.1.4 Work of Deformation for a Network of Gaussian Chains

The work required to deform a random network of Gaussian chains can be determined directly from Equation (3.35), using a similar approach to that employed to derive the equivalent expression for a single chain. If the network is assumed to possess the same internal energy in all deformation states, the work of deformation may be obtained from Equation (3.18) to give

$$W = \frac{1}{2} NkT(\lambda_1^2 + \lambda_2^2 + \lambda_3^2 - 3) \tag{3.37}$$

Equation (3.37) describes the accumulation of strain energy in random a network of Gaussian chains and is often referred to as the Neo-Hookean strain energy function. It is considered a fundamental relation in rubber elasticity and is sometimes written in the form

$$W = \frac{\mu}{2}(\lambda_1^2 + \lambda_2^2 + \lambda_3^2 - 3) \tag{3.38}$$

where $\mu = NkT$ is known as the shear modulus. It has been observed that Equation (3.38) and hence all the stress-strain relations derivable from it involve only a single physical parameter N, which is dependent on the structure of the material. Figure 3.4 shows a comparison of the stress-strain relations derived from Equation (3.38) with the experimental results of Treloar (1944). The Gaussian model agrees closely with the uniaxial data up to a strain of around 250%, above this level the difference between stresses predicted from Equation (3.38) and the experimentally determined values increases with increasing strain. The large differences which are observed at higher strains occur as an appreciable proportion of chains in the vulcanised rubber approach their limiting extensibility, so that the assumption employed in Gaussian theory that chains do not approach their fully extended length is no longer valid.

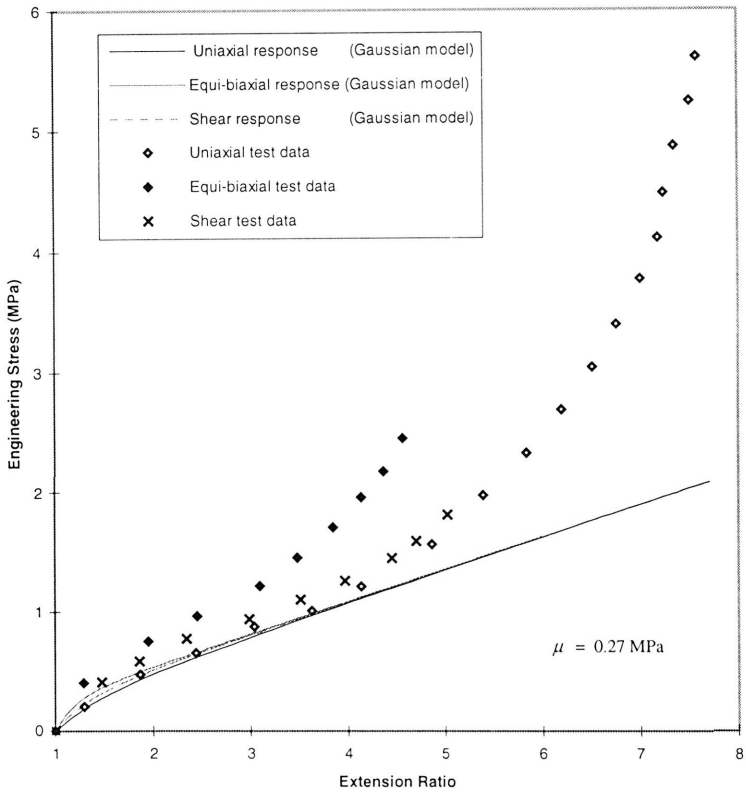


Figure 3.4 : A comparison of the experimental results of Treloar (1944) with the Gaussian model.

3.2.2.2 Non Gaussian Theory of Rubber Elasticity

For a randomly jointed chain, departures from Gaussian statistical theory first become significant when its vector length is between one-third and one-half of its fully extended length. This is independent of the number of links in the chain, or chain length. For a network of such chains Gaussian theory again becomes inadequate when the strain exceeds about one-third and one-half of the maximum deformability of the network. The maximum extensibility of a chain is defined as the ratio of its fully extended length to its length in the absence of external forces (*i.e.* its root mean square length) and is given by $\sqrt{n}$. The range of strain over which Gaussian theory is valid therefore becomes smaller as chain length is reduced. In the case of a network in which chain length is inversely related to the degree crosslinking, this implies that Gaussian theory becomes less satisfactory as the degree of crosslinking is increased. For chains which are very short, $n = 5$ or less, the mean chain extension in the unstrained state already exceeds that for which Gaussian approximation is valid. At chain extensions greater than one-third the fully extended length it is necessary to

investigate the properties of a network using a more accurate non-Gaussian statistical treatment, which can account for the finite extensibility of chains and hence networks.

As in Gaussian theory the problem is simplified by replacing the actual molecular structure with an idealised random chain, of n rigid links each of length l. The direction in space of any particular link is considered entirely random and independent of the direction of neighbouring links. Solution of the randomly jointed chain problem again involves determining the probability that one end of a chain B will occupy a small volume dv at a distance r from end A, Figure 3.2. The approximate solution of this problem using non-Gaussian statistics may be expressed in the form of the natural logarithm of the probability density function $\ln[p(r)]$

$$\ln[p(r)] = c - n\left[\frac{r}{nl}\beta + \ln\left\{\frac{\beta}{\sinh\beta}\right\}\right] \tag{3.39}$$

where c is a constant. The parameter β in Equation (3.39) is a function of the fractional chain extension (r/nl) and is defined in the following way

$$\frac{r}{nl} = \coth\beta - \frac{1}{\beta} \equiv \mathcal{L}(\beta) \tag{3.40}$$

where $\mathcal{L}(\beta)$ is known as the Langevin function. Alternatively one may write

$$\beta = \mathcal{L}^{-1}(r/nl) \tag{3.41}$$

where $\mathcal{L}^{-1}(r/nl)$ is the corresponding inverse Langevin function. It should be noted that Equation (3.41) represents an implicit relationship since an iterative scheme is required to determine an exact value of β. However as demonstrated by Treloar (1975) Equation (3.39) may be expanded in the form of the following series

$$\ln[p(r)] = c - n\left[\frac{3}{2}\left(\frac{r}{nl}\right)^2 + \frac{9}{20}\left(\frac{r}{nl}\right)^4 + \frac{99}{350}\left(\frac{r}{nl}\right)^6 + \ldots\right] \tag{3.42}$$

The equivalent expression derived from Gaussian theory is given by,

$$\ln[p(r)] = c - n\left[\frac{3}{2}\left(\frac{r}{nl}\right)^2\right] \tag{3.43}$$

which is observed to correspond to the first term of the series in Equation (3.42). Equation (3.43) therefore provides a good approximation for the more complex non-Gaussian distribution function so long as higher order terms are sufficiently small to be neglected. If $r/nl = 1/3$ the error in $\ln[p(r)]$ involved in the Gaussian approximation is only about 3%, while if $r/nl = 1/2$, the error is about 8%. At larger chain end extensions Equation (3.43) ceases to be a useful approximation.

3.2.2.2.1 Entropy of a Single non-Gaussian Chain

The entropy of a single non-Gaussian chain may be obtained using the Boltzmann's relation, where the entropy is taken as proportional to the logarithm of probability density, to give

$$s = k\ln[p(r)] = kc - kn\left[\frac{r}{nl}\beta + \ln\frac{\beta}{\sinh\beta}\right] \tag{3.44}$$

The function within the bracket is identical to that in Equation (3.39) and has the same series expansion as that given in Equation (3.42). The presence of the constant c in Equation (3.17) and Equation (3.44) is of no consequence since only relative probabilities or differences in entropy are of concern and not absolute values of these quantities. In addition it is important to bear in mind that a chain does not possess an entropy by the mere fact of having a specified conformation, but only by virtue of the large number of conformations accessible to it under specified conditions of restraint.

3.2.2.2.2 Work of Extension of a Single non-Gaussian Chain

The work required to extend a single non-Gaussian chain from the unstrained state is determined as in Gaussian theory, using Equation (3.18) to give

$$W = kTn\left[\frac{r}{nl}\beta + \ln\frac{\beta}{\sinh\beta}\right] - T\breve{c} \tag{3.45}$$

where $\breve{c}$ is a combination of the previously defined constants. The tension on a non-Gaussian chain when its ends are held at a distance r apart may also be derived as in Gaussian theory. From Equation (3.20) the tension f is given by

$$f = \frac{dW}{dr} \tag{3.46}$$

Substitution of Equation (3.45) for W thus gives

$$f = \frac{kT}{l}\mathcal{L}^{-1}\left(\frac{r}{nl}\right) \tag{3.47}$$

The series expansion employed for the inverse Langevin function $\mathcal{L}^{-1}(r/nl)$ takes the form

$$\mathcal{L}^{-1}\left(\frac{r}{nl}\right) = 3\left(\frac{r}{nl}\right) + \frac{9}{5}\left(\frac{r}{nl}\right)^3 + \frac{297}{175}\left(\frac{r}{nl}\right)^5 + \frac{1539}{875}\left(\frac{r}{nl}\right)^7 + \ldots\ldots \tag{3.48}$$

The form of the force-extension relation over the range of $r/nl = 0$ to $r/nl = 0.95$, represented by the inverse Langevin function is illustrated in Figure 3.5. If the fractional chain extension r/nl is less than about one-third, terms in Equation (3.48) involving powers of r/nl higher than one may be neglected. In this region the force-extension relation reduces to the linear form, corresponding to the Gaussian distribution. At higher values of the fractional chain extension the force required to extend the chain increases rapidly, as the inverse Langevin function tends to infinity as r/nl approaches unity. The representation of the inverse Langevin function by a limited number of terms in an expanded series while a useful approximation has persisted despite the wide spread availability of digital computers which allow for the efficient calculation of implicit functions using iterative solution techniques. Indeed it

is still common practice in literature to represent the inverse Langevin function as a six term series even though it only provides a satisfactory approximation for values of r/nl below 0.7.

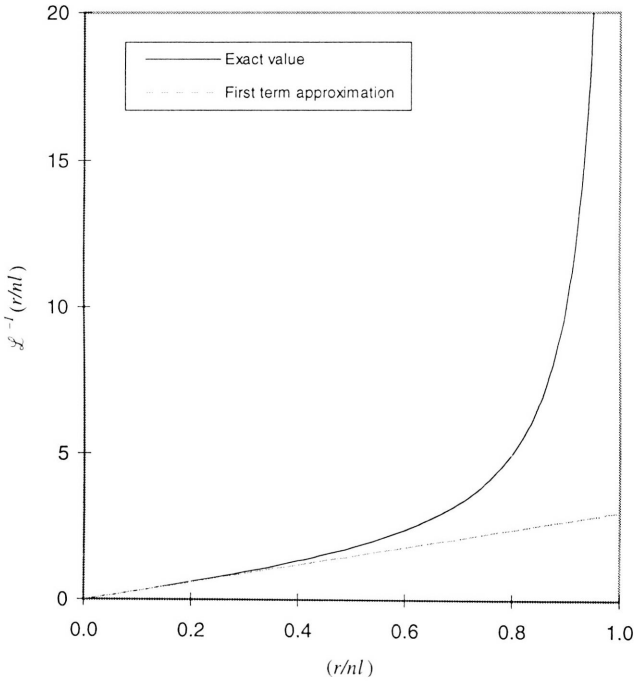


Figure 3.5 : The force-extension relation for a randomly jointed chain.

3.2.2.2.3 Non-Gaussian Chain Networks

The treatment of networks using non-Gaussian statistics has been considered by various authors including James and Guth (1943) in their three chain model, Treloar (1946) in his extension of the tetrahedron model of Flory and Rehner (1943) and later by Treloar and Riding (1979) who considered a large assembly of chains randomly orientated in space. However for he sake of brevity discussions will be confined to the models and James and Guth (1943) and Arruda and Boyce (1993) which form the basis of constitutive developments presented later. In considering the behaviour of a network of non-Gaussian chains it is convenient to express the fractional chain end separation in terms of $\lambda/\sqrt{n}$ rather than r/nl. The chain stretch λ is defined as current chain end separation r divided by the separation in the unstrained state r_0.

$$\lambda = \frac{r}{r_0} \tag{3.49}$$

Given that $r_0 = \sqrt{n}\, l$ the fractional chain end separation may be written as

$$\frac{r}{nl} = \frac{\lambda r_0}{nl} = \frac{\lambda}{\sqrt{n}} \tag{3.50}$$

The maximum allowable value of λ is referred to as the locking or limiting chain stretch λ_L. The limiting stretch is simply the ratio of the fully extended chain length $r_L = nl$ to the initial chain length and is given by

$$\lambda_L = \frac{r_L}{r_0} = \sqrt{n} \tag{3.51}$$

The work required to extend a non-Gaussian chain may be rewritten it terms of chain stretch using Equation (3.50) to give

$$W = kTn\left[\frac{\lambda}{\sqrt{n}}\beta + \ln\frac{\beta}{\sinh\beta}\right] - T\breve{c} \tag{3.52}$$

3.2.2.2.4 Three Chain Model

The earliest of the non-Gaussian network theories is that of James and Guth (1943). In their model the random network employed in Gaussian theory is replaced by three sets of independent chains aligned parallel to the axes OX, OY and OZ of a rectangular coordinate system, Figure 3.6. The network is considered to have a chain density of N with each set of independent chains containing $N/3$ chains. Chains are assumed to deform affinely and to be of length $r_0 = \sqrt{n}\, l$ in the unstrained state. The work required to deform the network can be determined by summing the contributions made by each chain set and may be written as

$$W = \frac{N}{3}\sum_{i=1}^{3}(W_i) \tag{3.53}$$

where W_i indicates the work performed on a particular chain set.

Replacing W_i with Equation (3.52) gives

$$W = \frac{\mu}{3}\sum_{i=1}^{3}\left\{n\left[\frac{\lambda_i}{\sqrt{n}}\beta_i + \ln\frac{\beta_i}{\sinh\beta_i}\right] - T\breve{c}\right\} \tag{3.54}$$

where $\mu = NkT$, λ_i represents the stretch in the i th chain set, and β_i is defined as

$$\beta_i = \mathcal{L}^{-1}\left(\frac{\lambda_i}{\sqrt{n}}\right) \tag{3.55}$$

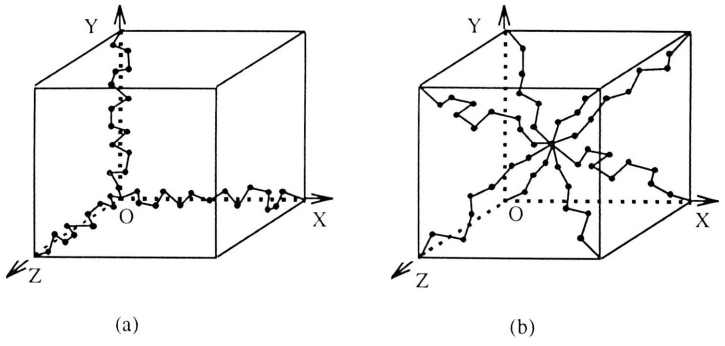


Figure 3.6 : Schematic of three chain model (a) and eight chain model (b).

Figure 3.7 shows the form of the uniaxial stress-strain curve derived from Equation (3.54), for three values of n, the stress (normalised by NkT) is defined as the tensile load divided by the unstrained cross sectional area. In contrast to Gaussian theory, the 3 chain model exhibits a pronounced upward curvature at higher strains, associated with the finite extensibility of the network. The ultimate extension at which the stress tends to infinity is the same as that for a single non-Gaussian chain which is equal to square root of the number of links per chain $\sqrt{n}$. Equation (3.54) contains two parameters which must be determined experimentally to model the behaviour of a real elastomer, the first, μ, which also occurs in the Gaussian theory defines the vertical scale or modulus in the region of small or moderate strains, while the second, n, which is specific to non-Gaussian theories determines the extent of the horizontal scale.

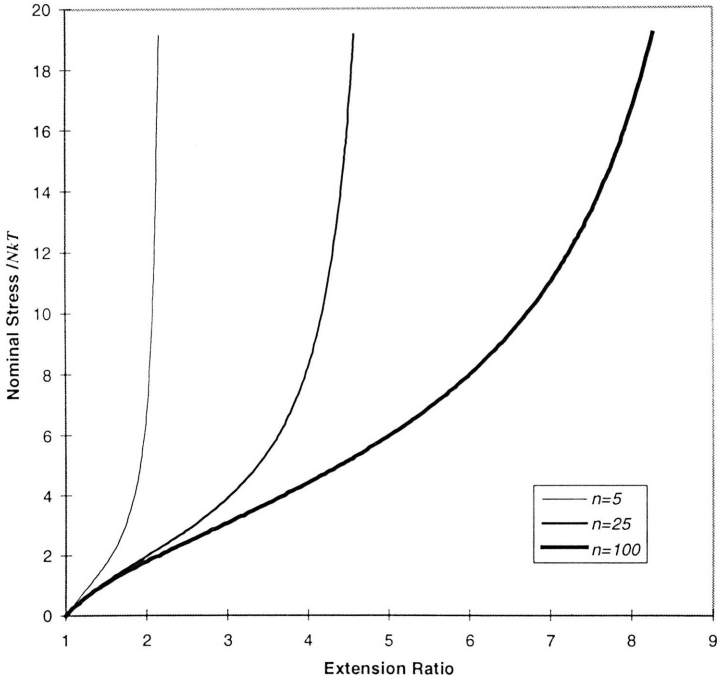


Figure 3.7 : Non-Gaussian force-extension curves from 3 chain model.

Figure 3.8 shows a comparison of the stress-strain relations derived from the strain energy function given in Equation (3.54) and the experimental results of Treloar (1944). The parameters μ and n were found by fitting the model to the uniaxial data. The 3 chain model is observed to reproduce the uniaxial and shear data but fails to predict the marked reduction in extensibility in equi-biaxial extension. The inability of the 3 chain model to distinguish between uniaxial and biaxial extension is a result of the assumption that the chain sets deform independently of one another. In uniaxial extension, chains parallel to the extension direction stretch until they reach their locking stretch. The stretch in the two remaining chain sets is determined by incompressibility. Under equi-biaxial extension, two coplanar chains extend independently until simultaneously reaching the locking stretch, the stretch in the remaining chain set is again dictated by the incompressibility condition. The limiting chain stretch in equi-biaxial extension predicted by the three chain model is therefore equal to that for uniaxial extension.

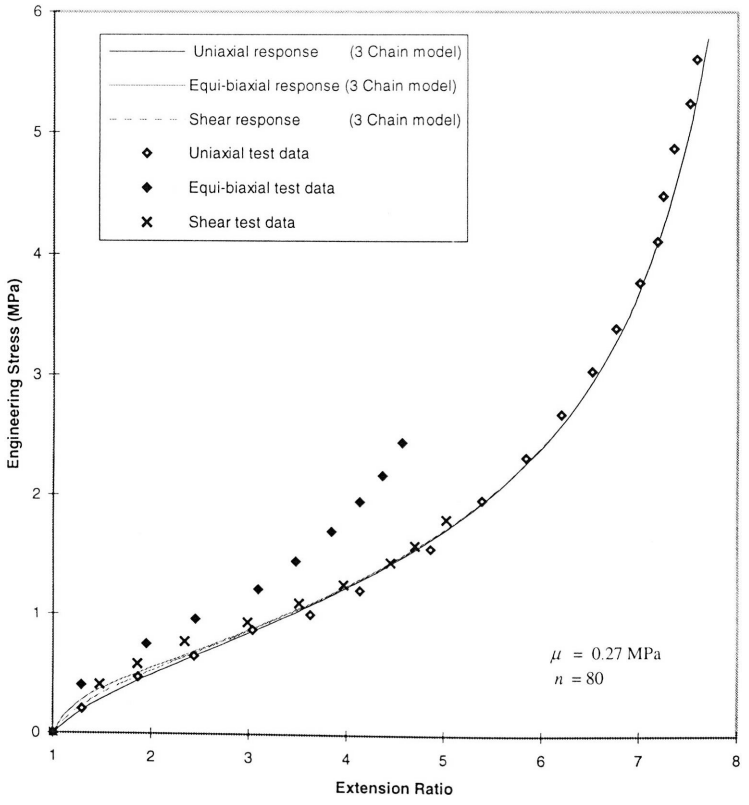


Figure 3.8 : A comparison of the experimental results of Treloar (1944) with the 3 chain model.

3.2.2.2.5 Eight Chain Model

Arruda and Boyce (1993) have proposed a network model that responds more realistically to multiaxial loading conditions. The network is made up of eight chains of length $r_0 = \sqrt{n}l$, which extend from the centre of a cube to the corners, Figure 3.6. In the unstained state the cube has a side length of a_0. From basic geometry a_0 and r_0 are related via

$$a_0 = \frac{2}{\sqrt{3}} r_0 \tag{3.56}$$

If the cube is stretched so that the edges measure $\lambda_1 a_0$, $\lambda_2 a_0$ and $\lambda_3 a_0$ in the X, Y and Z directions respectively each chain in the network has a length

$$r_{chain} = \frac{a_0}{2}\sqrt{\lambda_1^2 + \lambda_2^2 + \lambda_3^2} \tag{3.57}$$

The stretch for each chain in the network is given by

$$\lambda_{chain} = \frac{r_{chain}}{r_0} = \frac{\sqrt{\lambda_1^2 + \lambda_2^2 + \lambda_3^2}}{\sqrt{3}} \tag{3.58}$$

If λ_{chain} is substituted into Equation (3.52) and the network is assumed to contain N chains per unit volume, the work required to deform the network is given by

$$W = \mu \left\{ n \left[\frac{\lambda_{chain}}{\sqrt{n}} \beta_{chain} + \ln \frac{\beta_{chain}}{\sinh \beta_{chain}} \right] - T\breve{c} \right\} \tag{3.59}$$

where β_{chain} in the equation above is defined as

$$\beta_{chain} = \mathcal{L}^{-1}\left(\frac{\lambda_{chain}}{\sqrt{n}} \right) \tag{3.60}$$

It can be seen from Equation (3.59) that the strain energy function for the 8 chain model contains two parameters μ and n which are also present in the 3 chain model. (Note that this form of the strain energy function is not given explicitly in the work of Arruda and Boyce (1993), instead they provide a five term approximation obtained by the differentiation of Equation (3.59) and integration of the subsequent differential relation). It is clear from geometrical considerations that in the theory of Arruda and Boyce each chain in the network stretches equally in response to any given deformation state, and as such chains can be considered to deform in a cooperative manner. It has been argued by Arruda and Boyce that because chains deform cooperatively in their model, it provides a more realistic representation for the structure of a polymer network than other non-Gaussian theories. Figure 3.9 shows a comparison of the stress-strain relations derived from Equation (3.59) with the experimental results of Treloar (1944). The parameters μ and n were found by fitting the model to the uniaxial data. In common with the theory of James and Guth (1943) the 8 chain model accurately predicts the uniaxial and shear data. However it also captures the difference in limiting extensibility in uniaxial and biaxial extension. The success of the 8 chain model in reproducing the deformation state dependence

demonstrated by rubber-like materials has been attributed by the authors to the consideration of the finite extensibility parameter, n, as an averaged measure of applied stretches over eight spatial orientations.

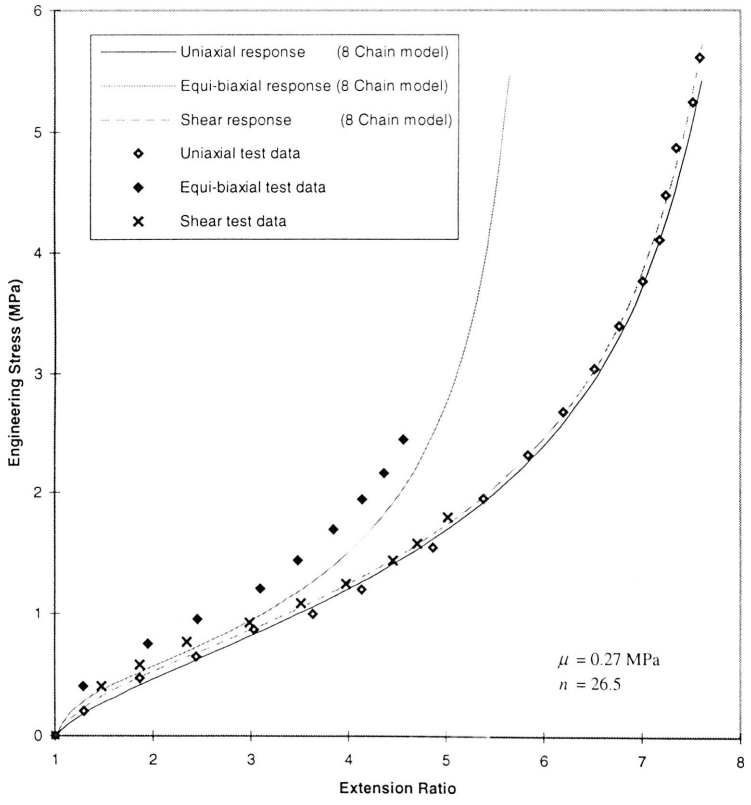


Figure 3.9 : A comparison of the experimental results of Treloar (1944) with the 8 chain model.

3.3 Final Remarks

The network models of James and Guth and Arruda and Boyce demonstrate that significant features of the mechanical behaviour of rubber-like materials can be reproduced using non-Gaussian statistical theory. While both theories capture the marked increase in stiffness observed at higher strains, the model of Arruda and Boyce can also account for the deformation state dependence. In practical terms both models offer several advantages over phenomenological alternatives. Firstly they provide a superior representation of the large strain behaviour of rubber-like materials compared with the Mooney-Rivlin model. Secondly they only require experimental data from single deformation state to determine a set of material constants, which are

thermodynamically stable, and so may be extrapolated beyond the range of the available experimental data with greater confidence than the Rivlin or Ogden models

Chapter 4

4. Implementation of Incompressible Forms of the Non-Gaussian Network Models into FE Software

4.1 Introduction

Constitutive models for the non-linear finite element analysis (FEA) of elastomeric materials are now frequently included as standard in many commercially available finite element (FE) packages. The most commonly available material models are those based on the theories of Rivlin (1948a) and Ogden (1972a), which being phenomenological in origin lack any direct link to the underlying mechanism of deformation. In contrast non-Gaussian network models like those of James and Guth (1943) and Arruda and Boyce (1993) have not attracted wide spread use in FEA despite requiring only two material parameters to describe the general deformation behaviour of elastomeric materials. One reason for this may be that traditional methods of implementation rely on an expanded series representation for the inverse Langevin function. This approach while still widely employed in literature leads to a set of constitutive relationships whose accuracy decreases rapidly as the argument of the inverse Langevin function approaches unity. In this chapter a new method to implement non-Gaussian network models into commercial FE codes is presented

which employs a simple iterative technique to determine the exact value of the inverse Langevin function and its derivative. This in turn allows exact expressions for the principal stresses and principal components of the tangent modulus to be derived. These quantities are then transformed to the axes of the base coordinate frame. Using this approach, compressible and incompressible forms of the 3 chain model of James and Guth and the 8 chain model of Arruda and Boyce have been implemented into the commercial FE code ABAQUS using the user defined material subroutine facility known as UMAT. The resulting constitutive equations are given in full in this chapter and are observed to be no more complex than those of standard phenomenological models. The chapter commences with a review of the scheme employed in the current work to determine the exact value of the inverse Langevin function and its derivative. This leads on to a discussion of the principal axes technique of Chadwick and Ogden (1971a,b) and its application to non-Gaussian network models. The results of numerical tests conducted on benchmark problems using UMAT routines developed for the analysis of plane stress problems are also presented at the end of the chapter to demonstrate the effectiveness of the proposed procedure.

4.2 Determination of the Inverse Langevin Function

The evaluation of the constitutive relationships for the 3 and 8 chain network models requires the calculation of the value of the inverse Langevin function. In the recent work of Allport and Day (1996) and Kaliske and Rothert (1997), concerned with the implementation of these models into FE codes, the inverse Langevin is determined using a series approximation. Though neither author specifies the number of terms employed in their series approximation of $\mathcal{L}^{-1}(x)$, a survey of related work reveals that the inverse Langevin function is most commonly represented as a six term series. Although such an approximation is accurate to a tolerance of 10^{-8} for values of x below 0.22, it provides an increasing poor estimate of $\mathcal{L}^{-1}(x)$ at higher values of x. In the current work an improved method is employed to calculate the inverse Langevin function, similar to that presented by Treloar (1979). The proposed method has the advantage of providing an accurate value of $\mathcal{L}^{-1}(x)$ for all values of x between the limits of 0 and 1.

At either end of this range, accurate approximations for $\mathcal{L}^{-1}(x)$ are available. For low values of x, the first six terms in the expanded series representation of Treloar (1975)

$$\mathcal{L}^{-1}(x) \approx 3x + \frac{9}{5}x^3 + \frac{297}{175}x^5 + \frac{1539}{875}x^7 + \frac{126117}{67375}x^9 + \frac{43733439}{21896875}x^{11} \qquad (4.1)$$

$$(x < 0.22)$$

and for values of x close to unity

$$\mathcal{L}^{-1}(x) \approx \frac{1}{1-x} \qquad (4.2)$$

$$(x > 0.9)$$

Each of these is accurate to 10^{-8}, or better within the specified range of x; one or the other is therefore used directly in the calculation of $\mathcal{L}^{-1}(x)$ for values of x within these ranges. Over the intermediate ranges of $0.22 < x < 0.7$ and $0.7 \leq x < 0.9$, Equation (4.1) and (4.2) respectively, are used to obtain a first approximation to $\mathcal{L}^{-1}(x)$, this is then refined by application of the Newton-Raphson technique. The essence of the procedure is as follows:

Let

$$y = \mathcal{L}^{-1}(x). \qquad (4.3)$$

Then

$$x = \mathcal{L}(y) = \coth y - \frac{1}{y}. \qquad (4.4)$$

Further, let

$$f(y) = \coth y - \frac{1}{y} - x = 0. \qquad (4.5)$$

For a given x, it is required to solve Equation (4.5) for y. Given any estimate of y, say y_i, the Newton-Raphson technique gives a better estimate, y_{i+1}, namely

$$y_{i+1} = y_i - \frac{f(y_i)}{f'(y_i)} \quad , \qquad (4.6)$$

where

$$f'(y) = \frac{df(y)}{dy} = \frac{1}{y^2} - \text{cosech}^2 y. \tag{4.7}$$

Hence given a first approximation y_0 from Equation (4.1) or Equation (4.2), Equation (4.6) can be used to generate a converging series of values $y_0, y_1, y_2, y_3 \ldots$ until two successive values differ by less than some (specified) small amount. In the present case it was found that for an accuracy of 10^{-8}, the number of iteration cycles (applications of Equation (4.6)) was approximately

$$\begin{aligned} 0.22 < x < 0.50: &\quad 2 \\ 0.50 < x < 0.90: &\quad 3 \end{aligned}$$

The derivative of the inverse Langevin function is also required in the constitutive formulations for the 3 and 8 chain models, and may be found by determining the derivative of the Langevin function. Differentiating the Langevin function, Equation (4.4), with respect to its argument gives

$$\frac{dx}{dy} = \frac{d}{dy}\left(\mathcal{L}(y)\right) = \frac{1}{y^2} - \text{cosech}^2 y \tag{4.8}$$

This expression may then be inverted to yield the derivative of the inverse Langevin function,

$$\frac{1}{\frac{dx}{dy}} = \frac{dy}{dx} = \frac{d}{dx}\left(\mathcal{L}^{-1}(x)\right) = \frac{y^2 \sinh^2 y}{\sinh^2 y - y^2} \tag{4.9}$$

Thus the derivative of the inverse Langevin function may be determined simply from Equation (4.9), if the value of the inverse Langevin function itself is known.

4.3 The Principal Axes Technique

The strain energy functions for the 3 and 8 chain models are phrased in terms of principal stretches. This enables the derivation of expressions for the principal stresses and principal components of the tangent modulus. However, since the axes of the base coordinate frame employed in the finite element scheme do not necessarily coincide with the principal directions, a coordinate transformation is usually required. This may be accomplished in several ways. In the method proposed by Simo and Taylor (1991) the eigenvector base is calculated using the closed-form formula of Morman (1986). In the alternative approach of Chadwick and Ogden (1971a,b) the stress and constitutive tensors are calculated in the principal directions and then rotated to the axial directions of the active coordinate frame. Various authors such as Gruttmann and Taylor (1992) and Reese and Wriggers (1995) have employed this method. It is also the approach that has been adopted in the current work because of its greater simplicity. Consider first the application of this method to the derivation of the constitutive relationship in the initial or material configuration. For a compressible hyperelastic material model, the second Piola-Kirchhoff stress tensor may be expressed as

$$\mathbf{S} = \frac{\partial W}{\partial \mathbf{E}} = \sum_{i=1}^{3} \frac{\partial W}{\partial \lambda_i} \frac{\partial \lambda_i}{\partial \mathbf{E}} \tag{4.10}$$

where $\mathbf{E}$ represents the Green strain tensor. Using the relationship $E_{ii}^{L} = \frac{1}{2}(\lambda_i^2 - 1)$ the principal second Piola-Kirchhoff stresses may be written as

$$S_{ii}^{L} = \frac{\partial W}{\partial \lambda_i} \frac{\partial \lambda_i}{\partial E_{ii}^{L}} = \frac{1}{\lambda_i} \frac{\partial W}{\partial \lambda_i} \tag{4.11}$$

where the L superscript in Equation (4.11) indicates the stress components in the principal directions, known as the Lagrangian triad. The components of the second Piola-Kirchhoff stress tensor in the Lagrangian triad and those in the axial directions of material coordinate system can be related using the standard tensor transformation

$$\mathbf{S} = \mathbf{Q}(\mathbf{N})\mathbf{Diag}\,[S_{ii}^{L}]\mathbf{Q}(\mathbf{N})^{T} \tag{4.12}$$

where $\mathbf{Q(N)} = [\mathbf{N}_1 \mathbf{N}_2 \mathbf{N}_3]$ is the matrix containing the principal direction vectors $\mathbf{N}_1$, $\mathbf{N}_2$ and $\mathbf{N}_3$ of the Lagrangian triad and $\mathbf{Diag}[S_{ii}^L]$ is the diagonal matrix containing the principal second Piola-Kirchhoff stresses S_{11}^L, S_{22}^L and S_{33}^L. Consider next the issue of obtaining the tangential relationship between the second Piola-Kirchhoff stress and the Green strain. Since the directions of the principal stresses and strains coincide we can complement Equation (4.12) with

$$\mathbf{E} = \mathbf{Q(N)Diag}[E_{ii}^L]\mathbf{Q(N)}^T, \tag{4.13}$$

where $\mathbf{Diag}[E_{ii}^L]$ is the diagonal matrix containing the principal Green strains E_{11}^L, E_{22}^L and E_{33}^L. Differentiation of Equations (4.12) and (4.13) leads to

$$\dot{\mathbf{S}} = \mathbf{Q(N)Diag}[\dot{S}_{ii}^L]\mathbf{Q(N)}^T + \dot{\mathbf{Q}}\mathbf{(N)Diag}[S_{ii}^L]\mathbf{Q(N)}^T + \mathbf{Q(N)Diag}[S_{ii}^L]\dot{\mathbf{Q}}\mathbf{(N)}^T, \tag{4.14}$$

$$\dot{\mathbf{E}} = \mathbf{Q(N)Diag}[\dot{E}_{ii}^L]\mathbf{Q(N)}^T + \dot{\mathbf{Q}}\mathbf{(N)Diag}[E_{ii}^L]\mathbf{Q(N)}^T + \mathbf{Q(N)Diag}[E_{ii}^L]\dot{\mathbf{Q}}\mathbf{(N)}^T. \tag{4.15}$$

Relating Equations (4.14) and (4.15) to the principal directions of the material frame known as the Lagrangian triad, gives

$$\dot{\mathbf{S}}^L = \mathbf{Q(N)}^T\dot{\mathbf{S}}\mathbf{Q(N)} = \mathbf{Diag}[\dot{S}_{ii}^L] + \mathbf{Q(N)}^T\dot{\mathbf{Q}}\mathbf{(N)Diag}[S_{ii}^L] + \mathbf{Diag}[S_{ii}^L]\dot{\mathbf{Q}}\mathbf{(N)}^T\mathbf{Q(N)}, \tag{4.16}$$

$$\dot{\mathbf{E}}^L = \mathbf{Q(N)}^T\dot{\mathbf{E}}\mathbf{Q(N)} = \mathbf{Diag}[\dot{E}_{ii}^L] + \mathbf{Q(N)}^T\dot{\mathbf{Q}}\mathbf{(N)Diag}[E_{ii}^L] + \mathbf{Diag}[E_{ii}^L]\dot{\mathbf{Q}}\mathbf{(N)}^T\mathbf{Q(N)}. \tag{4.17}$$

The spin of the Lagrangian triad is given by the antisymmetric spin tensor $\dot{\Omega}^{\mathrm{N}}$, defined as

$$\dot{\Omega}^{\mathrm{N}} = \dot{\mathbf{Q}}\mathbf{(N)Q(N)}^T, \tag{4.18}$$

while in relation to the Lagrangian triad,

$$\dot{\Omega}^{\mathrm{NL}} = \mathbf{Q(N)}^T\dot{\Omega}^{\mathrm{N}}\mathbf{Q(N)} = \mathbf{Q(N)}^T\dot{\mathbf{Q}}\mathbf{(N)}. \tag{4.19}$$

Using Equation (4.19), Equation (4.16) and (4.17) may be expressed

$$\dot{\mathbf{S}}^{L} = \mathbf{Q}(\mathbf{N})^{T}\dot{\mathbf{S}}\mathbf{Q}(\mathbf{N}) = \mathbf{Diag}[\dot{S}_{ii}^{L}] + \dot{\Omega}^{NL}\mathbf{Diag}[S_{ii}^{L}] - \mathbf{Diag}[S_{ii}^{L}]\,\dot{\Omega}^{NL}, \tag{4.20}$$

$$\dot{\mathbf{E}}^{L} = \mathbf{Q}(\mathbf{N})^{T}\dot{\mathbf{E}}\mathbf{Q}(\mathbf{N}) = \mathbf{Diag}[\dot{E}_{ii}^{L}] + \dot{\Omega}^{NL}\mathbf{Diag}[E_{ii}^{L}] - \mathbf{Diag}[E_{ii}^{L}]\,\dot{\Omega}^{NL}. \tag{4.21}$$

Expanding Equation (4.21) gives

$$\dot{\mathbf{E}}^{L} = \begin{bmatrix} \dot{E}_{11}^{L} & 0 & 0 \\ 0 & \dot{E}_{22}^{L} & 0 \\ 0 & 0 & \dot{E}_{33}^{L} \end{bmatrix} + \begin{bmatrix} 0 & \dot{\Omega}_{12}^{NL} & \dot{\Omega}_{13}^{NL} \\ \dot{\Omega}_{21}^{NL} & 0 & \dot{\Omega}_{23}^{NL} \\ \dot{\Omega}_{31}^{NL} & \dot{\Omega}_{32}^{NL} & 0 \end{bmatrix} \begin{bmatrix} E_{11}^{L} & 0 & 0 \\ 0 & E_{22}^{L} & 0 \\ 0 & 0 & E_{33}^{L} \end{bmatrix} - \begin{bmatrix} E_{11}^{L} & 0 & 0 \\ 0 & E_{22}^{L} & 0 \\ 0 & 0 & E_{33}^{L} \end{bmatrix} \begin{bmatrix} 0 & \dot{\Omega}_{12}^{NL} & \dot{\Omega}_{13}^{NL} \\ \dot{\Omega}_{21}^{NL} & 0 & \dot{\Omega}_{23}^{NL} \\ \dot{\Omega}_{31}^{NL} & \dot{\Omega}_{32}^{NL} & 0 \end{bmatrix} \tag{4.22}$$

where $\dot{\mathbf{\Omega}}_{ij}^{NL} = -\dot{\mathbf{\Omega}}_{ji}^{NL}$. It follows from Equation (4.22) that:

$$\dot{\mathbf{E}}^{L} = \begin{bmatrix} \dot{E}_{11}^{L} & (E_{22}^{L} - E_{11}^{L})\,\dot{\Omega}_{12}^{NL} & (E_{33}^{L} - E_{11}^{L})\,\dot{\Omega}_{13}^{NL} \\ (E_{22}^{L} - E_{11}^{L})\,\dot{\Omega}_{12}^{NL} & \dot{E}_{22}^{L} & (E_{33}^{L} - E_{22}^{L})\,\dot{\Omega}_{23}^{NL} \\ (E_{33}^{L} - E_{11}^{L})\,\dot{\Omega}_{13}^{NL} & (E_{33}^{L} - E_{22}^{L})\,\dot{\Omega}_{23}^{NL} & \dot{E}_{33}^{L} \end{bmatrix} \tag{4.23}$$

from which (provided $E_{ii}^{L} \neq E_{jj}^{L}$) $\dot{\mathbf{\Omega}}^{NL}$ may be expressed as

$$\dot{\mathbf{\Omega}}_{ij}^{NL} = \frac{\dot{E}_{ij}^{L}}{(E_{jj}^{L} - E_{ii}^{L})}. \tag{4.24}$$

Expanding Equation (4.20) for $\dot{\mathbf{S}}^{L}$, and substituting Equation (4.24) for the spin tensor $\dot{\mathbf{\Omega}}^{NL}$, yields

$$\dot{\mathbf{S}}^{L} = \begin{bmatrix} \dot{S}_{11}^{L} & \dfrac{(S_{22}^{L} - S_{11}^{L})}{(E_{22}^{L} - E_{11}^{L})}\dot{E}_{12}^{L} & \dfrac{(S_{33}^{L} - S_{11}^{L})}{(E_{33}^{L} - E_{11}^{L})}\dot{E}_{13}^{L} \\ \dfrac{(S_{22}^{L} - S_{11}^{L})}{(E_{22}^{L} - E_{11}^{L})}\dot{E}_{12}^{L} & \dot{S}_{22}^{L} & \dfrac{(S_{33}^{L} - S_{22}^{L})}{(E_{33}^{L} - E_{22}^{L})}\dot{E}_{23}^{L} \\ \dfrac{(S_{33}^{L} - S_{11}^{L})}{(E_{33}^{L} - E_{11}^{L})}\dot{E}_{13}^{L} & \dfrac{(S_{33}^{L} - S_{22}^{L})}{(E_{33}^{L} - E_{22}^{L})}\dot{E}_{23}^{L} & \dot{S}_{33}^{L} \end{bmatrix} \tag{4.25}$$

Considering first the diagonal terms in Equation (4.25), we can write

$$\begin{bmatrix} \dot{S}_{11}^{L} \\ \dot{S}_{22}^{L} \\ \dot{S}_{33}^{L} \end{bmatrix} = \begin{bmatrix} \dfrac{\partial S_{11}^{L}}{\partial E_{11}^{L}} & \dfrac{\partial S_{11}^{L}}{\partial E_{22}^{L}} & \dfrac{\partial S_{11}^{L}}{\partial E_{33}^{L}} \\ \dfrac{\partial S_{22}^{L}}{\partial E_{11}^{L}} & \dfrac{\partial S_{22}^{L}}{\partial E_{22}^{L}} & \dfrac{\partial S_{22}^{L}}{\partial E_{33}^{L}} \\ \dfrac{\partial S_{33}^{L}}{\partial E_{11}^{L}} & \dfrac{\partial S_{33}^{L}}{\partial E_{22}} & \dfrac{\partial S_{33}^{L}}{\partial E_{33}^{L}} \end{bmatrix} \begin{bmatrix} \dot{E}_{11}^{L} \\ \dot{E}_{22}^{L} \\ \dot{E}_{33}^{L} \end{bmatrix} \tag{4.26}$$

where the terms such as $\partial S_{11}^L / \partial E_{11}^L$ come from the differentiation of Equation (4.10) in conjunction with the relationship $E_{ii}^L = \frac{1}{2}(\lambda_i^2 - 1)$. For the off-diagonal shear components, we have:

$$\begin{bmatrix} \dot{S}_{12}^L \\ \dot{S}_{13}^L \\ \dot{S}_{23}^L \end{bmatrix} = \begin{bmatrix} \dfrac{(S_{11}^L - S_{22}^L)}{(E_{11}^L - E_{22}^L)} & 0 & 0 \\ 0 & \dfrac{(S_{11}^L - S_{33}^L)}{(E_{11}^L - E_{33}^L)} & 0 \\ 0 & 0 & \dfrac{(S_{22}^L - S_{33}^L)}{(E_{22}^L - E_{33}^L)} \end{bmatrix} \begin{bmatrix} \dot{E}_{12}^L \\ \dot{E}_{13}^L \\ \dot{E}_{23}^L \end{bmatrix} \tag{4.27}$$

The stiffness terms in Equation (4.27) are due to the change of direction of the principal axes. For the special case $E_{ii}^L = E_{jj}^L$, Equation (4.27) cannot be employed since it yields an undetermined expression. However following the approach of Reese and Wriggers (1995), L'Hopital's rule may be used to derive the limit value

$$\lim_{E_{ii}^L \to E_{jj}^L} \left(\frac{(S_{ii}^L - S_{jj}^L)}{(E_{ii}^L - E_{jj}^L)} \right) = \frac{\partial S_{ii}^L}{\partial E_{ii}^L} - \frac{\partial S_{jj}^L}{\partial E_{ii}^L}. \tag{4.28}$$

Equations (4.26), (4.27) and (4.28) permit the definition of the tangential constitutive matrix or tensor in Lagrangian triad such that:

$$\dot{S}_{ij}^L = D_{ijkl}^{K2L} \dot{E}_{kl}^L \tag{4.29}$$

The constitutive tensor in the Lagrangian triad D_{ijkl}^{K2L} may then be transformed back to the axial directions of the material coordinate frame using a standard tensor transformation as follows:

$$D_{ijkl}^{K2} = Q_{ia} Q_{jb} Q_{kc} Q_{ld} D_{abcd}^{K2L} \tag{4.30}$$

where the Q terms are the components from $\mathbf{Q}(\mathbf{N})$. If all the principal Green strains coincide $E_{11}^L = E_{22}^L = E_{33}^L$, we have

$$\frac{\partial S_{11}}{\partial E_{11}} = \frac{\partial S_{22}}{\partial E_{22}} = \frac{\partial S_{33}}{\partial E_{33}} = A \tag{4.31}$$

and

$$\frac{\partial S_{11}}{\partial E_{22}} = \frac{\partial S_{11}}{\partial E_{33}} = \frac{\partial S_{22}}{\partial E_{33}} = \frac{\partial S_{22}}{\partial E_{11}} = \frac{\partial S_{33}}{\partial E_{11}} = \frac{\partial S_{33}}{\partial E_{22}} = B. \tag{4.32}$$

Thus Equation (4.26) becomes

$$\begin{bmatrix} \dot{S}_{11} \\ \dot{S}_{22} \\ \dot{S}_{33} \end{bmatrix} = \begin{bmatrix} A & B & B \\ B & A & B \\ B & B & A \end{bmatrix} \begin{bmatrix} \dot{E}_{11} \\ \dot{E}_{22} \\ \dot{E}_{33} \end{bmatrix} \tag{4.33}$$

while Equation (4.27) may be expressed as

$$\begin{bmatrix} \dot{S}_{12} \\ \dot{S}_{13} \\ \dot{S}_{23} \end{bmatrix} = \begin{bmatrix} (A-B) & 0 & 0 \\ 0 & (A-B) & 0 \\ 0 & 0 & (A-B) \end{bmatrix} \begin{bmatrix} \dot{E}_{12} \\ \dot{E}_{13} \\ \dot{E}_{23} \end{bmatrix} \tag{4.34}$$

the subscript L for 'Lagrangian' has been dropped from Equations (4.33) and (4.34) because the same tangential properties now apply with respect to any orthogonal set of axes. Equations (4.33) and (4.34) can be re-expressed as

$$\dot{S}_{ij} = B\dot{E}_{kk}\delta_{ij} + (A-B)\dot{E}_{ij} \tag{4.35}$$

so that, allowing for the symmetry of $\dot{E}_{ij}$

$$D^{K2}_{ijkl} = B\delta_{ij}\delta_{kl} + \frac{(A-B)}{2}(\delta_{ik}\delta_{jl} + \delta_{il}\delta_{jk}) \tag{4.36}$$

Before moving on to consider the equivalent relationships with respect to the Eulerian triad, it is worth summarising those defined with respect to the Lagrangian triad. Provided all the principal stretch ratios (or Green strains) are distinct, the only non-zero components of $\mathscr{D}^{K2L}$ are from Equations (4.26) and (4.27):

$$D^{K2L}_{iijj} = \frac{\partial S^L_{ii}}{\partial E^L_{jj}} = \frac{1}{\lambda_j}\frac{\partial S^L_{ii}}{\partial \lambda_j} \tag{4.37}$$

$$D^{K2L}_{ijij} = D^{K2L}_{ijji} = D^{K2L}_{jiij} = D^{K2L}_{jiji} = \frac{S^L_{ii} - S^L_{jj}}{2(E^L_{ii} - E^L_{jj})} = \frac{S^L_{ii} - S^L_{jj}}{(\lambda_i^2 - \lambda_j^2)} \qquad i \neq j \tag{4.38}$$

If $E^L_{ii} = E^L_{jj}$ and (and $S^L_{ii} = S^L_{jj}$), from Equation (4.28), Equation (4.38) is replaced by

$$D^{K2L}_{ijij} = D^{K2L}_{ijji} = D^{K2L}_{jiij} = D^{K2L}_{jiji} = \frac{1}{2}\left(\frac{\partial S^L_{ii}}{\partial E^L_{ii}} - \frac{\partial S^L_{jj}}{\partial E^L_{ii}}\right) = \frac{1}{2\lambda_i}\left(\frac{\partial S_{ii}}{\partial \lambda_i} - \frac{\partial S_{jj}}{\partial \lambda_i}\right) \quad i \neq j \tag{4.39}$$

If we wish to derive the equivalent constitutive relationship with respect to the spatial configuration, we can simply use Equation (2.52) to transform the material constitutive tensor on the left hand side of Equation (4.30) so as to involve the Truesdell rate of Kirchhoff stress. However, following Chadwick and Ogden (1971a,b) it is simpler to work from the material tensor in the Lagrangian triad (as in Equation (4.29)) and initially obtain the equivalent spatial constitutive tensor in relation to the Eulerian triad. To this end we can write

$$d\mathbf{x} = \mathbf{Q}(\mathbf{n})\, d\mathbf{x}^E; \qquad d\mathbf{X} = \mathbf{Q}(\mathbf{N})\, d\mathbf{X}^L \tag{4.40}$$

so that $d\mathbf{x}$ can be expressed in terms of its components $d\mathbf{x}^E$ with respect to the Eulerian triad while $d\mathbf{X}$ can be expressed in terms of its components $d\mathbf{X}^L$ with respect to the Lagrangian frame. Substitution from Equation (4.40) into the relationship $d\mathbf{x} = \mathbf{F} d\mathbf{X}$ then leads to

$$d\mathbf{x}^E = \mathbf{Q}(\mathbf{n})^T \mathbf{F}\, \mathbf{Q}(\mathbf{N}) d\mathbf{X}^L = \mathbf{Diag}[\lambda] d\mathbf{X}^L = \hat{\mathbf{F}}\, d\mathbf{X}^L \tag{4.41}$$

where

$$\hat{\mathbf{F}} = \lambda_i \delta_{ij} \tag{4.42}$$

which gives the expected result that $dx^E_i = \lambda_i\, dX^L_i$. In moving from the second to the third expression in Equation (4.41), the following relationship has been used

$$\mathbf{Q}(\mathbf{n})\mathbf{F}\mathbf{Q}(\mathbf{N}) = \mathbf{Diag}[\lambda] \tag{4.43}$$

With respect to the Lagrangian and Eulerian coordinate systems, Equation (2.52) can now be directly applied using $\hat{\mathbf{F}}$ instead of $\mathbf{F}$. This leads to the transformation:

$$D_{ijkl}^{TKE} = \lambda_i \lambda_j \lambda_k \lambda_l \, D_{ijkl}^{K2L} \tag{4.44}$$

In addition the relationship $\boldsymbol{\tau} = \mathbf{F}\mathbf{S}\mathbf{F}^T$ gives:

$$S_{ii}^{L} = \frac{1}{\lambda_i^2} \tau_{ii}^{E} \tag{4.45}$$

so that:

$$\frac{\partial S_{ii}^{L}}{\partial \lambda_j} = \frac{1}{\lambda_i^2} \frac{\partial \tau_{ii}^{E}}{\partial \lambda_j} - \frac{2}{\lambda_i^3} \frac{\partial \lambda_i}{\partial \lambda_j} \tau_{ii}^{E} = \frac{1}{\lambda_i^2} \frac{\partial \tau_{ii}^{E}}{\partial \lambda_j} - \frac{2}{\lambda_i^3} \tau_{ii}^{E} \delta_{ij} \tag{4.46}$$

Substitution from Equation (4.44)-(4.46) into Equation (4.37)-(4.39) gives the non-zero components of $\mathscr{D}^{TKE}$ as

$$D_{iijj}^{TKE} = \lambda_j \frac{\partial \tau_{ii}^{E}}{\partial \lambda_j} - 2\tau_{ii}^{E} \delta_{ij} \tag{4.47}$$

$$D_{ijij}^{TLE} = D_{ijji}^{TKE} = D_{jiij}^{TKE} = D_{jiji}^{TKE} = \frac{\lambda_j^2 \tau_{ii}^{E} - \lambda_i^2 \tau_{jj}^{E}}{\lambda_i^2 - \lambda_j^2} \qquad i \neq j \tag{4.48}$$

If $\lambda_i = \lambda_j$ and ($\tau_{ii}^{E} = \tau_{jj}^{E}$), we have:

$$D_{ijij}^{TKE} = D_{ijji}^{TKE} = D_{jiij}^{TKE} = D_{jiji}^{TKE} = \frac{\lambda_i}{2} \frac{\partial \tau_{ii}^{E}}{\partial \lambda_i} - \tau_i^{E} - \frac{\lambda_i}{2} \frac{\partial \tau_{jj}^{E}}{\partial \lambda_i} \qquad i \neq j \tag{4.49}$$

The constitutive tensor in the Eulerian triad may then be transformed back to the axial directions of the spatial coordinate frame using a standard tensor transformation as follows:

$$D_{ijkl}^{TK} = Q_{ia} Q_{jb} Q_{kc} Q_{ld} \, D_{abcd}^{TKE} \tag{4.50}$$

where the Q terms are the components from $\mathbf{Q}(\mathbf{n})$. If all three principal stretch ratios coincide, we can directly compute $\mathscr{D}^{TK}$ from the equivalent of Equation (4.36) whereby:

$$D_{ijkl}^{TK} = B\delta_{ij}\delta_{kl} + \frac{(A-B)}{2}(\delta_{ik}\delta_{jl} + \delta_{il}\delta_{jl}) \tag{4.51}$$

Although in place of Equation (4.31) and (4.32) we now have

$$\lambda_1 \frac{\partial \tau_{11}}{\partial \lambda_1} - 2\tau_{11} = \lambda_2 \frac{\partial \tau_{22}}{\partial \lambda_2} - 2\tau_{22} = \lambda_3 \frac{\partial \tau_{33}}{\partial \lambda_3} - 2\tau_{33} = A \tag{4.52}$$

$$\lambda_2 \frac{\partial \tau_{11}}{\partial \lambda_2} = \lambda_3 \frac{\partial \tau_{11}}{\partial \lambda_3} = \lambda_3 \frac{\partial \tau_{22}}{\partial \lambda_3} = \lambda_1 \frac{\partial \tau_{22}}{\partial \lambda_1} = \lambda_1 \frac{\partial \tau_{33}}{\partial \lambda_1} = \lambda_2 \frac{\partial \tau_{33}}{\partial \lambda_2} = B \tag{4.53}$$

the superscript E for 'Eulerian' has been dropped from Equation (4.51) because the same tangential properties now apply with respect to any orthogonal set of axes.

4.4 Modelling Homogeneous Deformations

Closed-form solutions for boundary value problems involving homogeneous deformation are available for both the 3 and 8 chain models. These solutions are valuable as they provide a means to confirm accurately the response of the UMAT routines developed for the 3 and 8 chain models.

In common with the closed-form solutions presented for other hyperelastic models the assumption of material incompressibility is made. For the homogeneous deformation states examined in this chapter, namely uniaxial extension, equi-biaxial extension and pure shear, the volumetric strain observed in rubber-like solids is negligible. Therefore the assumption of material incompressibility brings simplicity to the theoretical treatment without sacrificing much in the way of accuracy. Substituting Equation (4.11) into Equation (4.45) and noting that $J = \det \mathbf{F} = 1$, the principal Cauchy stresses $\sigma_{11}^{E}, \sigma_{22}^{E}$ and σ_{33}^{E} for the incompressible forms of 3 and 8 chain models may be expressed as

$$\sigma_{ii}^{E} = \lambda_i \frac{\partial W}{\partial \lambda_i} - p \tag{4.54}$$

where p is the hydrostatic pressure (positive for compression) introduced because of the incompressibility constraint. The principal Cauchy stresses for the incompressible form of 3 chain model may be calculated from Equation (3.54) using Equation (4.54), to give

$$\sigma_{ii}^{E} = \frac{\mu\sqrt{n}}{3}\lambda_i \mathcal{L}^{-1}\left(\frac{\lambda_i}{\sqrt{n}}\right) - p\,. \tag{4.55}$$

The principal stresses for the incompressible form of 8 chain model can be calculated likewise from Equation (3.59), giving

$$\sigma_{ii}^{E} = \frac{\mu\sqrt{n}}{3}\frac{\lambda_i^2}{\lambda_{chain}}\mathcal{L}^{-1}\left(\frac{\lambda_{chain}}{\sqrt{n}}\right) - p\,. \tag{4.56}$$

The incompressibility constraint introduces the relation $\lambda_1\lambda_2\lambda_3 = 1$. In certain boundary value problems this relation may be exploited to eliminate the arbitrary hydrostatic pressure from Equations (4.55) and (4.56). This point will be demonstrated next with the development of stress-strain relations for the 3 and 8 chain models for the homogeneous deformation states of uniaxial extension, equi-biaxial extension and pure shear.

4.4.1 Homogenous Uniaxial Extension

Let $\lambda_1 = \lambda$ be the stretch ratio in the direction of extension, and $\sigma_{11} = \sigma$ be the corresponding principal Cauchy stress. The other two principal stresses are zero since no lateral forces are applied. By virtue of the incompressibility constraint, $\lambda_2 = \lambda_3 = \lambda^{-\frac{1}{2}}$. The independent stress-strain relations for the 3 chain model, from Equation (4.55), are then

$$\sigma = \frac{\mu\sqrt{n}}{3}\lambda \mathcal{L}^{-1}\left(\frac{\lambda}{\sqrt{n}}\right) - p \quad \text{and} \quad 0 = \frac{\mu\sqrt{n}}{3}\lambda^{-\frac{1}{2}}\mathcal{L}^{-1}\left(\frac{\lambda^{-\frac{1}{2}}}{\sqrt{n}}\right) - p\,. \tag{4.57}$$

Elimination of p yields

$$\sigma_{3chain}^{uni} = \frac{\mu\sqrt{n}}{3}\left\{\lambda\mathcal{L}^{-1}\left(\frac{\lambda}{\sqrt{n}}\right) - \lambda^{-\frac{1}{2}}\mathcal{L}^{-1}\left(\frac{\lambda^{-\frac{1}{2}}}{\sqrt{n}}\right)\right\}, \tag{4.58}$$

where the subscript in the above relation indicates the particular network model and the superscript the particular deformation state. Measurements in such tension tests are usually made in terms of force per unit unstrained area of cross section. This force is given by

$$f_{3chain}^{uni} = \frac{\sigma_{3chain}^{uni}}{\lambda} = \frac{\mu\sqrt{n}}{3}\left\{\mathcal{L}^{-1}\left(\frac{\lambda}{\sqrt{n}}\right) - \lambda^{-\frac{3}{2}}\mathcal{L}^{-1}\left(\frac{\lambda^{-\frac{1}{2}}}{\sqrt{n}}\right)\right\}. \tag{4.59}$$

The independent stress-strain relations for the 8 chain model, from Equation (4.56), may be calculated in a similar fashion, giving

$$\sigma = \frac{\mu\sqrt{n}}{3}\frac{\lambda^2}{\lambda_{chain}^{uni}}\mathcal{L}^{-1}\left(\frac{\lambda_{chain}^{uni}}{\sqrt{n}}\right) - p \quad \text{and} \quad 0 = \frac{\mu\sqrt{n}}{3}\frac{1}{\lambda\lambda_{chain}^{uni}}\mathcal{L}^{-1}\left(\frac{\lambda_{chain}^{uni}}{\sqrt{n}}\right) - p. \tag{4.60}$$

Elimination of p yields

$$\sigma_{8chain}^{uni} = \frac{\mu\sqrt{n}}{3\lambda_{chain}^{uni}}\left\{\lambda^2\mathcal{L}^{-1}\left(\frac{\lambda_{chain}^{uni}}{\sqrt{n}}\right) - \frac{1}{\lambda}\mathcal{L}^{-1}\left(\frac{\lambda_{chain}^{uni}}{\sqrt{n}}\right)\right\}. \tag{4.61}$$

The stress per unit volume unstrained area is calculated as before, giving

$$f_{8chain}^{uni} = \frac{\sigma_{8chain}^{uni}}{\lambda} = \frac{\mu\sqrt{n}}{3\lambda_{chain}^{uni}}\left\{\lambda\mathcal{L}^{-1}\left(\frac{\lambda_{chain}^{uni}}{\sqrt{n}}\right) - \frac{1}{\lambda^2}\mathcal{L}^{-1}\left(\frac{\lambda_{chain}^{uni}}{\sqrt{n}}\right)\right\}. \tag{4.62}$$

where from the incompressibility constraint λ_{chain}^{uni} in the above equations is given by

$$\lambda_{chain}^{uni} = \frac{\sqrt{\lambda^2 + 2/\lambda}}{\sqrt{3}} \tag{4.63}$$

4.4.2 Homogeneous Equi-biaxial Extension

In equi-biaxial tension two of the principal stresses are equal $\sigma_{22} = \sigma_{33} = \sigma$ say, while the third is zero. Correspondingly the principal stretches are written $\lambda_2 = \lambda_3 = \lambda$ and $\lambda_1 = \lambda^{-2}$. Elimination of p from the two remaining independent stresses in Equation (4.55) for the 3 chain model, yields

$$\sigma_{3chain}^{bi} = \frac{\mu\sqrt{n}}{3}\left\{\lambda\mathcal{L}^{-1}\left(\frac{\lambda}{\sqrt{n}}\right) - \frac{1}{\lambda^2}\mathcal{L}^{-1}\left(\frac{\lambda^{-2}}{\sqrt{n}}\right)\right\}. \tag{4.64}$$

Equation (4.64) may be rewritten in terms of force per unit unstrained area, as

$$f_{3chain}^{bi} = \frac{\sigma_{3chain}^{bi}}{\lambda} = \frac{\mu\sqrt{n}}{3}\left\{\mathcal{L}^{-1}\left(\frac{\lambda}{\sqrt{n}}\right) - \frac{1}{\lambda^3}\mathcal{L}^{-1}\left(\frac{\lambda^{-2}}{\sqrt{n}}\right)\right\}. \tag{4.65}$$

Elimination of p from the independent stresses in Equation (4.56) for the 8 chain model, yields

$$\sigma_{8chain}^{bi} = \frac{\mu\sqrt{n}}{3\lambda_{chain}^{bi}}\left\{\lambda^2\mathcal{L}^{-1}\left(\frac{\lambda_{chain}^{bi}}{\sqrt{n}}\right) - \frac{1}{\lambda^4}\mathcal{L}^{-1}\left(\frac{\lambda_{chain}^{bi}}{\sqrt{n}}\right)\right\}. \tag{4.66}$$

The relationship above may be expressed in terms of force per unit unstrained area, as

$$f_{8chain}^{bi} = \frac{\sigma_{8chain}^{bi}}{\lambda} = \frac{\mu\sqrt{n}}{3\lambda_{chain}^{bi}}\left\{\lambda\mathcal{L}^{-1}\left(\frac{\lambda_{chain}^{bi}}{\sqrt{n}}\right) - \frac{1}{\lambda^5}\mathcal{L}^{-1}\left(\frac{\lambda_{chain}^{bi}}{\sqrt{n}}\right)\right\}. \tag{4.67}$$

where from the incompressibility constraint λ_{chain}^{bi} in the equations above is given by

$$\lambda_{chain}^{bi} = \frac{\sqrt{2\lambda^2 + 1/\lambda^4}}{\sqrt{3}} \tag{4.68}$$

4.4.3 Homogeneous Pure Shear

In pure shear one of the principal stretches is held fixed, say $\lambda_2 = 1$. Setting $\lambda_1 = \lambda$ and $\lambda_3 = \lambda^{-1}$ the stress-strain relations for the 3 chain model reduce to

$$\sigma_{11} = \frac{\mu\sqrt{n}}{3}\lambda\mathcal{L}^{-1}\left(\frac{\lambda}{\sqrt{n}}\right) - p\,,\ \sigma_{22} = \frac{\mu\sqrt{n}}{3}\mathcal{L}^{-1}\left(\frac{1}{\sqrt{n}}\right) - p \quad \text{and} \quad \sigma_{33} = \frac{\mu\sqrt{n}}{3}\lambda^{-1}\mathcal{L}^{-1}\left(\frac{\lambda^{-1}}{\sqrt{n}}\right) - p \tag{4.69}$$

We are only concerned with the force in the direction of extension here so the force f per unit unstained area of cross-section in this direction is given by

$$f_{3chain}^{shear} = \frac{\mu\sqrt{n}}{3}\left\{\mathcal{L}^{-1}\left(\frac{\lambda}{\sqrt{n}}\right) - \frac{1}{\lambda^2}\mathcal{L}^{-1}\left(\frac{\lambda^{-1}}{\sqrt{n}}\right)\right\}. \tag{4.70}$$

The force per unit unstained area of cross-section for the 8 chain model is calculated as above, and may be expressed as

$$f_{8chain}^{shear} = \frac{\mu\sqrt{n}}{3\lambda_{chain}^{shear}}\left\{\lambda\mathcal{L}^{-1}\left(\frac{\lambda_{chain}^{shear}}{\sqrt{n}}\right) - \frac{1}{\lambda^3}\mathcal{L}^{-1}\left(\frac{\lambda_{chain}^{shear}}{\sqrt{n}}\right)\right\}. \tag{4.71}$$

where from the incompressibility constraint λ_{chain}^{shear} in Equation (4.71) is given by

$$\lambda_{chain}^{shear} = \frac{\sqrt{\lambda^2 + 1 + 1/\lambda^2}}{\sqrt{3}} \tag{4.72}$$

The response of the 3 and 8 chain models in the homogeneous deformation states of uniaxial extension, equi-biaxial extension and pure shear given by Equations (4.58), (4.62), (4.65), (4.67), (4.70) and (4.71) will be compared with the results from the UMAT routines developed in the next section at the end of this chapter.

4.5 ABAQUS User Defined Material Interface

Hyperelastic models may be implemented into the commercial finite element package ABAQUS using either the UHYPER or UMAT facilities, see the ABAQUS theory manual (1996) for details. The UHYPER or user defined hyperelastic material facility requires the user to submit a FORTRAN subroutine to define the strain energy function and the first and second derivatives of the strain energy function with respect to the invariants (I_1, I_2 and J). For incompressible models, only the first and second derivatives of the strain energy function with respect to the I_1 and I_2 are required. However the UHYPER facility does not permit the specification of other important features of the constitutive behaviour of elastomeric materials e.g. strain softening and viscous effects, and it was therefore decided to employ the more general UMAT facility in the current work. When the UMAT or user defined material subroutine is called, it is provided with the material state at the start of the increment (stress, solution dependent state variables, and temperature), the increment in temperature and strain and the time increment. The subroutine must then update the stresses and solution dependent state variables to their values at the end of the increment and provide the Jacobian matrix for the constitutive model. In finite deformation problems, the Jacobian matrix should take the form of the tangent of Jaumann rate of Cauchy stress, so as to remain consistent with the finite element formulation employed by ABAQUS. The accuracy with which the Jacobian matrix is defined has a strong effect on the rate of convergence of the solution, and so has a major influence on the computational efficiency. In the approach developed by the author to implement the 3 and 8 chain network models into ABAQUS, the Jacobian matrix is evaluated exactly using a two step procedure. The tangent of the Truesdell rate of Kirchhoff stress is determined first using the principal axes technique, the tangent of the Jaumann rate of Cauchy stress is then obtained using Equations 2.56 and 2.62.

4.6 Modelling Non-Homogeneous Deformations

The aim now is to derive a set of exact constitutive relationships for 3 and 8 chain models, suitable for implementation into the FE package ABAQUS. Discussion is initially limited to the development of constitutive relationships for the analysis of plane stress problems, where the incompressibility constraint may be employed to

eliminate the arbitrary hydrostatic pressure, which arises in Equation (4.54). Later in the chapter consideration is given to the development of relations for the analysis of plain strain, axisymmetric and three-dimensional problems by the extension of the 3 and 8 chain models to include a degree of material compressibility.

4.6.1 Constitutive Equations (2-D plane stress formulation)

Consider first the development of relations compatible with the family of two-dimensional axisymmetric shell elements provided by ABAQUS. The principal Cauchy stresses for the incompressible form of the 3 chain network model given in Equation (4.55), may be expressed as

$$\sigma_{ii} = \frac{\mu\sqrt{n}}{3}\lambda_i \beta_i - p \ , \tag{4.73}$$

where β_i is given by

$$\beta_i = \mathcal{L}^{-1}\left(\frac{\lambda_i}{\sqrt{n}}\right). \tag{4.74}$$

The E superscript has been omitted from Equation (4.73), since for two-dimensional axisymmetric elements considered here the principal directions of stretch coincide with those of the natural coordinate system. For the plane stress condition $\sigma_{33} = 0$, so that

$$p = \frac{\mu\sqrt{n}}{3}\lambda_3 \beta_3 \tag{4.75}$$

Substituting Equation (4.75) into Equation (4.73) we obtain expressions for the principal stresses σ_{11} and σ_{22}, of the form

$$\sigma_{11} = \frac{\mu\sqrt{n}}{3}\{\lambda_1 \beta_1 - \lambda_3 \beta_3\} \quad , \quad \sigma_{22} = \frac{\mu\sqrt{n}}{3}\{\lambda_2 \beta_2 - \lambda_3 \beta_3\} \tag{4.76}$$

To eliminate λ_3 from the relations above, the incompressibility constraint $\lambda_1\lambda_2\lambda_3 = 1$ is used, yielding

$$\sigma_{11} = \frac{\mu\sqrt{n}}{3}\left\{\lambda_1\beta_1 - \frac{1}{\lambda_1\lambda_2}\beta_3\right\} \quad , \quad \sigma_{22} = \frac{\mu\sqrt{n}}{3}\left\{\lambda_2\beta_2 - \frac{1}{\lambda_1\lambda_2}\beta_3\right\} \tag{4.77}$$

where β_3 may be expressed as

$$\beta_3 = \mathcal{L}^{-1}\left(\frac{1}{\lambda_1\lambda_2\sqrt{n}}\right) \tag{4.78}$$

The only remaining problem is the computation of the appropriate Jacobian matrix for the 3 chain model. Using the principal axes technique outlined in section 4.3, and in particular Equation (4.47) the principal components of the tangent of the Truesdell rate may be expressed in matrix form as

$$\hat{D}^T_{11} = \frac{\mu\sqrt{n}}{3}\left\{\frac{\lambda_1^2}{\sqrt{n}}\beta_1' - \lambda_1\beta_1 + \frac{3}{\lambda_1\lambda_2}\beta_3 + \frac{1}{\lambda_1^2\lambda_2^2\sqrt{n}}\beta_3'\right\} \tag{4.79}$$

$$\hat{D}^T_{22} = \frac{\mu\sqrt{n}}{3}\left\{\frac{\lambda_2^2}{\sqrt{n}}\beta_2' - \lambda_2\beta_2 + \frac{3}{\lambda_1\lambda_2}\beta_3 + \frac{1}{\lambda_1^2\lambda_2^2\sqrt{n}}\beta_3'\right\} \tag{4.80}$$

$$\hat{D}^T_{12} = \hat{D}^T_{21} = \frac{\mu\sqrt{n}}{3}\left\{\frac{3}{\lambda_1\lambda_2}\beta_3 + \frac{1}{\lambda_1^2\lambda_2^2\sqrt{n}}\beta_3'\right\} \tag{4.81}$$

where β_i' in Equations (4.79)-(4.81) represents the derivative of the inverse Langevin function with respect to its argument. The E superscript has been omitted from Equations (4.79)-(4.81), since the principal directions do not change. The K superscript has also been omitted from Equations (4.79)-(4.81), since the distinction between the Kirchhoff and Cauchy stress tensors vanishes when J equals unity. The fourth order constitutive tensor $\mathscr{D}^J$, corresponding to the tangent of the Jaumann rate, is finally obtained using Equation (2.56), which can be expressed in matrix form as

$$\hat{\mathbf{D}}^J = \hat{\mathbf{D}}^T + \check{\boldsymbol{\sigma}} \tag{4.82}$$

In this two dimensional case, the matrix $\bar{\boldsymbol{\sigma}}$ is given by

$$\bar{\boldsymbol{\sigma}} = \begin{bmatrix} 2\sigma_{11} & 0 \\ 0 & 2\sigma_{22} \end{bmatrix} \tag{4.83}$$

The superscript C has been omitted from Equation (4.82), because of the equality of the Kirchhoff and Cauchy stresses when J equals unity.

The constitutive relations for the 8 chain network model may be derived using exactly the same procedure as that adopted for the 3 chain model. The principal Cauchy stresses for the incompressible form of the 8 chain network model given in Equation (4.56), may be expressed as

$$\sigma_{ii} = \frac{\mu\sqrt{n}}{3}\frac{\lambda_i^2}{\lambda_c}\beta_c - p \tag{4.84}$$

where β_c is given by

$$\beta_c = \mathcal{L}^{-1}\left(\frac{\lambda_c}{\sqrt{n}}\right) \tag{4.85}$$

and

$$\lambda_c = \frac{\sqrt{\lambda_1^2 + \lambda_2^2 + \lambda_3^2}}{\sqrt{3}} \tag{4.86}$$

For the plane stress condition $\sigma_{33} = 0$, the arbitrary hydrostatic pressure in Equation (4.84) may be expressed as

$$p = \frac{\mu\sqrt{n}}{3}\frac{\lambda_3^2}{\lambda_c}\beta_c \tag{4.87}$$

Substituting Equation (4.87) into Equation (4.84), we obtain expressions for the principal stresses σ_{11} and σ_{22}, of the form

$$\sigma_{11} = \frac{\mu\sqrt{n}}{3}\frac{\beta_c}{\lambda_c}\left\{\lambda_1^2 - \lambda_3^2\right\} \quad , \quad \sigma_{22} = \frac{\mu\sqrt{n}}{3}\frac{\beta_c}{\lambda_c}\left\{\lambda_2^2 - \lambda_3^2\right\} \tag{4.88}$$

Using the incompressibility constraint λ_3 is eliminated from the relations above, yielding

$$\sigma_{11} = \frac{\mu\sqrt{n}}{3}\frac{\beta_c}{\lambda_c}\left\{\lambda_1^2 - \frac{1}{\lambda_1^2\lambda_2^2}\right\} \quad , \quad \sigma_{22} = \frac{\mu\sqrt{n}}{3}\frac{\beta_c}{\lambda_c}\left\{\lambda_2^2 - \frac{1}{\lambda_1^2\lambda_2^2}\right\} \tag{4.89}$$

where β_c is given by Equation (4.85) and λ_{chain} may expressed as

$$\lambda_c = \frac{\sqrt{\lambda_1^2 + \lambda_2^2 + \lambda_1^{-2}\lambda_2^{-2}}}{\sqrt{3}} \tag{4.90}$$

The Jacobian matrix for the 8 chain model can be obtained in the same way as that for the 3 chain model. The principal components of the tangent of the Truesdell rate are derived from Equation (4.89) using Equation (4.47), to give

$$\hat{D}_{11}^T = \frac{\mu\sqrt{n}}{3}\left\{\left(\frac{2}{3\lambda_2^2\lambda_c^2} + \frac{4}{\lambda_1^2\lambda_2^2} - \frac{\lambda_1^4}{3\lambda_c^2} - \frac{1}{3\lambda_1^4\lambda_2^4\lambda_c^2}\right)\frac{\beta_c}{\lambda_c} + \left(\lambda_1^4 + \frac{1}{\lambda_1^4\lambda_2^4} - \frac{2}{\lambda_2^2}\right)\frac{\beta_c'}{3\lambda_c^2\sqrt{n}}\right\} \tag{4.91}$$

$$\hat{D}_{22}^T = \frac{\mu\sqrt{n}}{3}\left\{\left(\frac{2}{3\lambda_1^2\lambda_c^2} + \frac{4}{\lambda_1^2\lambda_2^2} - \frac{\lambda_2^4}{3\lambda_c^2} - \frac{1}{3\lambda_1^4\lambda_2^4\lambda_c^2}\right)\frac{\beta_c}{\lambda_c} + \left(\lambda_2^4 + \frac{1}{\lambda_1^4\lambda_2^4} - \frac{2}{\lambda_1^2}\right)\frac{\beta_c'}{3\lambda_c^2\sqrt{n}}\right\} \tag{4.92}$$

$$\hat{D}_{12}^T = \hat{D}_{21}^T = \frac{\mu\sqrt{n}}{3}\left\{\left(\frac{(\lambda_1^2+\lambda_2^2)}{3\lambda_1^2\lambda_2^2\lambda_c^2} + \frac{2}{\lambda_1^2\lambda_2^2} - \frac{\lambda_1^2\lambda_2^2}{3\lambda_c^2} - \frac{1}{3\lambda_1^4\lambda_2^4\lambda_c^2}\right)\frac{\beta_c}{\lambda_c} + \left(\lambda_1^2\lambda_2^2 + \frac{1}{\lambda_1^4\lambda_2^4} - \frac{(\lambda_1^2+\lambda_2^2)}{\lambda_1^2\lambda_2^2}\right)\frac{\beta_c'}{3\lambda_c^2\sqrt{n}}\right\} \tag{4.93}$$

where β_c' in Equations (4.91)-(4.93) represents the derivative of the inverse Langevin function with respect to its argument. The Jacobian matrix for the 8 chain model corresponding to the tangent of Jaumann rate is obtained as before using Equation (4.82). The constitutive relations developed in this section are compatible with the SAX family of axisymmetric shell elements provided by ABAQUS Version 5.6.

4.6.2 Constitutive Equations (general 2-D plane stress formulation)

In this section we develop constitutive formulations for the incompressible forms of the 3 and 8 chain network models compatible with general two-dimensional plane stress elements. This is an important step as axisymmetric shell elements are only suitable for the analysis of very limited types of problems. The principal Cauchy stresses for the 3 and 8 chain models are same as those given by Equations (4.77) and (4.88), except these stresses are now related to the principal directions $\mathbf{n}_1, \mathbf{n}_2$. The principal Cauchy stresses may be rotated to the axial directions of the spatial coordinate frame using a standard tensor transformation of the form

$$\boldsymbol{\sigma} = \mathbf{Q}(\mathbf{n})\mathbf{Diag}[\sigma_i^E]\mathbf{Q}^T(\mathbf{n}) \tag{4.95}$$

where $\mathbf{Q}(\mathbf{n})$ is the matrix containing the principal direction vectors of the Eulerian triad, i.e. $\mathbf{Q}(\mathbf{n}) = [\mathbf{n}_1, \mathbf{n}_2]$ and $\mathbf{Diag}[\sigma_i^E]$ is the diagonal matrix formed by the principal Cauchy stresses σ_{11}^E and σ_{22}^E. However for our purposes it is more convenient and computationally efficient to follow the approach of Cook *et al* (1989) and use matrix equivalent of Equation (4.95). Taking into account the symmetry of $\boldsymbol{\sigma}$ we introduce for $\boldsymbol{\sigma}$: $\hat{\sigma}_i = [\sigma_{11}, \sigma_{22}, \sigma_{12}]$ and $\hat{\sigma}_i^E = [\sigma_{11}^E, \sigma_{22}^E, 0]$, which leads to the transformation

$$\hat{\sigma}_i = \hat{P}_{ij}\hat{\sigma}_j^E \tag{4.96}$$

where $\hat{P}_{ij}$ is a projection matrix defined as

$$\hat{\mathbf{P}} = \begin{bmatrix} Q_{11}^2 & Q_{12}^2 & 2Q_{11}Q_{12} \\ Q_{21}^2 & Q_{22}^2 & 2Q_{21}Q_{22} \\ Q_{11}Q_{21} & Q_{12}Q_{22} & Q_{11}Q_{22} + Q_{12}Q_{21} \end{bmatrix} \tag{4.97}$$

the Q terms in Equation (4.97) are the components of $\mathbf{Q}(\mathbf{n})$. Note that the matrix $\hat{\mathbf{P}}$ is neither symmetric nor orthogonal. Within the UMAT routines which have been developed in this work the principal stretches and directions are obtained from the left hand Cauchy Green deformation tensor, $\mathbf{B}$, via Jacobi diagonalisation.

The only remaining problem is the computation of an appropriate Jacobian matrix. As before we start by calculating the tangent of the Truesdell rate using the principal axes technique. The fourth order constitutive tensor $\mathscr{D}^{TE}$, corresponding to the tangent of the Truesdell rate in the Eulerian triad, may be expressed in matrix form as

$$\hat{\mathbf{D}}^{TE} = \begin{bmatrix} \begin{bmatrix} \hat{D}_{11}^{TE} & \hat{D}_{12}^{TE} \\ \hat{D}_{21}^{TE} & \hat{D}_{22}^{TE} \end{bmatrix} & \begin{matrix} 0 \\ 0 \end{matrix} \\ \begin{matrix} 0 & 0 \end{matrix} & \hat{D}_{33}^{TE} \end{bmatrix} \tag{4.98}$$

where the shear component $\hat{D}_{33}^{TE}$ is obtained from isotropy. Note that the sub matrix shown in Equation (4.98) is the same as that obtained for the 3 and 8 chain models in the previous section. The fourth order constitutive tensor $\mathscr{D}^{TE}$ may be rotated to the base coordinate frame using a standard tensor transformation of the form

$$D_{ijkl}^{T} = Q_{ia} Q_{jb} Q_{kc} Q_{ld} D_{abcd}^{TE} \tag{4.99}$$

where the Q terms in Equation (4.99) are the components of $\mathbf{Q}(\mathbf{n})$. However following the approach of Cook *et al* (1989) it is again more efficient and convenient to and employ the transformation

$$\hat{D}_{ij}^{T} = P_{ik} \hat{D}_{kl}^{TE} \hat{P}_{jl}, \tag{4.100}$$

where here we use the same transformation matrix as that used in calculation the components of the Cauchy stress tensor in Equation (4.96). To overcome the problem that occurs in the calculation of $\hat{D}_{33}^{TE}$ from Equation (4.98), when $\lambda_1 = \lambda_2$, the limit value given by Equation (4.49) is applied instead, this yields

$$\hat{D}_{33}^{TE} = \frac{\lambda_1}{2} \frac{\partial \sigma_{11}^{E}}{\partial \lambda_1} - \sigma_1^{E} - \frac{\lambda_1}{2} \frac{\partial \sigma_{22}^{E}}{\partial \lambda_1} = \frac{1}{2} \left(\hat{D}_{11}^{TE} - \hat{D}_{21}^{TE} \right) \tag{4.101}$$

The Jacobian matrix corresponding to the tangent of the Jaumann rate is obtained as before using Equation (2.57), and expressed in matrix form as

$$\hat{\mathbf{D}}^{J} = \hat{\mathbf{D}}^{T} + \breve{\boldsymbol{\sigma}} . \tag{4.102}$$

In two dimensions the matrix $\breve{\boldsymbol{\sigma}}$ is given by

$$\breve{\boldsymbol{\sigma}} = \begin{bmatrix} 2\sigma_{11} & 0 & \sigma_{12} \\ 0 & 2\sigma_{22} & \sigma_{21} \\ \sigma_{21} & \sigma_{12} & \dot{\sigma}_{12} \end{bmatrix} \tag{4.103}$$

where $\dot{\sigma}_{12} = (\sigma_{11} + \sigma_{22})/2$. The constitutive relations developed in this section are compatible with the CPS family of plane stress elements provided by ABAQUS Version 5.6.

4.7 Numerical Tests

Some examples will now be given to demonstrate the accuracy and effectiveness of the constitutive formulations developed for the 3 and 8 chain network models. The FE calculations were performed using ABAQUS (version 5.6) on a UNIX based Digital Alpha Station 200. The material constants employed for the 3 and 8 chain models come from a least squares fit to the uniaxial of Treloar (1944). The shear modulus for both models is $\mu = 0.27\,\text{MPa}$, the number of rigid links for the 3 chain model is $n = 80$, while that for the 8 chain model is $n = 26.5$.

4.7.1 Homogeneous Deformation Tests

In this set of tests the accuracy of the constitutive formulations for the 3 and 8 chain network models is examined in the homogeneous deformation states of uniaxial extension, equi-biaxial extension and pure shear. Tests were performed using a single CPS4 continuum plane stress element, and the results compared with the analytical solutions presented in section 4.4. Comparison of the FE and analytical solutions shows them to be in exact agreement. Figures 4.1 to 4.6 depict these results.

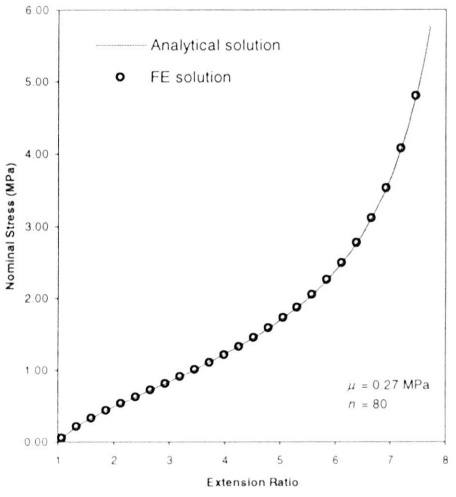


Figure 4.1 : Uniaxial response, 3 Chain Model.

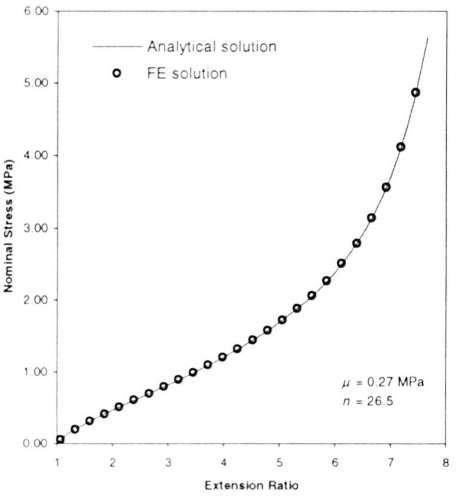


Figure 4.2 : Uniaxial response, 8 Chain Model.

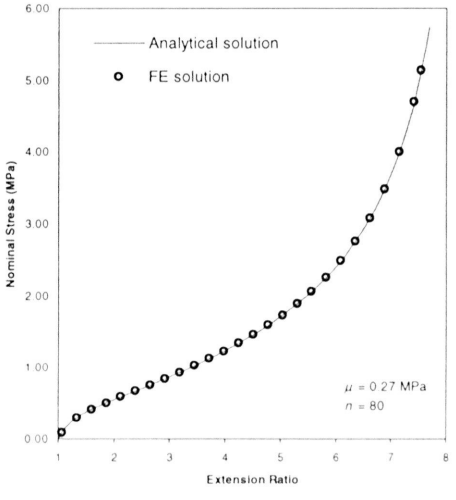


Figure 4.3 : Equi-biaxial response, 3 Chain Model.

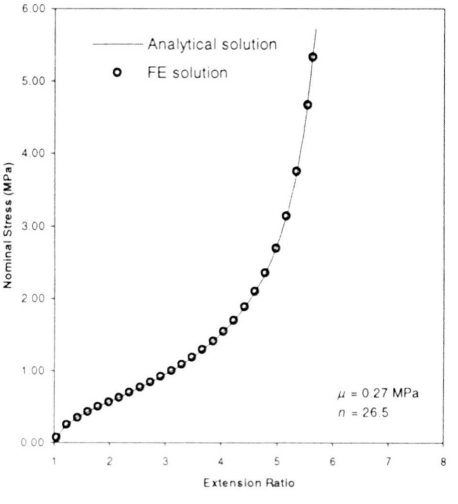


Figure 4.4 : Equi-biaxial response, 8 Chain Model.

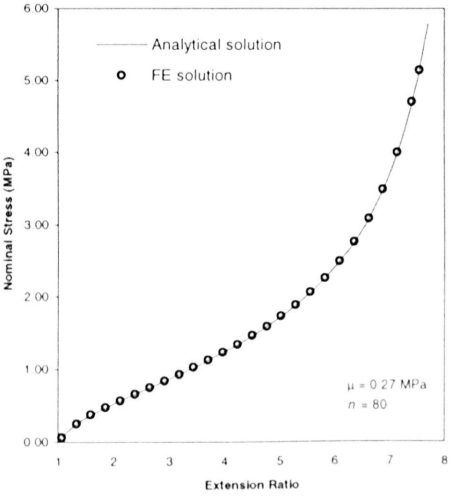


Figure 4.5 : Pure shear response, 3 Chain Model.

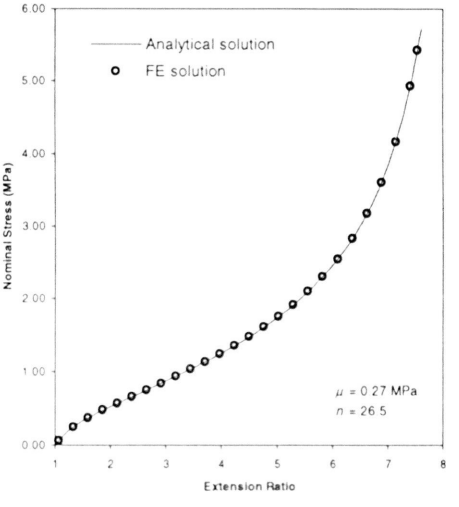


Figure 4.6 : Pure shear response, 8 Chain Model.

4.7.2 Stretching of a square sheet with a central circular hole

This example illustrates the stretching of square sheet with a circular hole. The same problem has been studied by Miehe (1995). The length of the square is $2L = 20\,\text{mm}$, the radius of the central hole is $r = 3\,\text{mm}$ and the thickness of the sheet is $t = 0.1\,\text{mm}$. The sheet is stretched in one direction, while the width is kept constant. One quarter of the sheet is modelled using 1000 CPS3 continuum plane stress elements. The material constants for the 3 and 8 chain networks models come from the experimental data of Treloar and are given at the beginning of this section. The response of the 3 and 8 chain models are also compared with the predictions of the Mooney-Rivlin and Ogden models (also fitted to the Treloar's experimental data), both of which are supplied as standard with ABAQUS. The material constants employed with the Mooney-Rivlin model, $C_1 = 0.1151\,\text{MPa}$ and $C_2 = 0.1013\,\text{MPa}$, are taken from Gent (1992), while those for Ogden model come from Ogden (1972a). The material constants chosen by Ogden are given in columns 2 and 4 of Table 4.1. However, because of the formulation of the Ogden model in ABAQUS, the moduli supplied in the input file, μ_r', take the form $\mu_r' = (\mu_r \alpha_r)/2$. The material constants for the Ogden model in ABAQUS are given in columns 3 and 4 of Table 4.1, for convenience the moduli are given in terms of MPa. Figure 4.7 shows the applied load (force) plotted against the edge displacement. The original and deformed meshes are shown in Figures 4.8-4.11.

r	μ_r (kg/cm^2)	μ_r (MPa)	μ_r' (MPa)	α_r
1	6.3	0.61803	0.40172	1.3
2	0.012	0.001177	0.00294	5.0
3	-0.1	-0.00981	0.00981	-2.0

Table 4.1 : Material properties for Ogden model, Treloar's experimental data.

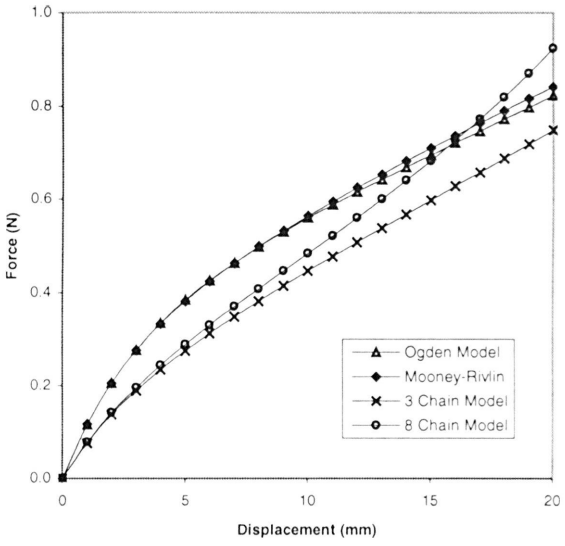


Figure 4.7 : Sheet with circular hole – force versus displacement.

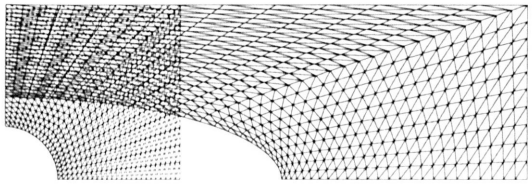


Figure 4.8 : Original and deformed meshes, 3 chain model.

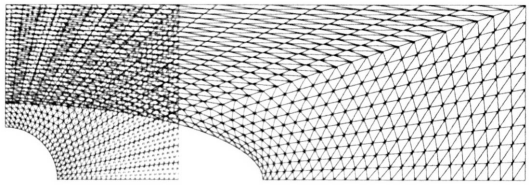


Figure 4.9 : Original and deformed meshes, 8 chain model.

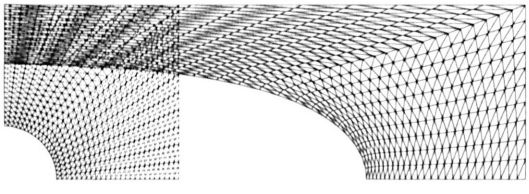


Figure 4.10 : Original and deformed meshes, M-R model.

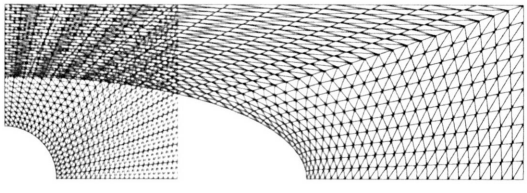


Figure 4.11 : Original and deformed meshes, Ogden model.

4.7.3 Inflation of a balloon

The inflation of a rubber balloon by an internal pressure is considered next. This problem has been widely studied and solutions can be found in the work of Needleman (1977), Wriggers and Taylor (1990) and Gruttmann and Taylor (1992). The balloon has an initial radius of R=30mm and a thickness of t=0.6 mm. The problem is axisymmetric and is modelled using ten SAX1 axisymmetric shell elements, representing one half of the sphere. The material constants employed in the analysis again come from the experimental data of Treloar (1944), and may be found in the section 4.7.2. The results of analysis can be represented by plots of the internal pressure against stretch, Figure 4.12. This problem also exhibits a snap-through, to pass the limit point an arc-length procedure is used in conjunction with the Newton-Raphson method to determine the complete solution path.

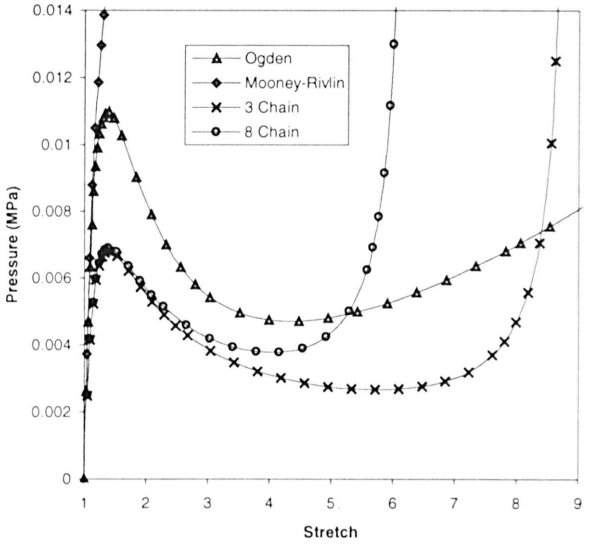


Figure 4.12 : Rubber balloon – pressure versus stretch.

4.7.4 Inflation of a shallow spherical cap

Now the inflation of a spherical cap is considered, Figure 4.13. This example has also been studied by Wriggers and Taylor (1990) and Gruttmann and Taylor (1992). The initial radius of the cap is R=10mm and the thickness is t=0.1mm. The cap is loaded normal to the current configuration by a uniform pressure. Twenty axisymmetric shell elements of the type SAX1 are used to model the cap. Since the maximum extension is expected to be at the centre of the cap, the length of the elements in the radial direction decreases from the circumference to the centre. As before we use material constants based on the experimental data of Treloar (1944). This example also requires the use of an arc-length procedure. Curves of the internal pressure against the mid surface displacement are given in Figure 4.14. Plots of the original meshes and deformed meshes for each model are given in Figures 4.15-4.18.

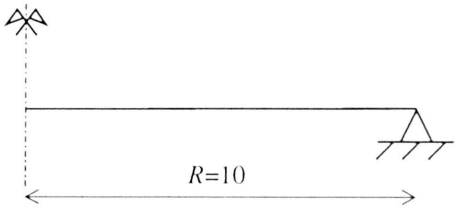


Figure 4.13 : Inflation of shallow spherical cap.

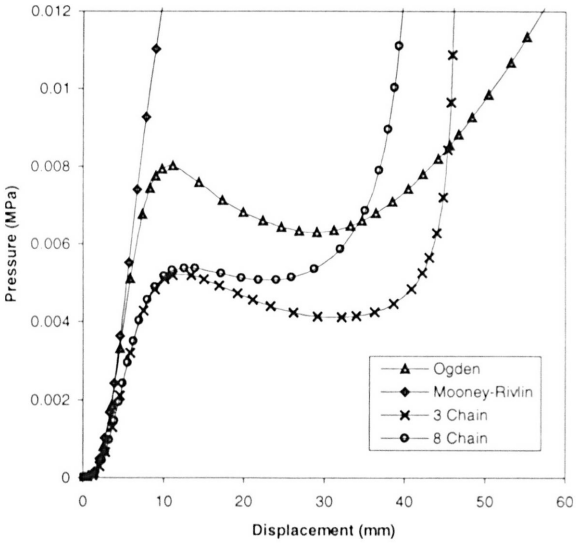


Figure 4.14 : Shallow spherical cap. Pressure versus displacement of the centre point.

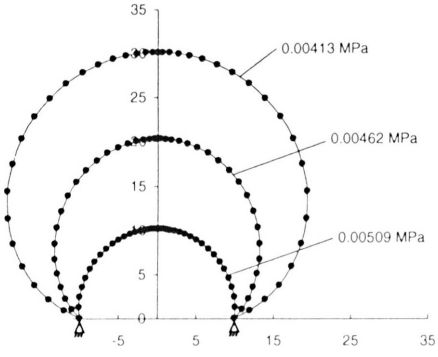


Figure 4.15 : Deformed configurations, 3 Chain model.

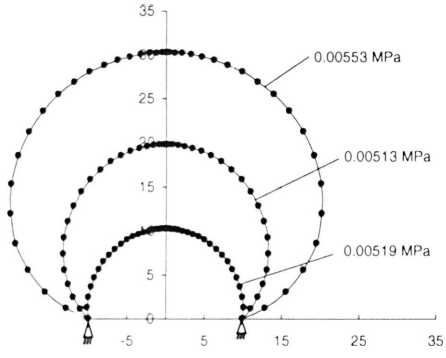


Figure 4.16 : Deformed configurations, 8 Chain model.

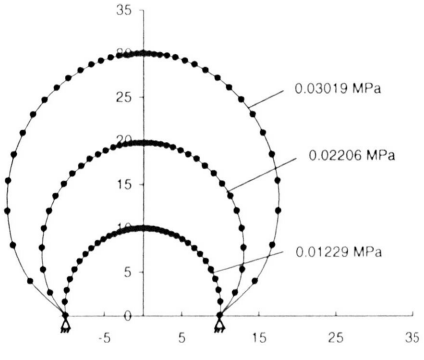


Figure 4.17 : Deformed configurations, Mooney Rivlin Model.

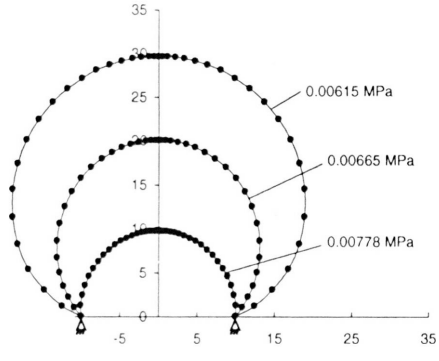


Figure 4.18 : Deformed configurations, Ogden Model.

A comparison of the results from this analysis shows that significant differences exist between the structural response predicted using the 3 and 8 chain models the Mooney-Rivlin Model and Ogden model. It is known from the experimental data of Treloar that the most accurate response is that obtained from the analysis conducted using the Ogden model. Given the fact that the cap is deformed in biaxial tension and the Ogden model is the only one of the four to make use of the experimental data for equi-biaxial extension (in the determination of material constants) this is not unexpected. Indeed the ability of the 3 and 8 chain models to reproduce the structural response of the cap can be improved significantly by determining the material constants from the equi-biaxial extension data, though this would have the effect over estimating the observed stress in uniaxial extension. Alternatively, the material constants could be obtained by performing a least squares fitting simultaneously to the experimental data for uniaxial extension and equi-biaxial extension, which would led to a slight underprediction of the observed stresses in biaxial extension and a slight overprediction in uniaxial

extension. Similar observations are also made with regard to the inflation of a sphere, analysed in the previous example.

4.8 Final Remarks

Using the principal axes technique a new approach has been developed to implement incompressible forms of the 3 and 8 chain network models into the commercial finite element program ABAQUS. The approach employs a simple iterative technique to determine the exact value of the inverse Langevin function and its derivative. Constitutive equations for the analysis of plane stress problems have been derived and given in full. In addition the analysis of problems involving the inflation of thin rubber-like membranes has demonstrated the importance of selecting appropriate values of the material constants for 3 and 8 models. In situations where one mode of deformation is dominant the best response is achieved by obtaining the material constants from experiments performed in that deformation state. Alternatively in situations where no one mode of deformation is dominant, satisfactory results can also be achieved using the material constants obtained from experiments performed in several deformation states.

Chapter 5

5. Implementation of Compressible Forms of the Non-Gaussian Network Models into FE Software

5.1 Introduction

In the previous chapter we considered the development of constitutive relations for the incompressible forms of the 3 and 8 chain network models. The incompressibility constraint was enforced exactly by the use of the plane stress condition and introduced no special problems. We now develop constitutive formulations suited to the analysis of axisymmetric, plane strain and three dimensional problems. However it is well known that the assumption of material incompressibility gives rise to severe numerical difficulties in these situations. As the Poisson's ratio approaches 0.5, the stiffness matrix becomes singular and the relationship between the hydrostatic pressure and strain becomes indeterminate. Several techniques have been developed to overcome the numerical difficulties arising from incompressibility. An explanation of these is provided by Hughes (1987). For a material which is incompressible the hydrostatic pressure is uncoupled from the displacements and must be determined directly from the equations of equilibrium. In the finite element analysis of such a material it is necessary to employ a mixed field approach where both the displacements and stresses

are treated as field variables. However for materials which are known to possess a degree of compressibility such as the majority of elastomers it is possible to employ an alternative approach referred to as the penalty method. This is a single field approach, which allows for a correlation between hydrostatic pressure and volume change by the extension of the constitutive formulation to account for material compressibility. It is this approach which has been employed in the current work because of its compatibility with the formulation of simple displacement based elements.

5.1.1 Deviatoric-volumetric multiplicative split

Compressibility is introduced into the constitutive formulations for the non-Gaussian network models considered here following a similar approach to that first proposed by Flory (1961). The deviatoric and hydrostatic responses are uncoupled by the introduction of the following multiplicative split of the deformation gradient

$$\mathbf{F} = \mathbf{F}_{vol}\tilde{\mathbf{F}}, \qquad \mathbf{F}_{vol} = J^{1/3}\mathbf{1}, \qquad \tilde{\mathbf{F}} = J^{-1/3}\mathbf{F} \tag{5.1}$$

where $J = \det \mathbf{F}$ and $\tilde{\mathbf{F}}$ represents the deviatoric or volume preserving component of the deformation gradient, such that $\det \tilde{\mathbf{F}} = 1$. Using this split, principal stretch based strain energy functions of a compressible type may be expressed in terms of a sum of separate deviatoric and volumetric components, as follows

$$W = \hat{W}^{dev}(\tilde{\lambda}_1, \tilde{\lambda}_2, \tilde{\lambda}_3) + \hat{W}^{vol}(J) \tag{5.2}$$

where the deviatoric or modified principal stretches, $\tilde{\lambda}_i$, are defined as

$$\tilde{\lambda}_i = J^{-1/3}\lambda_i, \tag{5.3}$$

Noting that

$$\tilde{\lambda}_1 \tilde{\lambda}_2 \tilde{\lambda}_3 = 1. \tag{5.4}$$

The first term in Equation (5.2), $\hat{W}^{dev}$, describes the change in strain energy as a result of deviatoric deformation, the second term $\hat{W}^{vol}$, is sometimes referred to as a

compressibility function and describes the change due to volumetric strain. A range of compressibility functions have been proposed to describe the volumetric response of rubberlike materials. Two of the most widely used functions in the non-linear stress analysis of elastomeric materials are of that Jankovich *et al* (1981)

$$\hat{W}^{vol}(J) = \frac{K}{2}\ln^2(J), \tag{5.5}$$

where K is the material constant, known as the bulk modulus, and that of Zdunek and Bercovier (1986)

$$\hat{W}^{vol}(J) = \frac{K}{2}(J-1)^2. \tag{5.6}$$

The compressibility functions above have been used in the analysis of rubberlike materials by various authors such as Moita (1995), Anand (1996) and Crisfield (1997). However a comparison of the response of Equation (5.5) and (5.6) with the experimental data of Bridgman (1945), who measured isothermal volume changes in a range of rubbers up to pressures of 2.5 GPa, shows that these functions only provide a satisfactory description of the volumetric response at low volumetric strains. A better description of the volumetric response of rubberlike materials at high volumetric strains is provided by the compressibility function of Ogden (1972b), who proposed a more sophisticated function of the form

$$\hat{W}^{vol}(J) = K\,g(J) \quad \text{with} \quad g(J) = \rho^{-2}\left[\rho\ln(J) + J^{-\rho} - 1\right] \tag{5.7}$$

where ρ denotes an empirical coefficient. Ogden demonstrated the ability of a function of this form to reproduce the experimental data of Bridgman (1944) for reductions in volume up to 20%, without significant deviation. Compressibility functions of this form have been used in the analysis of rubberlike materials in the work of authors like that of Holzapfel (1986), Reese and Wriggers (1995) and Peng and Chang (1997).

5.1.2 Uncoupled forms of the non-Gaussian network models

In the constitutive formulations for the non-Gaussian network models presented in the next section the volumetric response is modelled using Equation (5.5). As a result these formulations are only suitable for the analysis of problems involving small volumetric strains. The non-Gaussian network models considered here can easily be extended to deal with large volumetric strains using a compressibility function like that given in Equation (5.7). However because of the absence of experimental data for the volumetric response of the elastomers examined in this project, the use of a more sophisticated compressibility function cannot be justified. In addition since the deformation states examined in this work only give rise to small changes in volume, any difference in the hydrostatic pressure predicted by Equation (5.7) and (5.5) would itself be small. Using the multiplicative split introduced in Equation (5.1) the deviatoric and hydrostatic response of the 3 chain network model may be uncoupled to give a modified strain energy function of the form

$$W = \frac{\mu}{3}\sum_{i=1}^{3}\left\{ n\left[\frac{\tilde{\lambda}_i}{\sqrt{n}}\tilde{\beta}_i + \ln\frac{\tilde{\beta}_i}{\sinh\tilde{\beta}_i}\right] - T\,\hat{c}\right\} + \frac{K}{2}\ln^2(J), \tag{5.8}$$

where $\tilde{\beta}_i$ in Equation (5.8) is defined as

$$\tilde{\beta}_i = \mathcal{L}^{-1}\left(\frac{\tilde{\lambda}_i}{\sqrt{n}}\right) \tag{5.9}$$

Similarly the deviatoric and hydrostatic responses of the 8 chain model may be uncoupled to yield a strain energy function of the form

$$W = \mu\left\{ n\left[\frac{\tilde{\lambda}_{chain}}{\sqrt{n}}\tilde{\beta}_{chain} + \ln\frac{\tilde{\beta}_{chain}}{\sinh\tilde{\beta}_{chain}}\right] - T\,\hat{c}\right\} + \frac{K}{2}\ln^2(J) \tag{5.10}$$

where $\tilde{\beta}_{chain}$ in the equation on the previous page is defined as

$$\tilde{\beta}_{chain} = \mathcal{L}^{-1}\left(\frac{\tilde{\lambda}_{chain}}{\sqrt{n}}\right). \tag{5.11}$$

The modified or deviatoric chain stretch $\tilde{\lambda}_{chain}$ in Equation (5.11) is given by

$$\tilde{\lambda}_{chain} = \frac{\sqrt{\tilde{\lambda}_1^2 + \tilde{\lambda}_2^2 + \tilde{\lambda}_3^2}}{\sqrt{3}} \tag{5.12}$$

In the derivation the constitutive relations for the 3 and 8 chain models we regard $\tilde{\lambda}_i$ as a function of λ_i (and J) through Equation (5.3). By the chain rule we obtain

$$\frac{\partial \tilde{\lambda}_i}{\partial \lambda_j} = J^{-1/3}\left[\delta_{ij} - \frac{\lambda_i}{3\lambda_j}\right] \tag{5.13}$$

where we have used the fact that

$$\frac{\partial J}{\partial \lambda_i} = \frac{J}{\lambda_i} \tag{5.14}$$

5.1.3 Constitutive Equations (axisymmetric and plane strain formulations)

In considering the derivation of constitutive relations for the uncoupled form of the 3 and 8 chain models, it is useful especially with regard to later developments to continue with a strict separation of the deviatoric and hydrostatic responses. With this in mind, the Cauchy stress tensor may be expressed as

$$\boldsymbol{\sigma} = \boldsymbol{\sigma}^{dev} + \boldsymbol{\sigma}^{vol}, \tag{5.15}$$

where $\boldsymbol{\sigma}^{dev}$ and $\boldsymbol{\sigma}^{vol}$ represent the deviatoric and hydrostatic components of the Cauchy stress tensor, respectively. The principal deviatoric components of the Cauchy stress tensor for the 3 chain model may be obtained from Equation (5.8) using Equations (2.41), (4.11) and (4.45), giving

$$\sigma_{ii}^{E,dev} = \frac{\mu\sqrt{n}}{3J}\left[\tilde{\lambda}_i\,\tilde{\beta}_i - \frac{1}{3}\sum_{j=1}^{3}\tilde{\lambda}_j\tilde{\beta}_j\right]. \tag{5.16}$$

The volumetric component of the Cauchy stress tensor may be obtained similarly and expressed in tensor form as

$$\boldsymbol{\sigma}^{vol} = \frac{K}{J}\ln(J)\,\mathbf{I} \tag{5.17}$$

where $\mathbf{I}$ in the relation above represents the second order identity tensor. The principal components of the deviatoric part of Cauchy stress tensor given in Equation (5.16) are related to the principal directions $\mathbf{n}_1, \mathbf{n}_2, \mathbf{n}_3$ and may be rotated back to the base coordinate frame following the same approach as that adopted in section (4.6.2). Taking into account the symmetry of $\boldsymbol{\sigma}^{dev}$ we introduce for $\boldsymbol{\sigma}^{dev}$: $\hat{\sigma}_i^{dev} = [\sigma_{11}^{dev}, \sigma_{22}^{dev}, \sigma_{33}^{dev}, \sigma_{12}^{dev}]$, which leads to the transformation

$$\hat{\sigma}_i^{dev} = \hat{P}_{ij}\ \hat{\sigma}_j^{E,dev} \tag{5.18}$$

where $\hat{\sigma}_j^{E,dev}$ is the vector containing the deviatoric components of the Cauchy stress in the Eulerian triad, i.e. $\hat{\sigma}_j^{E,dev} = [\sigma_{11}^{E,dev}, \sigma_{22}^{E,dev}, \sigma_{33}^{E,dev}, 0]$ and P_{ij} is a projection matrix defined as

$$\hat{\mathbf{P}} = \begin{bmatrix} Q_{11}^2 & Q_{12}^2 & Q_{13}^2 & 2Q_{11}^2Q_{12}^2 \\ Q_{21}^2 & Q_{22}^2 & Q_{23}^2 & 2Q_{21}^2Q_{22}^2 \\ Q_{31}^2 & Q_{32}^2 & Q_{33}^2 & 2Q_{31}^2Q_{32}^2 \\ Q_{11}^2Q_{21}^2 & Q_{12}^2Q_{22}^2 & Q_{13}^2Q_{23}^2 & Q_{11}Q_{22} + Q_{12}Q_{21} \end{bmatrix} \tag{5.19}$$

The Q terms in Equation (5.19) are components of $\mathbf{Q}(\mathbf{n})$, the tensor containing the principal direction vectors of the Eulerian triad, i.e. $\mathbf{Q}(\mathbf{n}) = [\mathbf{n}_1, \mathbf{n}_2, \mathbf{n}_3]$. The principal stretches and directions may be obtained as before by the diagonalisation of the left hand Cauchy Green deformation tensor $\mathbf{B}$, defined in Equation (2.31). However, in axisymmetric and plane strain problems it is only necessary to calculate λ_1, λ_2 and $\mathbf{n}_1, \mathbf{n}_2$ via diagonalisation methods. The total Cauchy stress is finally evaluated by adding the deviatoric and volumetric components of the Cauchy stress tensor.

To complete the formulation it is only necessary to find the appropriate Jacobian matrix. We start as in the previous chapter by calculating the tangent of the Truesdell rate of Kirchhoff stress. Here we again maintain a strict separation of the deviatoric and volumetric responses, such that the tangent of the Truesdell rate of Kirchhoff stress may be written in tensor form as

$$\mathscr{D}^{TK} = \mathscr{D}^{TK,dev} + \mathscr{D}^{TK,vol} \tag{5.20}$$

where $\mathscr{D}^{TK,dev}$ and $\mathscr{D}^{TK,vol}$ represent the deviatoric and volumetric components of the fourth order constitutive tensor, respectively. Using the principal axes technique we first calculate the tangent of the Truesdell rate of Kirchhoff stress in the Eulerian triad. For our convenience we can arrange the components of $\mathscr{D}^{TK,dev}$ and $\mathscr{D}^{TKE,dev}$ into the 4×4 matrices $\hat{\mathbf{D}}^{TK,dev}$ and $\hat{\mathbf{D}}^{TKE,dev}$. Using Equation (4.47), the components of $\hat{\mathbf{D}}^{TKE,dev}$ for $i = j$ $(i = 1,2,3)$ are given by

$$\hat{D}_{ii}^{TKE,dev} = \frac{\mu\sqrt{n}}{3}\left[\frac{\tilde{\lambda}_i^2}{3\sqrt{n}}\tilde{\beta}_i' - \frac{16\tilde{\lambda}_i}{9}\tilde{\beta}_i + \sum_{k=1}^{3}\frac{\tilde{\lambda}_k^2}{9\sqrt{n}}\tilde{\beta}_k' + \frac{7\tilde{\lambda}_k}{9}\tilde{\beta}_k\right] \tag{5.21}$$

and for $i \neq j$ $(i = 1,2,3)$

$$\hat{D}_{ij}^{TKE,dev} = \hat{D}_{ji}^{TKE,dev} = \frac{\mu\sqrt{n}}{3}\left[\sum_{k=1}^{3}\frac{\tilde{\lambda}_k^2}{9\sqrt{n}}\tilde{\beta}_k' + \frac{\tilde{\lambda}_k}{9}\tilde{\beta}_k - \frac{\tilde{\lambda}_i^2}{3\sqrt{n}}\tilde{\beta}_i' - \frac{\tilde{\lambda}_i}{3}\tilde{\beta}_i - \frac{\tilde{\lambda}_j^2}{3\sqrt{n}}\tilde{\beta}_j' - \frac{\tilde{\lambda}_j}{3}\tilde{\beta}_j\right] \tag{5.22}$$

For the shear component $\hat{D}_{44}^{TKE,dev}$, we have from Equation (4.48)

$$\hat{D}_{44}^{TKE,dev} = \frac{\lambda_2^2\tau_{11}^{E,dev} - \lambda_1^2\tau_{22}^{E,dev}}{\lambda_1^2 - \lambda_2^2} \tag{5.23}$$

where $\tau_{ii}^{E,dev}$ in the above equation represents the principal deviatoric components of the Kirchhoff stress, i.e. $\tau_{ii}^{E,dev} = J\sigma_{ii}^{E,dev}$.

If $\lambda_1 = \lambda_2$ the limit value of Equation (5.23) is applied instead, yielding

$$\hat{D}_{44}^{TKE,dev} = \frac{1}{2}\left(\hat{D}_{11}^{TKE,dev} - \hat{D}_{21}^{TKE,dev}\right) \tag{5.24}$$

The volumetric component of the tangent of the Truesdell rate of Kirchhoff stress may be similarly evaluated and expressed as

$$\hat{D}_{ii}^{TK,vol} = K(1 - 2\ln(J)) \qquad i = j \quad (i = 1,2,3) \tag{5.25}$$

$$\hat{D}_{ij}^{TK,vol} = K \qquad i \neq j \quad (i = 1,2,3) \tag{5.26}$$

For the shear component $\hat{D}_{44}^{TK,vol}$, we have from Equation (4.47)

$$\hat{D}_{44}^{TK,vol} = -K\ln(J) \tag{5.27}$$

The constitutive tensor, $\mathscr{D}^{TKE,dev}$, corresponding to the tangent of the Truesdell rate in the Eulerian triad may be rotated back to the base coordinate frame using a standard fourth order tensor transformation, Equation (4.101). However following the approach adopted in section (4.6.2), it is again more convenient to employ the matrix transformation

$$\hat{D}_{ij}^{TK,dev} = \hat{P}_{ik}\hat{D}_{kl}^{TKE,dev}\hat{P}_{jl} \tag{5.28}$$

where we use the same transformation matrix as that used in the calculation of the deviatoric components of the Cauchy stress tensor, Equation (5.19). The deviatoric and volumetric components are then summed to give the total tangent of the Truesdell rate of Kirchhoff stress. The tangent of the Jaumann rate of Kirchhoff stress may then be obtained using Equation (2.56), which may be expressed in matrix form as

$$\hat{\mathbf{D}}^{JK} = \hat{\mathbf{D}}^{TK} + \breve{\boldsymbol{\tau}} \ . \tag{5.29}$$

In two dimensions, the matrix $\breve{\boldsymbol{\tau}}$ is given by

$$\breve{\boldsymbol{\tau}} = \begin{bmatrix} 2\tau_{11} & 0 & 0 & \tau_{12} \\ 0 & 2\tau_{22} & 0 & \tau_{21} \\ 0 & 0 & 2\tau_{33} & 0 \\ \tau_{21} & \tau_{12} & 0 & \dot{\tau}_{12} \end{bmatrix} \tag{5.30}$$

where τ_{ij} represent the components of the Kirchhoff stress tensor, i.e. $\tau_{ij} = J\sigma_{ij}$ and $\dot{\tau}_{12} = (\tau_{11} + \tau_{22})/2$. The tangent of the Jaumann rate of Kirchhoff stress is finally transformed to give the tangent of the Jaumann rate of Cauchy stress using Equation (2.63), which may also be expressed in matrix form as

$$\hat{\mathbf{D}}^{JC} = \frac{1}{J}\hat{\mathbf{D}}^{JK} - \breve{\boldsymbol{\sigma}}. \tag{5.31}$$

In two dimensions, the non-symmetric matrix $\breve{\boldsymbol{\sigma}}$ is given by

$$\breve{\boldsymbol{\sigma}} = \begin{bmatrix} \sigma_{11} & \sigma_{11} & \sigma_{11} & 0 \\ \sigma_{22} & \sigma_{22} & \sigma_{22} & 0 \\ \sigma_{33} & \sigma_{33} & \sigma_{33} & 0 \\ \sigma_{12} & \sigma_{12} & \sigma_{12} & 0 \end{bmatrix} \tag{5.32}$$

Constitutive relations for the compressible form of the 8 chain network model may be derived using the same procedure as that employed for the 3 chain model. The principal deviatoric components of the Cauchy stress tensor are obtained from Equation (5.10) using Equations (2.41), (4.11) and (4.45), to yield

$$\sigma_{ii}^{E,dev} = \frac{\mu\sqrt{n}}{3J}\frac{\tilde{\lambda}_i^2 - \frac{1}{3}\tilde{I}_1}{\tilde{\lambda}_c}\tilde{\beta}_c, \tag{5.33}$$

where $\tilde{I}_1 = \tilde{\lambda}_1^2 + \tilde{\lambda}_2^2 + \tilde{\lambda}_3^2$. The volumetric component of the Cauchy stress is the same as that given in Equation (5.17). The principal deviatoric components of the Cauchy stress tensor may then be rotated back to the base coordinate frame using Equation (5.18), and summed with the volumetric components to give the total Cauchy stress.

The Jacobian matrix for the 8 chain model is obtained in a similar manner to that for the 3 chain model. Using the principal axes technique we first evaluate the tangent of the Truesdell rate of Kirchhoff stress in the Eulerian triad and then rotate it back to the base coordinate frame. As before it is computationally more convenient for our purposes to arrange the components of the constitutive tensors $\mathscr{D}^{TK,dev}$ and $\mathscr{D}^{TKE,dev}$ into the 4×4 matrices $\hat{\mathbf{D}}^{TK,dev}$ and $\hat{\mathbf{D}}^{TKE,dev}$. Using Equation (4.47) the components of $\hat{\mathbf{D}}^{TKE,dev}$ for $i=j$ $(i=1,2,3)$ are given by

$$\hat{D}_{ii}^{TKE,dev}=\mu\sqrt{n}\left[\frac{1}{\sqrt{n}}\{F(i)\}^2\tilde{\beta}_c'-\left(\frac{\tilde{\lambda}_i^4}{\tilde{\lambda}_c^3}+\frac{2\tilde{\lambda}_i^2}{\tilde{\lambda}_c}+7\tilde{\lambda}_c\right)\frac{\tilde{\beta}_c}{9}\right] \tag{5.34}$$

and for $i\neq j$ $(i=1,2,3)$

$$\hat{D}_{ij}^{TKE,dev}=\hat{D}_{ji}^{TKE,dev}=\mu\sqrt{n}\left[\frac{1}{\sqrt{n}}F(i)F(j)\tilde{\beta}_c'-\left(\frac{\tilde{\lambda}_i^2\tilde{\lambda}_j^2}{\tilde{\lambda}_c^3}+\frac{\tilde{\lambda}_i^2}{\tilde{\lambda}_c}+\frac{\tilde{\lambda}_j^2}{\tilde{\lambda}_c}+\lambda_c\right)\frac{\tilde{\beta}_c}{9}\right] \tag{5.35}$$

where the term $F(k)$ in Equations (5.34) and (5.35) is defined as

$$F(k)=\frac{\tilde{\lambda}_k^2-\frac{1}{3}\tilde{I}_1}{3\tilde{\lambda}_c}. \tag{5.36}$$

When $\lambda_i\neq\lambda_j$, the shear component $\hat{D}_{44}^{TKE,dev}$ is calculated from Equation (5.23), for $\lambda_i=\lambda_j$ the limit value given in Equation (5.24) is applied instead. The volumetric component of the tangent of the Truesdell rate of Kirchhoff stress is the same as that given in Equations (5.25), (5.26) and (5.27). The principal deviatoric components of the Truesdell rate of Kirchhoff stress are again rotated back to the base coordinate frame using Equation (5.28), and summed with the volumetric components to give the total tangent of the Truesdell rate of Kirchhoff stress. The tangent of the Jaumann rate of Cauchy stress is finally obtained using Equations (5.29)and (5.31). The constitutive relations presented in this section are compatible with the CPE and CAX families of plane strain and axisymmetric elements provided by ABAQUS.

5.1.4 Constitutive Equations (3-D formulation)

The principal deviatoric components of the Cauchy stress tensor for the 3 and 8 chain network models are identical those given in Equation (5.16) and (5.33), respectively. The volumetric component of the Cauchy stress for both models is the same as that given in Equation (5.17). The principal components of the deviatoric part of the Cauchy stress are related to the principal directions $\mathbf{n}_1, \mathbf{n}_2, \mathbf{n}_3$ and may be rotated back to the base coordinate frame following the same approach as that adopted in the previous section. Taking into account the symmetry of $\boldsymbol{\sigma}^{dev}$ we introduce for $\boldsymbol{\sigma}^{dev}$: $\sigma_i^{dev} = [\sigma_{11}^{dev}, \sigma_{22}^{dev}, \sigma_{33}^{dev}, \sigma_{12}^{dev}, \sigma_{13}^{dev}, \sigma_{23}^{dev}]$, which as before leads to the transformation

$$\sigma_i^{dev} = \hat{P}_{ij}\, \sigma_j^{E,dev} \tag{5.37}$$

where $\hat{\sigma}_j^{E,dev}$ is the vector containing the deviatoric components of the Cauchy stress in the Eulerian triad, i.e. $\hat{\sigma}_j^{E,dev} = [\sigma_{11}^{E,dev}, \sigma_{22}^{E,dev}, \sigma_{33}^{E,dev}, 0, 0, 0]$ and $\hat{P}_{ij}$ is a projection matrix defined as

$$\hat{\mathbf{P}} = \begin{bmatrix} Q_{11}^2 & Q_{12}^2 & Q_{13}^2 & 2Q_{11}Q_{12} & 2Q_{13}Q_{11} & 2Q_{12}Q_{13} \\ Q_{21}^2 & Q_{22}^2 & Q_{23}^2 & 2Q_{21}Q_{22} & 2Q_{23}Q_{21} & 2Q_{22}Q_{23} \\ Q_{31}^2 & Q_{32}^2 & Q_{33}^2 & 2Q_{31}Q_{32} & 2Q_{33}Q_{31} & 2Q_{32}Q_{33} \\ Q_{11}Q_{21} & Q_{12}Q_{22} & Q_{13}Q_{23} & Q_{11}Q_{22}+Q_{12}Q_{21} & Q_{13}Q_{21}+Q_{11}Q_{23} & Q_{12}Q_{23}+Q_{13}Q_{22} \\ Q_{31}Q_{11} & Q_{32}Q_{12} & Q_{33}Q_{13} & Q_{31}Q_{12}+Q_{32}Q_{11} & Q_{33}Q_{11}+Q_{31}Q_{13} & Q_{32}Q_{13}+Q_{33}Q_{12} \\ Q_{21}Q_{31} & Q_{22}Q_{32} & Q_{23}Q_{33} & Q_{21}Q_{32}+Q_{22}Q_{31} & Q_{23}Q_{31}+Q_{21}Q_{33} & Q_{22}Q_{33}+Q_{23}Q_{32} \end{bmatrix} \tag{5.38}$$

The Q terms in Equation (5.38) are components of $\mathbf{Q}(\mathbf{n})$, the tensor containing the principal direction vectors of the Eulerian triad, i.e. $\mathbf{Q}(\mathbf{n}) = [\mathbf{n}_1, \mathbf{n}_2, \mathbf{n}_3]$. The principal stretches and directions may be obtained as before by the diagonalisation of the left hand Cauchy Green deformation tensor $\mathbf{B}$. The deviatoric and volumetric components may then be summed to give the total Cauchy stress.

The only remaining problem is the computation of the appropriate Jacobian matrix. Following a similar approach to that adopted in section 5.1.3 we start by calculating the deviatoric component of the tangent Truesdell rate of Kirchhoff stress in the Eulerian triad, and then rotate this back to the base coordinate frame. For our convenience we arrange the components of the constitutive tensors $\mathscr{D}^{TK,dev}$ and $\mathscr{D}^{TKE,dev}$ into the 6×6 matrices $\hat{\mathbf{D}}^{TK,dev}$ and $\hat{\mathbf{D}}^{TKE,dev}$. The matrix $\hat{\mathbf{D}}^{TKE,dev}$ corresponding to the tangent of the Truesdell rate of Kirchhoff stress in the Eulerian triad has the form

$$\hat{\mathbf{D}}^{TKE,dev} = \begin{bmatrix} \begin{bmatrix} \hat{D}_{11}^{TKE,dev} & \hat{D}_{12}^{TKE,dev} & \hat{D}_{13}^{TKE,dev} & 0 \\ \hat{D}_{21}^{TKE,dev} & \hat{D}_{22}^{TKE,dev} & \hat{D}_{23}^{TKE,dev} & 0 \\ \hat{D}_{31}^{TKE,dev} & \hat{D}_{32}^{TKE,dev} & \hat{D}_{33}^{TKE,dev} & 0 \\ 0 & 0 & 0 & \hat{D}_{44}^{TKE,dev} \end{bmatrix} & \begin{matrix} 0 & 0 \\ 0 & 0 \\ 0 & 0 \\ 0 & 0 \end{matrix} \\ \begin{matrix} 0 & 0 & 0 & 0 \\ 0 & 0 & 0 & 0 \end{matrix} & \begin{matrix} \hat{D}_{55}^{TKE,dev} & 0 \\ 0 & \hat{D}_{66}^{TKE,dev} \end{matrix} \end{bmatrix} \tag{5.39}$$

where the submatrix shown in Equation (5.39) is identical to that obtained for the 3 and 8 chain network models in the previous section. When $\lambda_1 \neq \lambda_3$ the shear term $\hat{D}_{55}^{TKE,dev}$ may be obtained from Equation (5.23), yielding

$$\hat{D}_{55}^{TKE,dev} = \frac{\lambda_3^2 \tau_{11}^{E,dev} - \lambda_1^2 \tau_{33}^{E,dev}}{\lambda_1^2 - \lambda_3^2}. \tag{5.40}$$

Likewise when $\lambda_2 \neq \lambda_3$ the shear term $\hat{D}_{66}^{TKE,dev}$ is given by

$$\hat{D}_{66}^{TKE,dev} = \frac{\lambda_3^2 \tau_{22}^{E,dev} - \lambda_2^2 \tau_{33}^{E,dev}}{\lambda_2^2 - \lambda_3^2}. \tag{5.41}$$

To overcome the problem that occurs in the calculation of $\hat{D}_{55}^{TKE,dev}$ when $\lambda_1 = \lambda_3$ the limit value of Equation (5.40) is applied instead, giving

$$\hat{D}_{55}^{TKE,dev} = \frac{1}{2}\left(\hat{D}_{11}^{TKE,dev} - \hat{D}_{31}^{TKE,dev}\right). \tag{5.42}$$

Similarly when $\lambda_2 = \lambda_3$ the limit value of Equation (5.41) is applied, which yields

$$\hat{D}_{66}^{TKE,dev} = \frac{1}{2}\left(\hat{D}_{22}^{TKE,dev} - \hat{D}_{32}^{TKE,dev}\right). \tag{5.43}$$

The volumetric component of the tangent of the Truesdell rate for the 3 and 8 chain models is the same as that given in Equations (5.25), (5.26) and (5.27), with the addition that

$$\hat{D}_{55}^{TK,vol} = -K\ln(J), \tag{5.44}$$

and

$$\hat{D}_{66}^{TK,vol} = -K\ln(J). \tag{5.45}$$

The total tangent of the Truesdell rate of Kirchhoff stress may then be obtained by the rotation of $\hat{\mathbf{D}}^{TKE,dev}$ back to the base coordinate frame using a similar matrix operation to that given in Equation (5.28), followed the addition of the volumetric component of the tangent. If all three principal stretches coincide, $\hat{\mathbf{D}}^{TK,dev}$ may be calculated directly from Equation (4.51). The tangent of the Jaumann rate of Kirchhoff stress may then be obtained using Equation (2.56), and expressed in matrix form as

$$\hat{\mathbf{D}}^{JK} = \hat{\mathbf{D}}^{TK} + \breve{\boldsymbol{\tau}} \tag{5.46}$$

In three dimensions the matrix $\breve{\boldsymbol{\tau}}$ is given by

$$\breve{\boldsymbol{\tau}} = \begin{bmatrix} 2\tau_{11} & 0 & 0 & \tau_{12} & \tau_{13} & 0 \\ 0 & 2\tau_{22} & 0 & \tau_{21} & 0 & \tau_{23} \\ 0 & 0 & 2\tau_{33} & 0 & \tau_{31} & \tau_{32} \\ \tau_{21} & \tau_{12} & 0 & \dot{\tilde{\tau}}_{12} & \frac{1}{2}\tau_{23} & \frac{1}{2}\tau_{13} \\ \tau_{31} & 0 & \tau_{13} & \frac{1}{2}\tau_{32} & \dot{\tilde{\tau}}_{13} & \frac{1}{2}\tau_{12} \\ 0 & \tau_{32} & \tau_{23} & \frac{1}{2}\tau_{31} & \frac{1}{2}\tau_{21} & \dot{\tilde{\tau}}_{23} \end{bmatrix} \tag{5.47}$$

where $\dot{\tilde{\tau}}_{ij} = (\tau_{ii} + \tau_{jj})/2$.

The tangent of the Jaumann rate of Kirchhoff stress is finally transformed to give the tangent of the Jaumann rate of Cauchy stress using Equation (2.62), which may also be expressed in matrix form as

$$\hat{\mathbf{D}}^{JC} = \frac{1}{J}\hat{\mathbf{D}}^{JK} - \breve{\boldsymbol{\sigma}}. \tag{5.48}$$

In three dimensions the non-symmetric matrix $\breve{\boldsymbol{\sigma}}$ is given by

$$\breve{\boldsymbol{\sigma}} = \begin{bmatrix} \sigma_{11} & \sigma_{11} & \sigma_{11} & 0 & 0 & 0 \\ \sigma_{22} & \sigma_{22} & \sigma_{22} & 0 & 0 & 0 \\ \sigma_{33} & \sigma_{33} & \sigma_{33} & 0 & 0 & 0 \\ \sigma_{12} & \sigma_{12} & \sigma_{12} & 0 & 0 & 0 \\ \sigma_{13} & \sigma_{13} & \sigma_{13} & 0 & 0 & 0 \\ \sigma_{23} & \sigma_{23} & \sigma_{23} & 0 & 0 & 0 \end{bmatrix} \tag{5.49}$$

5.2 Numerical Tests

Examples are now provided to demonstrate the accuracy of the constitutive formulations developed for the compressible forms of the 3 and 8 chain non-Gaussian network models. Comparisons are again made with the predictions of the Mooney-Rivlin and Ogden models.

5.2.1 Homogeneous Deformation Tests

We commence by examining the accuracy of the 3 and 8 models in the homogeneous deformation states of uniaxial extension, equibiaxial extension and pure shear. Tests are performed using a single C3D8I, where the use of an element with incompatible mode is necessary to avoid problems associated with volumetric locking. The material constants employed again come from a least squares fit to the uniaxial experimental data of Treloar (1944), a Poisson's ratio of $\nu = 0.4999$ is also used to simulate an (almost) incompressible bulk response. The FEA results are compared with the analytical solutions in Figures (5.1) to (5.6), and can be seen to be in good agreement.

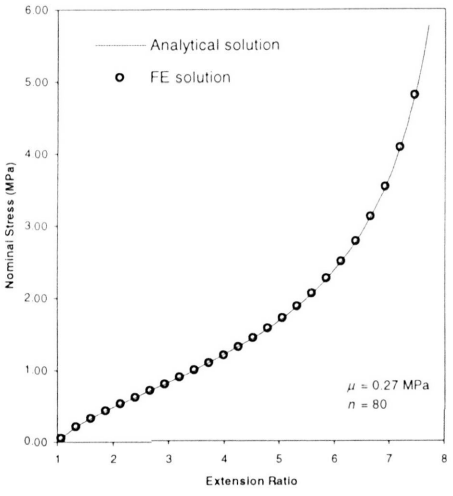


Figure 5.1 : Uniaxial response, 3 Chain model.

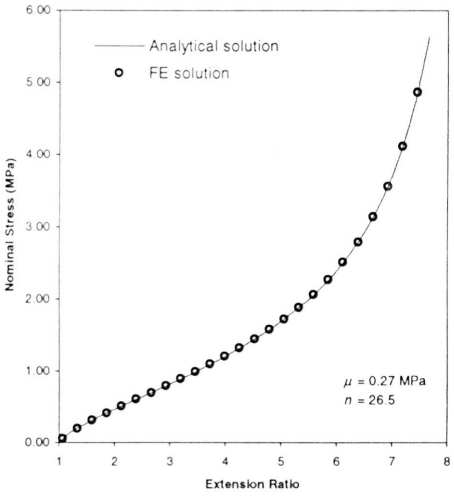


Figure 5.2 : Uniaxial response, 8 Chain model.

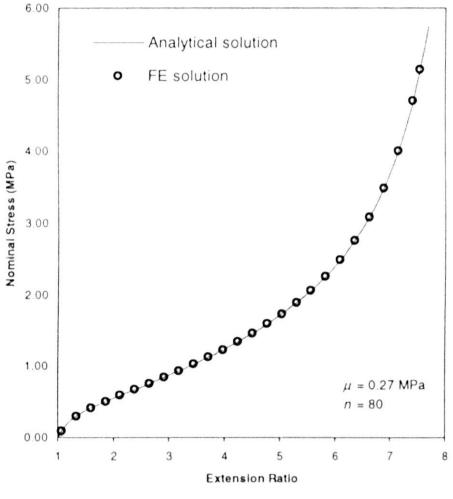


Figure 5.3 : Equibiaxial response, 3 Chain model.

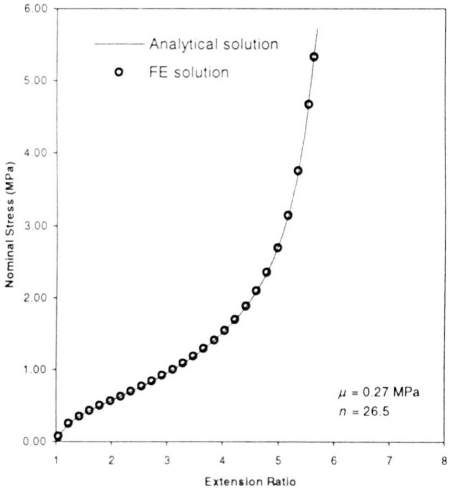


Figure 5.4 Equibiaxial response, 8 Chain model.

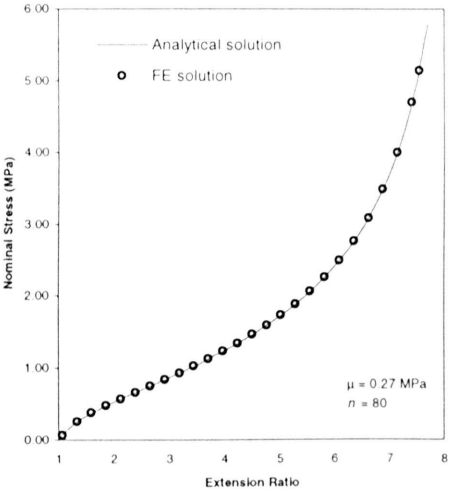


Figure 5.5 : Pure shear response, 3 Chain model.

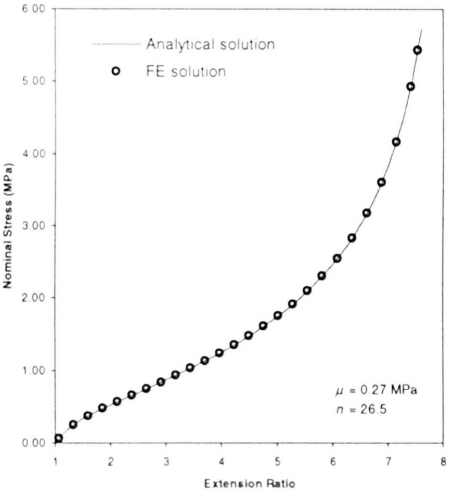


Figure 5.6: Pure shear response, 8 Chain model.

5.2.2 Compression of a bonded cylindrical block

This example illustrates the compression of a cylindrical block bonded between two rigid plates, Figure 5.7. Problems of a similar nature have also been studied in the work of Morman and Pan (1988) and Lee and Rivin (1996) among others. The block has a diameter of $d = 25.4\,mm$, and a height of $h = 25.4\,mm$. One quarter of the cylinder is modelled using 900 CAX4I axisymmetric elements. Problems associated with volumetric locking are avoided by employing an element type with incompatible modes. The response of the 3 and 8 chain models is compared with that of the Mooney-Rivlin and Ogden models. The material constants employed come from the experimental data of Treloar (1944), and are the same as those given in section 4.7.2. A Poisson's ratio of $\nu = 0.4999$ is also used to simulate an (almost) incompressible bulk response with each model. Figure 5.8 shows the load displacement response of the block. The original and deformed meshes are shown in Figures 5.9-5.12.

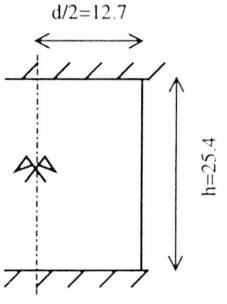


Figure 5.7 : Compression of bonded cylindrical block.

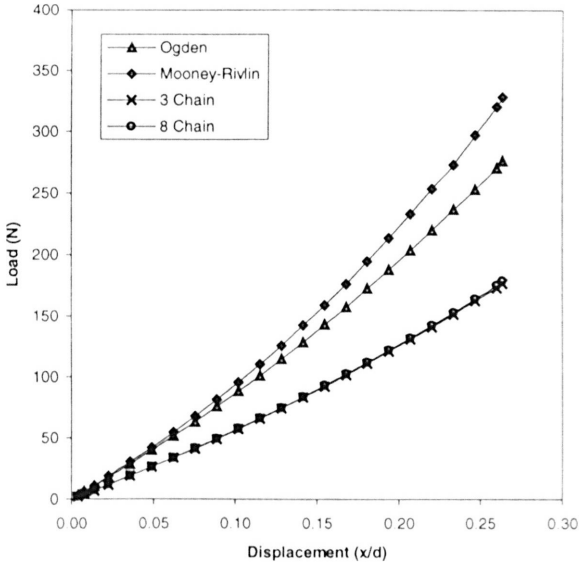


Figure 5.8 : Bonded cylindrical block, load versus normalised axial displacement.

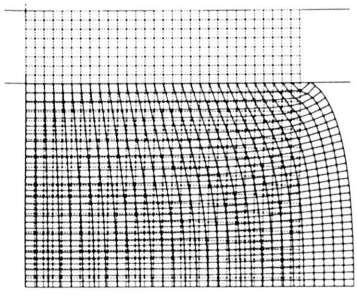


Figure 5.9 : Original and deformed meshes, 3 chain model.

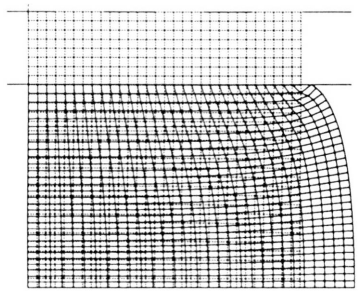


Figure 5.10 : Original and deformed meshes, 8 chain model.

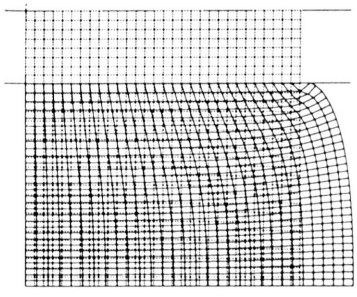


Figure 5.11 : Original and deformed meshes, M-R model.

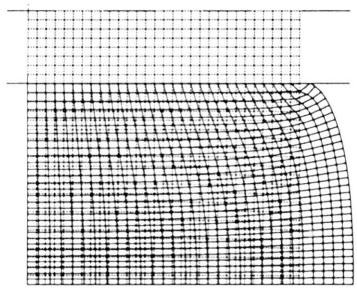


Figure 5.12 : Original and deformed meshes, Ogden model.

A comparison of the results of this analysis demonstrates that in common with the example problems examined at the end of chapter 4, there are significant differences between the between the structural response predicted using the 3 and 8 chain models and that of the Mooney-Rivlin and Ogden models. Unfortunately since experimental data for the behaviour of this material in compression is unavailable it is not known which models provides the most accurate description of the structural response. However given the similarities of the deformation states of equi-biaxial extension and uniaxial compression states, differences between the predictions of the 3 and 8 chain models and the Ogden model can be explained by the fact that the materials constants for the former were obtained by comparison with the experimental data for uniaxial extension. As a final note it is worth mentioning that in tests conducted on polyurethane and neoprene, discussed later in Chapter 8, material constants for the 8 model obtained by comparison with uniaxial tensile data were also successful at describing the response of these materials in uniaxial compression.

5.2.3 Cook's membrane problem

The final example to be examined is Cook's membrane problem. This problem has also been studied in the non-linear environment by Simo and Armero (1992) and Moita (1994). Consider a tapered panel clamped on one edge and subjected to a shearing load F on the opposite edge, as is shown in Figure 5.13. A plane strain analysis is performed using 400 CPE4I plane strain elements to represent the panel. The material constants employed are the same as those given in the previous example. Problems associated with volumetric locking are again overcome by employing an element type with incompatible modes. Figure 5.14 shows a plot of the vertical displacement of the top right hand corner of the panel against the applied load. The original and deformed meshes for each of the 4 models employed are shown in Figures 5.15 to 5.18.

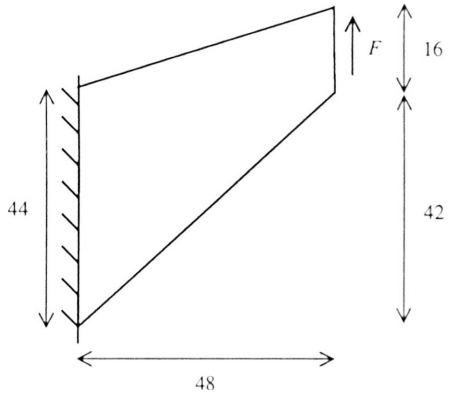


Figure 5.13 : Cook's membrane problem.

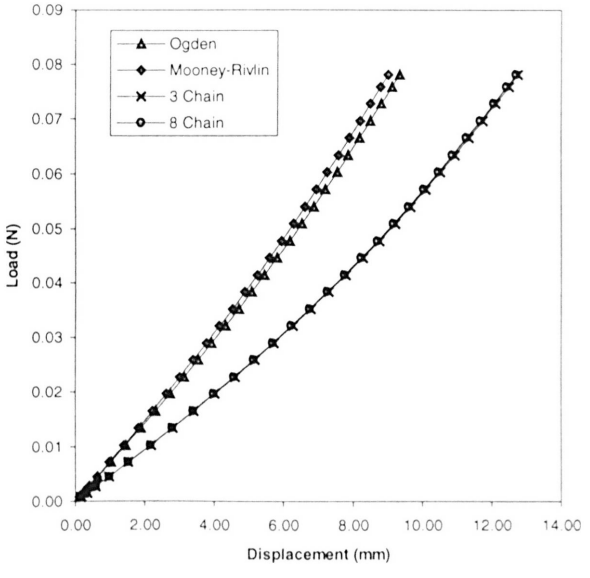


Figure 5.14 : Cooks membrane, applied load versus displacement of top right hand corner of panel.

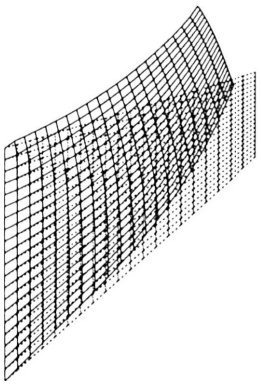


Figure 5.15 : Original and deformed meshes, 3 chain model.

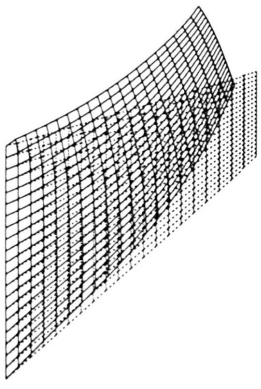


Figure 5.16 : Original and deformed meshes, 8 chain model.

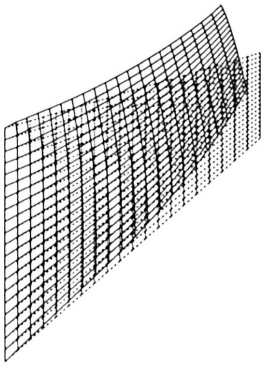


Figure 5.17 : Original and deformed meshes, M-R model.

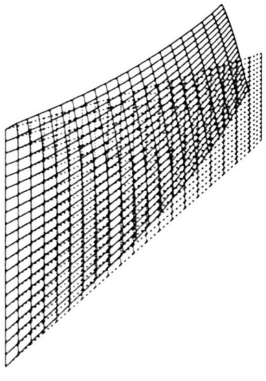


Figure 5.18 : Original and deformed meshes, Ogden model.

This example again demonstrates the difference in the structural response predicted using the 3 and 8 chain models and the Mooney-Rivlin and Ogden models. As in the previous example the difference can be explained in terms of the experimental data, which was employed to determine the material constants for the 3 and 8 chain models.

5.3 Final Remarks

Material compressibility has been introduced into the constitutive formulations for the 3 and 8 chain models by uncoupling the deviatoric and volumetric responses. Constitutive relations for the analysis of plane strain, axisymmetric and three-dimensional problems have also been derived. Comparisons between the response of the 3 chain, 8 chain, Mooney-Rivlin and Ogden models have been made, which again demonstrate the importance of obtaining material constants from experiments conducted in the deformation state that most closely represents the dominant mode of deformation in the particular situation of interest.

Chapter 6

6. Strain Induced Softening

6.1 Introduction

Fillers are commonly added to the elastomers used in engineering applications in order to enhance mechanical properties like tensile strength, stiffness and abrasion resistance. Indeed, tenfold increases in the strength and stiffness of elastomeric materials have been reported by Eirich (1978) and Gent (1992), respectively. However the addition of fillers is also known to cause a form of strain induced softening or damage often referred as the Mullins effect. The chapter commences with a discussion of filler reinforcement and the Mullins effect and goes on to review the various theories that have been proposed for their origin. Later in the chapter, the 3 and 8 chain network models are extended to account for the effect of strain induced softening using continuum damage mechanics, in an approach similar to that first presented by Simo (1987). The most commonly employed fillers are carbon black, zinc oxide, and the carbonates and silicates of calcium and magnesium. Fillers generally fall into one of two categories: reinforcing and non-reinforcing. Fillers are considered to be reinforcing if they can increase the stiffness of an elastomer without impairing its strength or destroying its rubbery characteristics. The degree of reinforcement provided by a particular filler depends on a number of variables, one of the most

important of which is the development of a large polymer-filler interface. This typically requires the use of filler particles that are between 100-4700 Å in diameter, Blow and Hepburn (1982). The strain induced softening of filled loaded elastomers was first studied in detail by Holt (1932) who examined the effect in carbon black filled NR. The phenomenon is most easily understood by considering an idealised quasi-static strain driven cyclic tension test, Figure 6.1. Quasi static in the present context means inertial and viscous effects are negligible; *i.e.* the loading is slow not only with respect to the inertial time scale but also with respect to the time scales of the viscous relaxation mechanisms in the elastomer. The material starts out in the virgin (undamaged) state (0). Upon loading to strain (1), path (a) defines the material response; upon subsequent unloading and loading between strain (1) and strain (0), path (b) defines the new material response. The material has experienced a change in its response due to the loading up to strain (1). If the strain is increased beyond strain (1), path (a) is again activated in the region above strain (1). Assume the loading is increased to strain (2). Then upon subsequent unloading between strain (2) and strain (0), path (c) will define the material response. From a phenomenological viewpoint this is a strain induced softening or damaging of the material; this is known as the Mullins effect. The mechanical response of filled elastomers is thus rather ill defined, depending on the degree to which they have been previously strained.

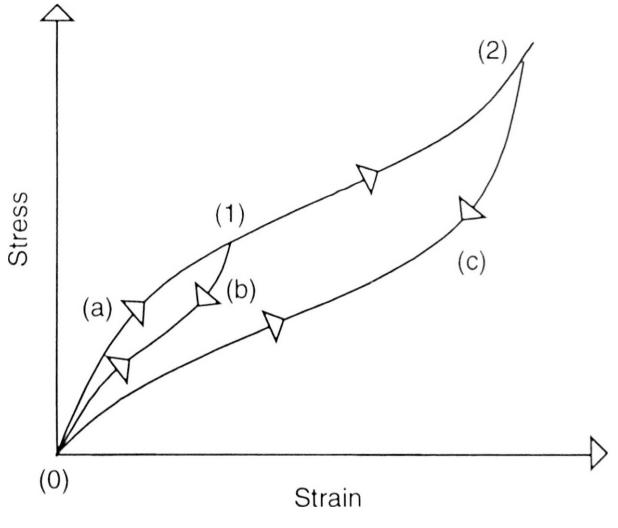


Figure 6.1 : Schematic of cyclic tension test demonstrating the Mullins effect.

Holt (1932) further demonstrated that while the majority of softening occurs during the first extension cycle, additional cycles also soften the material but to a lesser extent. In addition, Holt showed that NR regains a portion of its stiffness if allowed to rest in the relaxed state. Although this recovery was very slow at room temperature, up to 50% recovery was noted after about an hour at 100°C. Similar softening was also noted in the unfilled NR examined by Holt, but the effects were less marked than in the filled material. The strain induced softening of filled rubbers was later examined in more detail in the experimental study of Mullins (1948). Mullins confirmed and extended the earlier results of Holt, and also speculated about the mechanisms involved but did not come to any definite conclusion in that regard. The observed phenomenon apparently gets its name from this early work.

6.2 Mechanisms of Reinforcement and Mullins effect

The phenomenon of filler reinforcement and associated strain softening still remains a poorly defined and only partially understood subject. This situation results from the chemical and physical complexity of the commercially important elastomeric composites. It is probable however that the particulate reinforcement of elastomers is not the result of any single phenomenon or molecular process. The dispersed rigid phase can influence mechanical behaviour in many ways depending upon the chemical and physical nature of the network and the chemical, physical and morphological characteristics of the particles. A number of so-called hydrodynamic and molecular theories have been proposed to account for filler reinforcement and the inevitable strain induced softening which accompanies it, these will be discussed next.

6.2.1 Hydrodynamic Theories of Smallwood and Guth

Early theories of reinforcement attempted to establish a relationship between the volume fraction of filler and the observed increase in stiffness. Studies of this type are derived mainly from the analogous problem of the increase in the viscosity of a liquid caused by a suspension of solid particles. In this approach the vulcanised rubber surrounding the filler particles is considered to be an isotropic elastic continuum having the same elastic properties as the rubber without filler. The rubber is assumed to adhere to the filler surface, and, by considering stresses in the neighbourhood of

particles, expressions can be derived relating the Young's modulus E_f of the filled rubber to E_0 the Young's modulus of the matrix. For spherical particles at low concentrations, Smallwood (1944) showed that at small strains

$$E_f = E_0\left(1 + 2.5V_f\right) \tag{6.1}$$

where V_f is the volume fraction of filler. Guth (1945) modified Equation (6.1) to account for particle interactions at higher volume fractions of filler by adding an extra term involving the square of the volume fraction, such that

$$E_f = E_0\left(1 + 2.5V_f + 14.1V_f^2\right) \tag{6.2}$$

This equation fitted the data for fine thermal blacks up to volume fractions of 0.3. However for more strongly reinforcing fillers serious departures from Equation (6.2) were observed. Guth suggested that this was due to the asymmetric nature of the aggregates of carbon black and modified the above relation to include a shape factor, η , the ratio of the length to the width of the aggregates

$$E_f = E_0\left(1 + 2.5\eta V_f + 14.1\eta^2 V_f^2\right) \tag{6.3}$$

with a proper choice for the value of η this equation gives fair agreement with the modulus-volume fraction data for many systems. The marked softening caused by prestretching is attributed to a reduction in η and is therefore considered to be influenced by the presence of transient carbon black structure. In an alternative correction of the Guth-Smallwood relation proposed Medalia (1972) the "occluded rubber" volume is added to the actual filler volume to obtain the "effective" volume of the rigid phase. Medalia demonstrated that this procedure leads to a significant improvement in the agreement of Equation (6.2) with experimental data. "Occluded rubber" was defined by Medalia as the elastomeric matrix which penetrated the void space of individual aggregates of carbon black, thereby partially shielding it from deformation.

6.2.2 Strain-amplification theory of Mullins *et al*

In a series of papers by Mullins and Tobin (1965), Harwood, Mullins and Payne (1965) and Harwood and Payne (1966a,b) the authors proposed a theory for materials that undergo strain induced crystallisation, based on the notion of strain amplification. The authors argued that since the particles of filler are considerably more rigid than the surrounding matrix the local strain in the matrix must be larger than the overall measured strain, thus causing an increase in stress and an associated increase in the observed stiffness. Various strain amplification factors have been suggested. Mullins and Tobin (1965) proposed the use of the Guth-Smallwood Equation (6.2) to estimate the effective strain λ' in the rubber matrix,

$$\lambda' = \lambda\left(1 + 2.5V_f + 14.1\,V_f^2\right). \tag{6.4}$$

This factor agrees with the available experimental data only for large-particle size thermal blacks at moderate strains. For reinforcing blacks one must assume abnormally large shape factors in the modified form of the Guth-Smallwood Equation (6.3), to obtain better agreement, or use an adjusted filler volume fraction. Mullins and Tobin attribute the softening observed in their experimental data to strain induced crystallisation. There are however several limitations to the work and Mullins and Tobin. Firstly there are doubts as to whether Equation (6.4) can apply at finite strains, Rigbi (1980) has argued that at strains as low as 10% the Guth-Smallwood factor is not even approximately applicable for any carbon black except N-990. Secondly the theory proposes that the Mullins effect arises from strain induced crystallisation, whereas it is known that the effect also occurs in materials that do not undergo strain induced crystallisation.

6.2.3 Blanchard and Parkinson mechanisms

A completely different approach to the problem was pursued in the work of Blanchard and Parkinson (1952), who argued that strain amplification could not provide a satisfactory explanation of the reinforcing effect of fillers. Instead Blanchard and Parkinson speculated that the reinforcing effect of fillers was due to the formation of strong and weak linkages between the rubber network and filler particles. They attributed the strain induced softening or Mullins effect to the breakage of weak

linkages. The strength of the weak linkages was estimated from the energy consumed to obtain varying degrees of softening up to the point of rupture. Strength and reinforcement were attributed to the relatively few strong linkages that survived up to rupture.

6.2.4 Bueche's Interparticle Chain Breakage Mechanism

Bueche (1960,1961) proposed a mechanism of stress softening and reinforcement based on the simple concept of the breakage of network chains, or their attachments to adjacent filler particles. These interparticle chains have a distribution of lengths, the shorter of which are considered to rupture first. Since the stress on a chain in the fully extended state just before rupture is large, it contributes greatly to the stiffness or modulus. Bueche argued that chains broken on the first stretch would not be able to affect the stiffness on the second stretch and so softening will occur. In addition to chain breakage, Bueche mentions another possible process of softening involving the movement of filler particles through the surrounding matrix, particularly important at high temperatures and in slow tests. It is proposed that small motions of filler particles are sufficient to release most of the tension on highly extended chains. Bueche attributes the increase in strength to the filler particles acting effectively as a means of distributing the load more equitably. The breakage of a single chain between particles does not cause the stress to be transferred to the relatively few adjacent chains-as for an unfilled network, but the stress is distributed to the much larger number of chains attached to the filler particles. Except for the emphasis on chain breakage and the omission of chain alignment, Bueche's reinforcement processes are similar to those in the molecular slippage mechanism.

6.2.5 Molecular Slippage Mechanism

Dannenburg (1974) proposed a mechanism of reinforcement and softening which assumes that under stress, the surface absorbed network segments move relative to the surface, accommodating the imposed stress and preventing molecular chain rupture. As a consequence of this movement or slippage process, the stress is redistributed to the neighbouring molecules. It is argued by Dannenburg that stress redistribution in this way results in molecular chain alignment and increased strength. Dannenburg considers this process to first absorb strain energy, and then dissipate it as frictional

heat, and in this manner act as a source of hysteresis. Energy requirements for rupture processes are thus increased by the dissipation of a portion of the strain energy as heat.

6.3 Continuum models

Although the mechanisms that give rise to the Mullins effect have been the subject of intensive research, few attempts seem to have been made to formulate continuum models suitable for incorporation into numerical procedures for the simulation of large scale problems. Standard hyperelastic models by themselves are of only limited usefulness in the description of the behaviour of filled elastomers because of their failure to capture the strain induced loss of stiffness to which these materials are subject. One approach often adopted to avoid this phenomenon is to apply a prestretch up to a specified maximum strain. This process known in industry as scragging has the effect of increasing the reproducibility of the stress-strain response, at least up to the maximum previously attained strain. Standard hyperelastic formulations may then be used to describe the behaviour of the damaged material. A more recent development is a class of theory that relies on continuum damage mechanics to account for strain induced softening. These theories offer the distinct advantage of being able to describe the behaviour of filled elastomers in the virgin and damaged states. A number of theories of this type have been proposed, though differing in origin each assumes softening to result from the evolution of internal damage, these theories will be discussed next.

6.3.1 Gurtin and Francis 1-D Phenomenological Damage Model

One of the earliest models to account for the Mullins effect in filled elastomers using damage mechanics was that of Gurtin and Francis (1981). Gurtin and Francis proposed a one-dimensional model in which the current state of internal damage is characterised by the maximum axial strain, ε^m, attained up to the present time t:

$$\varepsilon^m(t) = \max_{0 \le s \le t} \{\varepsilon(s)\} \tag{6.5}$$

The axial stress $\sigma(t)$ is defined via a constitutive equation of the form

$$\sigma(t) = \mathrm{g}\left(\varepsilon(t), \varepsilon^{m}(t)\right) \tag{6.6}$$

and hence depends only on the current values of strain and damage. For the material examined in their work (a highly filled elastomeric compound) Gurtin and Francis proposed a specialised form of Equation (6.6), which may be written as follows

$$\sigma(t) = \bar{\mathrm{f}}(\zeta)\,\bar{\mathrm{g}}(\varepsilon^{m}) \tag{6.7}$$

where ζ is the relative strain, defined as

$$\zeta = \frac{\varepsilon}{\varepsilon^{m}} \tag{6.8}$$

and the function $\bar{\mathrm{f}}(\zeta)$, named the master damage curve, defines the loss of stiffness experienced by filled elastomers at strain levels below the previously attained maximum strain ε^{m}.

The function $\bar{\mathrm{f}}(\zeta)$ satisfies the condition

$$\bar{\mathrm{f}}(1) = 1 \tag{6.9}$$

So that when the maximum strain occurs at the current time $(\varepsilon = \varepsilon^{m})$ the uniaxial stress is given by

$$\sigma = \bar{\mathrm{g}}(\varepsilon^{m}) \tag{6.10}$$

The stress strain curve defined by Equation (6.10) is called the virgin curve. To characterise the material parameters for this model it is necessary to determine both the virgin and master damage curves. The virgin curve may be obtained from uniaxial loading experiments and the master damage curve from unloading experiments. Although Equation (6.7) can reproduce single cycle hysteresis, such an expression suffers from the serious drawback that over a wide range of strain rates, hysteresis associated with viscous effects is incorrectly attributed to Mullins effect.

6.3.2 Simo's 3-D Finite Strain Isotropic Damage Model

A generalisation of Equation (6.6) to three-dimensions has been proposed in the work Simo (1987). In common with the approach of Gurtin and Francis, the current state of internal damage is governed by the maximum strain previously attained. This notion is extended to 3-D by introducing an equivalent strain ε_{eq} as a scalar measure of the maximum strain. The equivalent strain ε_{eq} is defined as

$$\varepsilon_{eq}(s) = \sqrt{2\hat{W}_0\left(\mathbf{E}(s)\right)} \tag{6.11}$$

where $\hat{W}_0\left(\mathbf{E}(s)\right)$ is a function representing the effective strain energy of the undamaged material, and $\mathbf{E}(s)$ the Green strain at time s. The degree of internal damage is controlled by the maximum value of the equivalent strain ε_{eq}^m attained up to the present time t:

$$\varepsilon_{eq}^m(t) = \max_{0\le s\le t}\{\varepsilon_{eq}(s)\} \tag{6.12}$$

For a material initially characterised by a general strain energy function W_0 undergoing an isotropic damage process the constitutive response is defined via a strain energy function of the form

$$\hat{W}(\mathbf{E}, d) = (1-d)W_0 \qquad with \qquad W_0 = \hat{W}_0(\mathbf{E}) \tag{6.13}$$

where d is the damage parameter and $(1-d)$ a reduction factor of the form suggested by Kachanov (1986). The damage variable d is described by the equation

$$d = \hat{d}(\varepsilon_{eq}^m) \tag{6.14}$$

where $\hat{d}$ is a shape function relating the current state of internal damage to the maximum equivalent strain. In this model no account is made of the limited degree of damage that occurs at values of the effective strain energy below the previously attained maximum, *i.e.* the damage accumulates discontinuously. However Miehe (1995) has suggested an additional contribution to the damage evolution governed by

the arclength of the effective strain energy W_0 . This part of the damage is assumed to accumulate continuously during a cyclic loading history.

6.3.3 Govindjee and Simo Phenomenological/Micromechanical Model

Govindjee and Simo (1992) proposed a phenomenological model, which approximates the response of a more complex micromechanically based model previously developed by the authors. The micromechanical mechanism for the Mullins effect that is followed in this work was originally proposed in varying form by Bueche (1960), Dannenburg (1975) and Rigbi (1980). Unlike the model of Simo (1987) the current state of internal damage is governed by the maximum principal stretch previously attained during the loading history. The model consists of a free energy function W for the composite system that depends upon the volume average principal stretches, λ_A, and a scalar damage variable, χ , *i.e.* isotropic damage. The strain energy of the system is split into two parts and is given by

$$W(\lambda_A, d) = (1 - V_f)\left[W_{cc}(\lambda_A^M) + W_{pp}(\lambda_A^M, \chi)\right] \tag{6.15}$$

where W_{cc} represents the strain energy of the polymer chains that crosslinked at both ends (given in their work by the Ogden model : Ogden (1972a)), and W_{pp} represents the strain energy of the polymer chains that are attached on both ends to the carbon black particles, V_f is the volume fraction of filler particles, and λ_A^M are volume average stretches averaged over the polymer matrix volume. Polymer chains that do not fall into the two classes mentioned above are assumed to be accounted for by the effective material properties. The relation between the volume average stretch and the matrix volume average stretch is given by

$$\lambda_A^M = \frac{\lambda_A - V_f}{1 - V_f} \tag{6.16}$$

Govindjee and Simo demonstrated that a model of this form can accurately reproduce the load drop at a given level of strain due to an extension to a higher strain by comparison with the experimental data of Mullins (1957) and Bueche (1961).

However a major drawback of such an approach is its complexity, 12 material parameters are required to completely define the response of the model, 6 to describe the non-linear elastic response given by the Ogden model (though these are actually obtained by performing a curve fit to the multiaxial behaviour of the 3 chain model of James and Guth(1943)) and a further 6 parameters to describe the evolution of damage.

6.4 Extension of non-Gaussian Network Models to account for the Mullins Effect

In this section we describe a simple method by which the 3 and 8 chain non-Gaussian models may be extended to reproduce the strain induced softening observed in filled elastomers. The approach employed is similar to that outlined in the work of Simo (1987) and Miehe (1995). Although the approach is purely phenomenological in origin, it has the advantage of much greater simplicity when compared with the method of Govindjee and Simo (1992). As in chapter 4, discussion is initially limited to the development of constitutive relationships for the analysis of plane stress problems, where the incompressibility constraint may be employed to eliminate the arbitrary hydrostatic stress in Equation (4.54). Later in the chapter consideration is also given to the development of relations suitable for the analysis of three-dimensional problems.

6.4.1 Constitutive Equations (2-D general plane stress formulation)

Consider first the development of constitutive relations compatible with the family of two-dimensional plane stress elements provided by ABAQUS. Let W denote the free energy, assumed to be given by the constitutive expression

$$\hat{W}(\mathbf{E}, d) = (1 - d)\, W_0 \qquad with \qquad W_0 = \hat{W}_0(\mathbf{E}) \tag{6.17}$$

in terms of an effective strain energy function W_0, where $\mathbf{E}$ represents the Green strain and d is a scalar internal variable which describes an isotropic damage effect characterised by an elastic softening of the material. The effective strain energy function W_0 for the incompressible forms of the 3 and 8 chain non-Gaussian network

models are given by Equation (3.54) and (3.59), respectively. The second Piola-Kirchhoff stresses for the constitutive expression given in Equation (6.17) may be derived via Equation (2.43), to yield

$$\mathbf{S} = (1-d)\,\mathbf{S}_0 \qquad \text{with} \qquad \mathbf{S}_0 = \frac{\partial W_0}{\partial \mathbf{E}} \tag{6.18}$$

Using Equation (2.41) the above relation may be transformed to give the equivalent expression in terms of Cauchy stresses

$$\boldsymbol{\sigma} = (1-d)\,\boldsymbol{\sigma}_0 . \tag{6.19}$$

Here we denote $\boldsymbol{\sigma}$ as the nominal stress and $\boldsymbol{\sigma}_0$ as the effective stress. The effective Cauchy stress tensor $\boldsymbol{\sigma}_0$ for the 3 and 8 chain models can be obtained as in chapter 4, using the principal axes technique. The principal effective Cauchy stresses are determined first using either Equation (4.77) or (4.88), and then rotated to the base coordinate frame using Equation (4.95).

6.4.1.1 Damage Force

The Clausius-Duhem inequality for internal dissipation reads $\mathbf{S} : \dot{\mathbf{E}} - \dot{W} \geq 0$. Time differentiation of Equation (6.17) yields, $\dot{W} = (1-d)\,\partial_{\mathbf{E}} W_0 : \dot{\mathbf{E}} - W_0\,\dot{d}$, where $\partial_{\mathbf{E}} W_0$ indicates the derivative with respect to $\mathbf{E}$, insertion of this equation into the expression for internal dissipation gives $[\mathbf{S} - (1-d)\,\partial_{\mathbf{E}} W_0\,] : \dot{\mathbf{E}} + W_0\,\dot{d} \geq 0$. Thus the Clausius-Duhem inequality is reduced to

$$f\,\dot{d} \geq 0 \qquad \textit{with} \qquad f = \hat{W}_0\,(\mathbf{E}), \tag{6.20}$$

where by definition f is the thermodynamic variable conjugate to the damage variable d. We denote f as the thermodynamic force, which drives the damage evolution. Here f is identical to the strain energy of the undamaged material and its evolution

$$\dot{f} = \mathbf{S}_0 : \dot{\mathbf{E}} \tag{6.21}$$

is the same as the effective stress power of the undamaged material. Since f is always positive , the inequality requires that $\dot{d} \geq 0$. Damage defined in this way can therefore only increase or remain constant. Therefore the phenomenon of recovery of the elastic modulus, observed when filled elastomers are allowed to rest at high temperature is not permitted within the current model.

6.4.1.2 Damage Evolution

In order to complete the damage model it is necessary to determine an evolution equation for the internal damage variable d. Following the approach of Simo (1987) a Mullins effect type discontinuous damage evolution is assumed, where the damage accumulation occurs only within the first cycle of a strain controlled loading process. Further strain cycles below a maximum strain energy do not contribute to this type of damage. The damage variable d is described by the constitutive equation

$$d = \hat{d}(\alpha) \tag{6.22}$$

Here $\hat{d}(\alpha)$ is a monotonicly increasing smooth function with the properties $\hat{d}(0) = 0$ and $\hat{d}(\infty) = 1$. $\hat{d}(\alpha)$ can be considered a shape function relating the damage variable d to a new variable α which describes discontinuous damage. The new variable α is defined as

$$\alpha(t) = \max_{0 \leq s \leq t} f(s) \tag{6.23}$$

Thus α is simply the maximum thermodynamic force or effective strain energy which has been achieved up to the current time t. The evolution of Equation (6.23) becomes

$$\dot{\alpha} = \begin{cases} \dot{f} = \mathbf{S}_0 : \dot{\mathbf{E}} & for \quad f - \alpha = 0 \quad \wedge \quad \dot{f} > 0 \\ 0 & otherwise \end{cases} \tag{6.24}$$

with the initial condition that $\alpha(0) = 0$. This underlines the discontinuous character of this damage effect. There is no damage accumulation if the thermodynamic force f

lies inside the damage domain. Following the approach of Miehe (1995) the damage function $\hat{d}(\alpha)$, is assumed to have the saturation form

$$\hat{d}(\alpha) = d_{\alpha}^{\infty}\left[1 - \exp\left(-\frac{\alpha}{\eta_{\alpha}}\right)\right] \tag{6.25}$$

The constant d_{α}^{∞} dictates the maximum possible damage, thus there is the restriction that $0 \le d_{\alpha}^{\infty} \le 1$. The constant η_{α} referred to as the damage saturation parameter specifies the approach to the maximum state of damage.

The only remaining problem is the computation of an appropriate Jacobian matrix. We commence by first determining the tangent of the second Piola-Kirchhoff stress and then use Equation (2.52) to transform this result to the tangent of the Truesdell rate. Using the chain rule in conjunction with Equation (2.45), the tangent of the second Piola-Kirchhoff stress is given by

$$\mathscr{D}^{K2} = (1-d)\frac{\partial^2 W_0}{\partial \mathbf{E}^2} - e\frac{\partial W_0}{\partial \mathbf{E}} \otimes \frac{\partial W_0}{\partial \mathbf{E}} = (1-d)\mathscr{D}_0^{K2} - e\,\mathbf{S}_0 \otimes \mathbf{S}_0 \tag{6.26}$$

The second term in Equation (6.26) represents the softening effect due to the progress of damage. The continuous tangent factor e is given by

$$e = \begin{cases} \hat{d}'(\alpha) & \textit{for} \quad f - \alpha = 0 \quad \wedge \quad \dot{f} > 0 \\ 0 & \textit{otherwise} \end{cases} \tag{6.27}$$

where $\hat{d}'(\alpha)$ is given by

$$\hat{d}'(\alpha) = \frac{d_{\alpha}^{\infty}}{\eta_{\alpha}}\exp\left(-\frac{\alpha}{\eta_{\alpha}}\right) \tag{6.28}$$

Using Equation (2.52) the tangent of the second Piola-Kirchhoff stress can be pushed forward to give the tangent of the Truesdell rate

$$\mathscr{D}^{T} = (1-d)\mathscr{D}_0^{T} - e\,\boldsymbol{\sigma}_0 \otimes \boldsymbol{\sigma}_0 \tag{6.29}$$

We denote $\mathscr{D}^T$ and $\mathscr{D}_0^T$ as the nominal and effective tangents of the Truesdell rate. The effective tangent of the Truesdell rate $\mathscr{D}_0^T$ for the 3 and 8 chain models can be obtained using a similar approach to that adopted in Chapter 4. The principal components of the effective tangent of the Truesdell rate are determined first using either Equations (4.79)-(4.81) or (4.91)-(4.94), and then rotated back to the base coordinate frame using Equation (4.102). The tangent of the Truesdell rate $\mathscr{D}^T$ is finally transformed to the tangent of the Jaumann rate $\mathscr{D}^J$, using Equation (4.104).

6.4.2 Constitutive Equations (3-D formulation)

We now consider the development of constitutive relations suitable for the analysis of three-dimensional problems. Based on the multiplicative split introduced in Equation (5.1), an uncoupled constitutive representation of the free energy function is assumed

$$\hat{W}(\mathbf{E}, d) = (1-d)\, W_0^{dev} + \hat{W}^{vol}(J) \qquad with \qquad W_0^{dev} = \hat{W}_0^{dev}(\tilde{\mathbf{E}}) \tag{6.30}$$

where W_0^{dev} describes the change in the effective strain energy of the undamaged material due solely to the deviatoric deformation, and W^{vol} the change due to volume change. Thus Equation (6.30) restricts the damage phenomenon to the deviatoric part of the deformation while the volumetric behaviour is assumed to be elastic. The effective deviatoric strain energy functions for the 3 and 8 chain network models are similar to those given in Equation (5.8) and (5.10), while the volumetric strain energy function is identical to that given Equation (5.5). The split of the nominal free energy into deviatoric and volumetric components also leads to an additive split of the nominal Cauchy stress

$$\boldsymbol{\sigma} = (1-d)\, \boldsymbol{\sigma}_0^{dev} + \boldsymbol{\sigma}^{vol}. \tag{6.31}$$

Here we denote $\boldsymbol{\sigma}$ the nominal stress, $\boldsymbol{\sigma}_0^{dev}$ the effective deviatoric stress and $\boldsymbol{\sigma}^{vol}$ the volumetric stress. The effective deviatoric stress $\boldsymbol{\sigma}_0^{dev}$ for the 3 and 8 chain models can be obtained as in chapter 5, using the principal axes technique. The principal effective deviatoric Cauchy stresses are determined first using either Equation (5.16) or (5.33), and then rotated to the base coordinate frame using Equation (5.37). The

volumetric stresses are determined from Equation (5.17). The deviatoric and volumetric contributions are then summed to give the nominal Cauchy stress.

The thermodynamic force $f \geq 0$ conjugated to d is now assumed to be the deviatoric effective strain energy W_0^{dev} of the undamaged material. Equation (6.20) and (6.21) are therefore replaced by

$$f = \hat{W}_0^{dev}(\tilde{\mathbf{E}}) \qquad and \qquad \dot{f} = \mathbf{S}_0^{dev} : \mathbf{E} . \tag{6.32}$$

The split of the nominal free energy also results in a additive split of the tangent of the Truesdell rate of Kirchhoff stress

$$\mathscr{D}^{TK} = \mathscr{D}^{TK,dev} + \mathscr{D}^{TK,vol} . \tag{6.33}$$

The deviatoric part of Equation (6.33) has a structure analogous to Equation (6.29) and has the form

$$\mathscr{D}^{TK,dev} = (1-d)\mathscr{D}_0^{TK,dev} - e\ \boldsymbol{\tau}_0^{dev} \otimes \boldsymbol{\tau}_0^{dev} \tag{6.34}$$

where $\boldsymbol{\tau}_0^{dev}$ is the effective deviatoric Kirchhoff stress, *i.e.* $\boldsymbol{\tau}_0^{dev} = J\boldsymbol{\sigma}_0^{dev}$. The second term in Equation (6.34) only appears in the case of damage loading. The effective deviatoric tangent of the Truesdell rate of Kirchhoff stress $\mathscr{D}_0^{TK}$, for the 3 and 8 chain models can be obtained using a similar approach to that presented in chapter 5. The principal components of the effective deviatoric tangent of the Truesdell rate of Kirchhoff stress are determined first using either Equations (5.21)-(5.22) or (5.34)-(5.35), and then rotated to the base coordinate frame using a similar matrix transformation as that given in Equation (5.28). The volumetric component of the tangent of the Truesdell rate of Kirchhoff stress, $\mathscr{D}^{TK,vol}$, is identical to that given in section 5.1.4. The tangent of the Truesdell rate of Kirchhoff stress $\mathscr{D}^{TK}$ is finally transformed to the tangent of the Jaumann rate of Cauchy stress $\mathscr{D}^{JC}$, using Equation (5.46) and (5.48).

6.5 Numerical Examples

6.5.1 Cyclic Tension Tests

In this section we compare the response of the 3 and 8 chain models which have been extended to display isotropic damage with the experimental data of Bueche (1961), for cyclic tension tests on 30 HAF SBR. In the work of Bueche the material was loaded to a stretch of 3 then unloaded, then loaded again to a stretch of 4, and finally unloaded. All of the data points were recorded in the quasi-static state to remove viscous effects. The material constants used here were obtained via a least square fit to the plane stress versions of the 3 and 8 chain models. Numerical tests were performed using both CPS4 and C3D8I element types, to check the accuracy of the plane stress and three-dimensional formulations. For the three-dimensional analysis a Poisson's ratio of $\nu = 0.4999$ was assumed to simulate an almost incompressible response. The results of the analyses are compared with the experimental data of Bueche in Figure 6.2 and 6.3. Note that the first unloading cycle is indicated by the boxes and the second by the diamonds. Agreement between the plane stress and three-dimensional versions of the same model is excellent, as would be expected. Taking into account the simplicity of the damage evolution equation that has been employed, the 3 and 8 chain damage models are observed to provide a good approximation of the experimental data of Bueche.

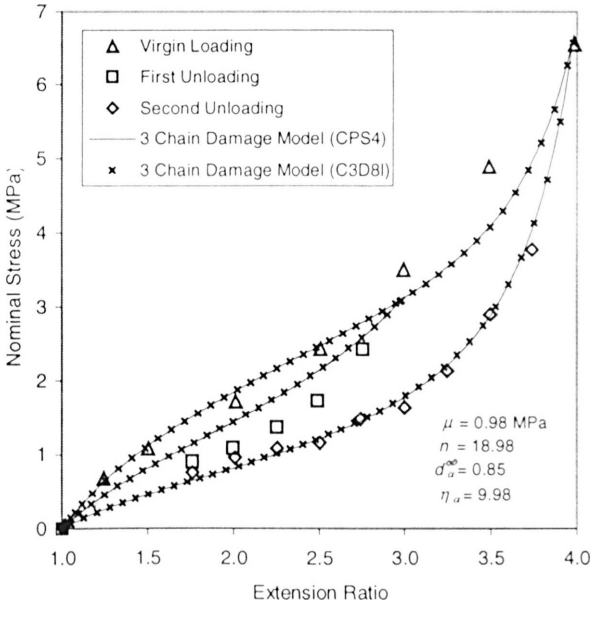


Figure 6.2 : Comparison of 3 chain damage model with the experimental data of Bueche.

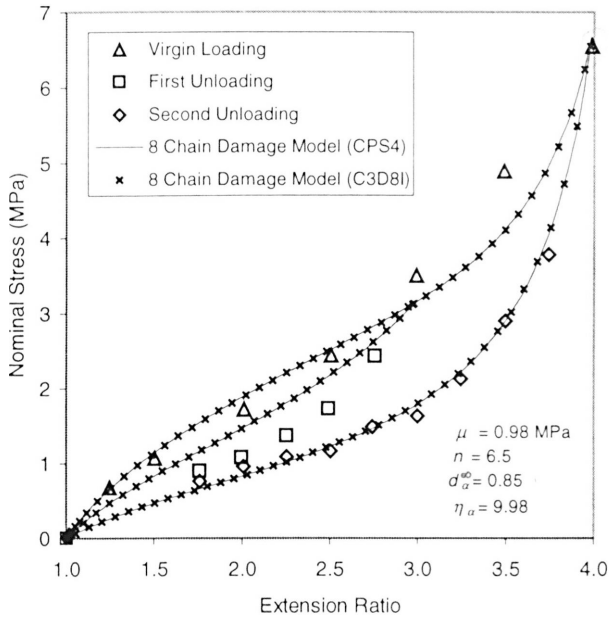


Figure 6.3 : Comparison of 8 chain damage model with the experimental data of Bueche.

6.5.2 Stretching of a square sheet with a central circular hole

This example illustrates the stretching of a square sheet with a circular hole. The problem is analysed using the plane stress formulations for the 3 and 8 chain models incorporating isotropic damage. The geometry of the sheet is the same as in section 4.7.2. One quarter of the sheet is modelled using 1000 CPS3, 3-noded continuum plane stress elements. The material constants employed come from a least square fit to the experimental data of Bueche (1961), and are the same as those given in the previous example. Figure 6.4 and 6.5 show contour plots of the damage variable d on the undeformed configuration, after a stretch to λ=3. Both figures demonstrate an inhomogeneity near the circular hole with a high value of accumulated damage.

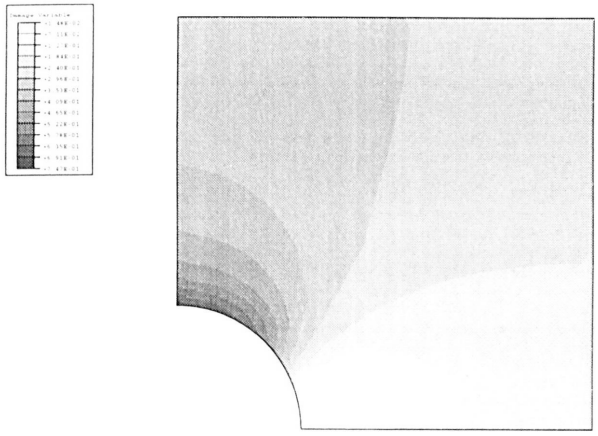


Figure 6.4 : Sheet with circular hole, 3 chain model, contour of damage variable d.

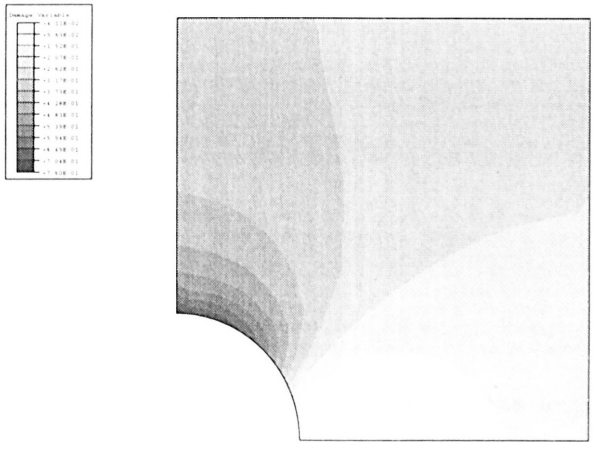


Figure 6.5 : Sheet with circular hole, 8 chain model, contour of damage variable d.

6.6 Final Remarks

Using continuum damage mechanics, the 3 and 8 chain models have been extended to account for the strain induced softening that occurs in filled elastomers by the introduction of an isotropic dam age mechanism into the constitutive formulations. Discussions were initially limited to the development of constitutive relations suitable for the analysis of plane stress problems, where the incompressibility constraint was employed to eliminate the arbitrary hydrostatic pressure, which arises in the analysis of volume preserving materials. Later in the chapter relations were also derived for the analysis of three-dimensional problems, by introduction a degree of material compressibility. A comparison of the experimental data of Bueche (1961) and the response of the modified network models indicates that despite the simplicity of the damage evolution equations which have been employed, the models still provide a good approximation of the material behaviour.

Chapter 7

7. Viscoelasticity

7.1 Introduction

In the discussion of the mechanical behaviour of elastomers in previous chapters we ignored the time dependent nature of these materials and considered only the equilibrium or long term response. We now extend the discussion by considering the contribution made by time dependent processes. The chapter commences with a discussion of two of the most prominent features of the time dependent behaviour of elastomeric materials, creep and stress relaxation, and leads on to a brief review of the constitutive theories that have been proposed to describe the phenomena. In the second half of the chapter the kinetic theory of rubber elasticity (in the form of the 3 and 8 chain non-Gaussian network models) is generalised to include time dependent effects in a similar manner to that proposed by Christensen (1980) and O'Dowd and Knauss (1995). To enhance the ability of the proposed model to predict the behaviour of filled elastomers, the Mullins effect is also accounted for, via the inclusion of an isotropic damage mechanism, introduced into the constitutive formulation of the 3 and 8 chain models in the previous chapter. The chapter concludes with a comparison of published experimental data and the response of the proposed models.

7.2 Stress Relaxation and Creep

Creep is defined as the time dependent change in strain following a step change in stress. However unlike the creep phenomenon observed in metals, creep in elastomeric solids is almost completely recoverable after unloading. Stress relaxation on the other hand is defined as the time dependent change in stress following a step change in strain. It is important to appreciate that there are two distinct causes for the phenomena of creep and stress relaxation: the first is physical and the second is chemical. The physical effect is due the viscoelastic nature of elastomeric materials, *i.e.* the response to a stress or strain is not instantaneous but develops with time, and is discussed in more detail the next section. The chemical effect is due to ageing of the elastomer by oxidative chain scission. In practice it is often rather difficult to distinguish between the two, and as pointed out by Brown (1996) it could be argued that, if experimental measurements are conducted under the same conditions as in service, it matters relatively little what caused, e.g. the creep, as long as it can be measured. However if any form of accelerated conditioning, such as increased temperatures, are employed it follows that results could be very misleading. Generally, physical effects are dominant at short times and low temperatures and the chemical effects are more apparent at longer times and higher temperatures.

7.3 Linear Viscoelasticity and the Superposition Principal

A cornerstone of the theory of linear viscoelasticity is the Boltzmann superposition principal. This principal states that the total deformation produced at any time due to a complex loading history is the sum of the deformations of each of the individual loads, removal of a load being regarded as the application of a negative load. For a linearly viscoelastic body deformed in simple shear this principal may be expressed in the form of a constitutive relationship, given by

$$\sigma_{12}(t) = \int_{-\infty}^{t} \mu(t-u) \frac{d\gamma_{12}(u)}{du} du = \int_{-\infty}^{t} \mu(t-u)\, \dot{\gamma}_{12}(u)\, du \tag{7.1}$$

where σ_{12} is the time dependent shear stress, $\dot{\gamma}_{12}$ is the shear strain rate and μ is known as the shear relaxation modulus. In simple shear the change in shape is not accompanied by any change in volume. However in other deformation states changes

in volume may occur. To describe the mechanical behaviour under such conditions it is necessary to introduce a more complicated constitutive equation including all of the components the stress tensor. For (initially) isotropic materials the small strain or engineering stress in that context is given by

$$\boldsymbol{\sigma}(t) = \int_{-\infty}^{t} 2\mu(t-u)\frac{d\boldsymbol{\varepsilon}(u)}{du}du + \mathbf{I}\int_{-\infty}^{t} K(t-u)\frac{d\theta}{du}du \tag{7.2}$$

where $\boldsymbol{\sigma}$ is the time dependent stress tensor, $\boldsymbol{\varepsilon}$ is the deviatoric strain tensor, θ is the volumetric strain and μ and K are the shear and bulk relaxation moduli respectively. The latter are the only (mutually independent) two functions that need to be evaluated in order to determine the response of the material to any deformation history. For many elastomeric materials the relaxation functions μ and K are well represented in the form of the Prony series, *i.e.*

$$\mu(t-u) = \mu_{\infty} + \sum_{j=1}^{N^{\mu}} \mu_j \exp\left\{\frac{-(t-u)}{\xi_j^{\mu}}\right\} \tag{7.3}$$

$$K(t-u) = K_{\infty} + \sum_{j=1}^{N^{K}} K_j \exp\left\{\frac{-(t-u)}{\xi_j^{K}}\right\} \tag{7.4}$$

where μ_{∞} and K_{∞} denote the long term shear and bulk response and μ_j and K_j are components of the viscous part of the shear and bulk moduli with the relaxation times ξ_j^{μ} and ξ_j^{K} respectively. A more detailed discussion of linear viscoelasticity is provided in the work of McCrum *et al* (1988).

7.4 Finite Strain Viscoelasticity

The constitutive relation for linear viscoelasticity given by Equation (7.2) is not objective and so cannot provide an appropriate description of mechanical behaviour at finite strains. Several authors have however proposed theories for finite strain viscoelasticity (also referred to as non-linear viscoelasticity or viscohyperelasticity by some authors). In theories such as that of Chang (1976), time dependence is still described by the Boltzmann superposition integral (or equivalently by linear differential

equations with constant coefficients), but the infinitesimal strain measure is replaced by a finite strain measure. Christensen (1980) has also proposed a non-linear viscoelastic constitutive model for elastomers, which has limits of linear viscoelasticity under small strains and rubber elasticity at long times. A similar approach has also been pursued in the work of O'Dowd and Knauss (1995), in their model for the time dependent large principal deformation of polymers.

Among the various theories for finite strain viscoelasticity the most widely cited in connection with the non-linear FEA of elastomers appears to be that of Simo (1987). Simo assumed viscoelasticity in elastomeric materials to be mainly associated with deviatoric deformation and proposed a constitutive relation of the form

$$\mathbf{S}(t^{n+1}) = \mathbf{S}_{\infty}^{dev}(t^{n+1}) + \sum_{j=1}^{N} \mathbf{H}_{j}(t^{n+1}) + \mathbf{S}_{\infty}^{vol}(t^{n+1}) \tag{7.5}$$

where the first and second terms on the right hand side of Equation (7.5) represent the elastic and viscous components of the deviatoric second Piola-Kirchhoff stress tensor, respectively, and the last term represents the elastic volumetric component. A similar approach has also been employed in the work of and Govindjee and Simo (1992), Holzapfel (1996) and Kaliske and Rothert (1997). The description in the reference configuration is required in order to preserve the principal objectivity. In one-dimension this approach is analogous to a generalised Maxwell element, and may be represented pictorially as a collection of springs and dashpots, (see Figure 7.1).

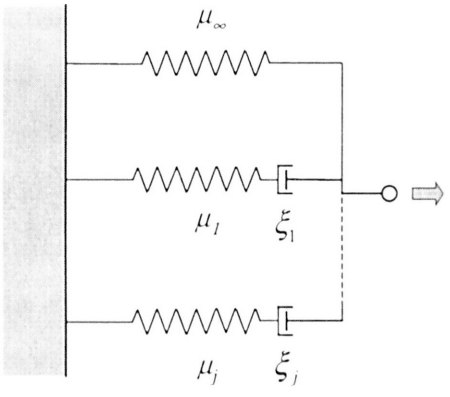


Figure 7.1 : Generalised Maxwell element.

The internal stress variables $\mathbf{H}_j$ are defined via the linear rate equation

$$\dot{\mathbf{H}}_j + \frac{1}{\xi_j}\mathbf{H}_j = \varsigma_j \dot{\mathbf{S}}_\infty^{dev} \tag{7.6}$$

which leads to the convolution integral

$$\mathbf{H}_j(t) = \varsigma_j \int_0^t \exp\left\{-\frac{(t-u)}{\xi_j}\right\} \frac{d\mathbf{S}_\infty^{dev}(u)}{du} du \tag{7.7}$$

Here ς_j represents the normalised shear modulus given by

$$\varsigma_j = \frac{\mu_j}{\mu_\infty} \tag{7.8}$$

7.5 Incorporation of time dependent effects in non-Gaussian network Models

Elastomers utilised in engineering applications are often subject to loading rates at or above the rate at which viscous relaxation mechanisms operate. As these materials usually contain a significant number of crosslinks the degree of viscoelasticity displayed is relatively small. Nevertheless since some viscoelasticity is exhibited it must be taken into account in any theory attempting to provide a general description of the mechanical behaviour of these materials. To this end we now adopt an approach similar to that proposed in the work of Christensen (1980) and O'Dowd and Knauss (1995) and extend the kinetic theory of rubber elasticity (in the form of the 3 and 8 chain non-Gaussian network models) to include rate effects, using the theoretical framework of finite strain viscoelasticity of Simo (1987). To enhance the ability of the proposed model to describe the mechanical behaviour of filled elastomers we also take into account the Mullins effect, via the inclusion of isotropic damage, introduced into the constitutive formulations for the 3 and 8 chain models in the previous chapter. Discussion is again initially limited to the development of relations for plane stress problems, where the incompressibility constraint is employed to eliminate the arbitrary hydrostatic stress in Equation (4.54). Later consideration is

also given to the development of relations suitable for the analysis of three-dimensional problems.

7.5.1 Constitutive Equations (2-D general plane stress formulation)

We commence as in the previous chapter by considering the development of constitutive relations compatible with the family of two dimensional plane stress elements provided by ABAQUS. Our starting point is the constitutive relationship of Simo (1987), given in Equation (7.5). Here the absence of volumetric strain that derives from the assumption of material incompressibility permits the use of the following two-term specialisation of Equation (7.5)

$$\mathbf{S}(t^{n+1}) = \mathbf{S}_{\infty}(t^{n+1}) + \sum_{j=1}^{N} \mathbf{H}_j(t^{n+1}) \tag{7.9}$$

The nominal elastic or equilibrium second Piola-Kirchhoff stress tensor, $\mathbf{S}_{\infty}$, in the above relation is defined as

$$\mathbf{S}_{\infty} = (1-d)\frac{\partial W_0}{\partial \mathbf{E}} = (1-d)\mathbf{S}_{0,\infty}. \tag{7.10}$$

where d is the damage variable. The effective strain energy function W_0 for the incompressible forms of the 3 and 8 chain non-Gaussian network models are given by Equations (3.54) and (3.59), respectively. The effective elastic second Piola-Kirchhoff stress tensor $\mathbf{S}_{0,\infty}$ for both models can be obtained using a similar approach to that adopted in chapter 6 to calculate the effective elastic Cauchy stress tensor. The principal effective elastic second Piola-Kirchhoff stresses are determined first from either Equation (3.54) or (3.59), using Equation (4.11), and then rotated to the base coordinate frame using the material equivalent of Equation (4.95).

The internal stress variables $\mathbf{H}_j$ are defined via linear rate equations similar to that given in Equation (7.6)

$$\dot{\mathbf{H}}_j + \frac{1}{\xi_j}\mathbf{H}_j = \varsigma_j \dot{\mathbf{S}}_{\infty} \tag{7.11}$$

and may be re-expressed in the form of a convolution integrals as

$$\mathbf{H}_j(t) = \varsigma_j \int_0^t \exp\left\{\frac{-(t-u)}{\xi_j}\right\} \frac{d\mathbf{S}_\infty(u)}{du} du \,. \tag{7.12}$$

To calculate the value of the second Piola-Kirchhoff stress tensor, $\mathbf{S}$, given in Equation (7.9), it is necessary to integrate Equation (7.12), for the internal stress variables $\mathbf{H}_j$. This may be achieved following a similar approach to that presented by Taylor *et al* (1970).

Consider the time interval $[t^n, t^{n+1}]$ with a time step $\Delta t = t^{n+1} - t^n$, utilising the multiplicative of the exponential expression

$$\exp\left\{-\frac{t^{n+1}}{\xi_j}\right\} = \exp\left\{-\frac{(t^n + \Delta t)}{\xi_j}\right\} = \exp\left\{-\frac{t^n}{\xi_j}\right\} \exp\left\{-\frac{\Delta t}{\xi_j}\right\} \tag{7.13}$$

and the separation of the deformation history into a period $0 \le u \le t^n$ when the result is known and into the current unknown time step $t^n \le u \le t^{n+1}$

$$\mathbf{H}_j(t^{n+1}) = \exp\left\{-\frac{\Delta t}{\xi_j}\right\} \varsigma_j \int_0^{t^n} \exp\left\{-\frac{(t^n - u)}{\xi_j}\right\} \frac{d\mathbf{S}_\infty(u)}{du} du + \varsigma_j \int_{t^n}^{t^{n+1}} \exp\left\{-\frac{(t^{n+1} - u)}{\xi_j}\right\} \frac{d\mathbf{S}_\infty(u)}{du} du \tag{7.14}$$

The integral in the first term of Equation (7.14) can be replaced by Equation (7.12) to yield

$$\mathbf{H}_j(t^{n+1}) = \exp\left\{-\frac{\Delta t}{\xi_j}\right\} \mathbf{H}_j(t^n) + \varsigma_j \int_{t^n}^{t^{n+1}} \exp\left\{-\frac{(t^{n+1} - u)}{\xi_j}\right\} \frac{d\mathbf{S}_\infty(u)}{du} du \tag{7.15}$$

an exact recursive formula for the current value of the stress quantity $\mathbf{H}_j(t^{n+1})$. The transition from differential coefficient to discrete time steps

$$\frac{d\mathbf{S}_\infty(u)}{du} = \lim_{\Delta s \to 0} \frac{\Delta \mathbf{S}_\infty(u)}{\Delta u} \lim_{\Delta t \to 0} \frac{\mathbf{S}_\infty(t^{n+1}) - \mathbf{S}_\infty(t^n)}{\Delta t} \tag{7.16}$$

introduces a time approximation of second order into the formula which was exact so far. The remaining expression

$$\mathbf{H}_j(t^{n+1}) = \exp\left\{-\frac{\Delta t}{\xi_j}\right\}\mathbf{H}_j(t^n) + \varsigma_j \int_{t^n}^{t^{n+1}} \exp\left\{-\frac{(t^{n+1}-u)}{\xi_j}\right\}\frac{\mathbf{S}_\infty(t^{n+1}) - \mathbf{S}_\infty(t^{n+1})}{\Delta t}\,du \tag{7.17}$$

may then be integrated analytically, to give

$$\mathbf{H}_j(t^{n+1}) = \exp\left\{-\frac{\Delta t}{\xi_j}\right\}\mathbf{H}_j(t^n) + \varsigma_j \frac{1-\exp\left\{-\dfrac{\Delta t}{\xi_j}\right\}}{\dfrac{\Delta t}{\xi_j}}\left[\mathbf{S}_\infty(t^{n+1}) - \mathbf{S}_\infty(t^n)\right] \tag{7.18}$$

In addition to the current elastic stress, $\mathbf{S}_\infty(t^{n+1})$, determination of the current value of the internal stress variables $\mathbf{H}_j(t^{n+1})$, requires knowledge of the quantities $\mathbf{H}_j(t^n)$ and $\mathbf{S}_\infty(t^n)$. Within the UMAT routines developed by the author $\mathbf{H}_j(t^n)$ and $\mathbf{S}_\infty(t^n)$ are stored as a state dependent variables for this purpose. Inserting Equation (7.18) into Equation (7.9) the complete stress update can be written as

$$\mathbf{S}(t^{n+1}) = \mathbf{S}_\infty(t^{n+1}) + \sum_{j=1}^{N^\mu} \exp\left\{-\frac{\Delta t}{\xi_j}\right\}\mathbf{H}_j(t^n) + \varsigma_j \frac{1-\exp\left\{-\dfrac{\Delta t}{\xi_j}\right\}}{\dfrac{\Delta t}{\xi_j}}\left[\mathbf{S}_\infty(t^{n+1}) - \mathbf{S}_\infty(t^n)\right] \tag{7.19}$$

The value of the Cauchy stress at the end of the increment is finally obtained by the push forward transformation of the second Piola-Kirchhoff stress, utilising the deformation gradient at the end of the increment

$$\boldsymbol{\sigma}(t^{n+1}) = \mathbf{F}(t^{n+1})\mathbf{S}(t^{n+1})\mathbf{F}^T(t^{n+1}). \tag{7.20}$$

The only remaining problem is the calculation of an appropriate Jacobian matrix. Following a similar approach to that in Chapter 6, we start by determining the tangent of the second Piola-Kirchhoff stress using Equation (2.45) and then employ Equation (2.52) to transform this result to the tangent of the Truesdell rate. Differentiating

Equation (7.19) with respect to Green strain yields the tangent of the second Piola-Kirchhoff stress, which may be expressed as follows

$$\mathscr{D}^{K2}(t^{n+1}) = \left[1 + \sum_{j=1}^{N^{\mu}} \varsigma_j \frac{1 - \exp\left\{ -\dfrac{\Delta t}{\xi_j} \right\}}{\dfrac{\Delta t}{\xi_j}} \right] \mathscr{D}_{\infty}^{K2}(t^{n+1}) \tag{7.21}$$

Here the elastic or equilibrium tangent of the second Piola-Kirchhoff stress, $\mathscr{D}_{\infty}^{K2}(t^{n+1})$, is given by

$$\mathscr{D}_{\infty}^{K2}(t^{n+1}) = (1 - d(t^{n+1}))\mathscr{D}_{0,\infty}^{K2}(t^{n+1}) - e\mathbf{S}_{0,\infty}(t^{n+1}) \otimes \mathbf{S}_{0,\infty}(t^{n+1}) \tag{7.22}$$

In Equation (7.22), d is the damage parameter and e is the same as that given in Equation (6.27). Using Equation (2.52) the tangent of the second Piola-Kirchhoff stress can be pushed forward to give the corresponding tangent of the Truesdell rate

$$\mathscr{D}^{T}(t^{n+1}) = \left[1 + \sum_{j=1}^{N^{\mu}} \varsigma_j \frac{1 - \exp\left\{ -\dfrac{\Delta t}{\xi_j} \right\}}{\dfrac{\Delta t}{\xi_j}} \right] \mathscr{D}_{\infty}^{T}(t^{n+1}) \tag{7.23}$$

From Equation (7.23) the important conclusion can be drawn that the structure of the viscoelastic tangent of the Truesdell rate, $\mathscr{D}^{T}(t^{n+1})$, is same as the accompanying elastic tangent, $\mathscr{D}_{\infty}^{T}(t^{n+1})$, merely modified by a scalar quantity. This result leads to a very efficient numerical implementation of the viscoelastic formulation. The elastic or equilibrium tangent of the Truesdell rate, $\mathscr{D}_{\infty}^{T}(t^{n+1})$, in Equation (7.23) is given by

$$\mathscr{D}_{\infty}^{T}(t^{n+1}) = (1 - d(t^{n+1}))\mathscr{D}_{0,\infty}^{T}(t^{n+1}) - e\boldsymbol{\sigma}_{0,\infty}(t^{n+1}) \otimes \boldsymbol{\sigma}_{0,\infty}(t^{n+1}) \tag{7.24}$$

The effective elastic tangent of the Truesdell rate $\mathscr{D}_{0,\infty}^{T}(t^{n+1})$ for the 3 and 8 chain models can be obtained following a similar approach to that used in chapter 6. The principal components of the effective tangent of the Truesdell rate are determined first

and then rotated back to the base coordinate frame. The tangent of the Truesdell rate, $\mathscr{D}^T(t^{n+1})$, is finally transformed to the tangent of the Jaumann rate, $\mathscr{D}^J(t^{n+1})$, using Equation (4.104). Lastly, it is worth mentioning that although the algorithm that has just been outlined requires knowledge of the principal directions of both the material and spatial configurations, it is not necessary to calculate both by diagonalisation methods. If the principal directions of one configuration are known then the principal directions of the other can be found trivially via polar decomposition of the deformation gradient.

7.5.2 Constitutive Equations (3-D formulation)

We now consider the development of constitutive relations suitable for the analysis of three-dimensional problems. Our starting point is again the constitutive relationship of Simo (1987) given by Equation (7.9), which relies on the multiplicative split of the deformation gradient introduced in chapter 5.

$$\mathbf{S}(t^{n+1}) = \mathbf{S}_{\infty}^{dev}(t^{n+1}) + \sum_{j=1}^{N} \mathbf{H}_j(t^{n+1}) + \mathbf{S}_{\infty}^{vol}(t^{n+1}) \tag{7.25}$$

Here $\mathbf{S}_{\infty}^{dev}$ denotes the nominal elastic deviatoric second Piola-Kirchhoff stress tensor, $\mathbf{H}_j$ the internal stress variables and $\mathbf{S}_{\infty}^{vol}$ the elastic volumetric stress. Equation (7.25) restricts damage and rate effects to the deviatoric part of the deformation while the volumetric behaviour is assumed rate independent. The nominal elastic deviatoric second Piola-Kirchhoff stress tensor, $\mathbf{S}_{\infty}^{dev}$, is defined as

$$\mathbf{S}_{\infty}^{dev} = (1-d)\frac{\partial W_0^{dev}}{\partial \mathbf{E}} = (1-d)\mathbf{S}_{0,\infty}^{dev}. \tag{7.26}$$

where the effective deviatoric strain energy function, W_0^{dev}, for the compressible forms of the 3 and 8 chain models are given by Equation (5.8) and (5.10), respectively. The effective elastic deviatoric second Piola-Kirchhoff stress tensor, $\mathbf{S}_{0,\infty}^{dev}$, can be obtained following a similar approach to that adopted in the previous chapter to calculate the effective elastic deviatoric Cauchy stress tensor. The principal effective elastic

deviatoric second Piola-Kirchhoff stresses are determined first from either Equation (5.8) or (5.10) using Equation (4.11) and then rotated back to the base coordinate frame using the material equivalent of Equation (5.37).

The internal stress variables $\mathbf{H}_j$ are defined via the linear rate equation and convolution integral given in Equations (7.6) and (7.7), and may be integrated in a similar way to that outlined in the previous section, to yield the following expression

$$\mathbf{H}_j(t^{n+1}) = \exp\left\{-\frac{\Delta t}{\xi_j}\right\}\mathbf{H}_j(t^n) + \varsigma_j \frac{1-\exp\left\{-\dfrac{\Delta t}{\xi_j}\right\}}{\dfrac{\Delta t}{\xi_j}}\left[\mathbf{S}_\infty^{dev}(t^{n+1}) - \mathbf{S}_\infty^{dev}(t^n)\right] \tag{7.27}$$

To determine the value of the Cauchy stress at the end of the increment the deviatoric components of the second Piola-Kirchhoff stress are simply 'pushed forward' and summed with the volumetric component of the Cauchy stress

$$\boldsymbol{\sigma}(t^{n+1}) = \frac{1}{J(t^{n+1})}\mathbf{F}(t^{n+1})\left[\mathbf{S}_\infty^{dev}(t^{n+1}) + \sum_{j=1}^{N^\mu}\mathbf{H}_j(t^{n+1})\right]\mathbf{F}^T(t^{n+1}) + \boldsymbol{\sigma}_\infty^{vol}(t^{n+1}). \tag{7.28}$$

The volumetric component of the Cauchy stress tensor, $\boldsymbol{\sigma}_\infty^{vol}(t^{n+1})$, for both models is given by Equation (5.17).

To determine the Jacobian matrix corresponding to the tangent Jaumann rate of Cauchy stress we start by calculating the tangent of the second Piola-Kirchhoff stress using Equation (2.45), and then 'push forward' this result to give the tangent of the Truesdell rate of Kirchhoff stress using Equation (2.52). Following this approach the tangent of the Truesdell rate of Kirchhoff stress may be expressed as follows

$$\mathscr{D}^{TK}(t^{n+1}) = \left[1 + \sum_{j=1}^{N^\mu}\varsigma_j \frac{1-\exp\left\{-\dfrac{\Delta t}{\xi_j}\right\}}{\dfrac{\Delta t}{\xi_j}}\right]\mathscr{D}_\infty^{TK,dev}(t^{n+1}) + \mathscr{D}_\infty^{TK,vol}(t^{n+1}). \tag{7.29}$$

The deviatoric part of Equation (7.29) has a similar structure to that of Equation (7.21) and is defined as

$$\mathscr{D}_{\infty}^{TK,dev}(t^{n+1}) = (1-d(t^{n+1}))\mathscr{D}_{0,\infty}^{TK,dev}(t^{n+1}) - e\,\boldsymbol{\tau}_{0,\infty}^{dev}(t^{n+1}) \otimes \boldsymbol{\tau}_{0,\infty}^{dev}(t^{n+1}) . \tag{7.30}$$

Here the effective elastic Kirchhoff stress, $\boldsymbol{\tau}_{0,\infty}^{dev}(t^{n+1})$, is given by

$$\boldsymbol{\tau}_{0,\infty}^{dev}(t^{n+1}) = \mathbf{F}\ (t^{n+1})\ \mathbf{S}_{0,\infty}^{dev}(t^{n+1})\mathbf{F}^{T}(t^{n+1}) . \tag{7.31}$$

The effective elastic deviatoric tangent of the Truesdell rate of Kirchhoff stress, $\mathscr{D}_{0,\infty}^{TK,dev}(t^{n+1})$, for the 3 and 8 chain models may be obtained following the same approach as that adopted in chapter 5. The principal components of the effective elastic deviatoric tangent of the Truesdell rate of Kirchhoff stress are determined first using either Equations (5.21)-(5.22) or (5.34)-(5.35) and then rotated back to the base coordinate frame. The volumetric component of the tangent of the Truesdell rate of Kirchhoff stress, $\mathscr{D}_{\infty}^{TK,vol}(t^{n+1})$, is identical to that given in section 5.1.4. The tangent of the Truesdell rate of Kirchhoff stress, $\mathscr{D}^{TK}(t^{n+1})$, is finally transformed to the tangent of the Jaumann rate of Cauchy stress, $\mathscr{D}^{JC}(t^{n+1})$, using Equations (5.46) and (5.48).

7.6 Numerical Examples

7.6.1 Stress Relaxation

The response of the viscoelastic forms of the 3 and 8 chain non-Gaussian network models, developed in this chapter, are now compared with published experimental data. We begin by comparing the response of the plane stress formulations with the experimental data of Quigley *et al* (1995). Quigley *et al* performed a series of stress relaxation tests on 20 N121 HNBR, in both tension and compression. The Mullins effect is ignored in this example because of the preconditioning routine to which the specimens employed in this study were subject. For the stress relaxation tests in tension, specimens were loaded at a strain rate of 0.2 s^{-1}. Numerical tests were performed using a single CPS4 element. The time independent material constants for

the proposed model (μ_∞, n), which describe equilibrium response, were obtained from the quick pull test data. The time dependent material constants (μ_i, ξ_i where i=1,..,N), which take the form of a Prony series were obtained from the normalised relaxation data using a new approach developed by the author. This approach accounts for the stress relaxation that occurs during the loading-up phase of a typical relaxation test, and as a result leads to a more accurate description of viscoelastic behaviour than traditional methods employed to determine the values of the Prony series. This approach is discussed in detail in Chapter 9. Comparisons of the experimentally determined stress relaxation behaviour at a stretch of $\lambda = 1.5$ with the predictions of the viscoelastic forms of the 3 and 8 chain models are given in Figure 7.2 and 7.3, respectively. Both figures show close agreement between the experimental data and the predicted rate of stress relaxation.

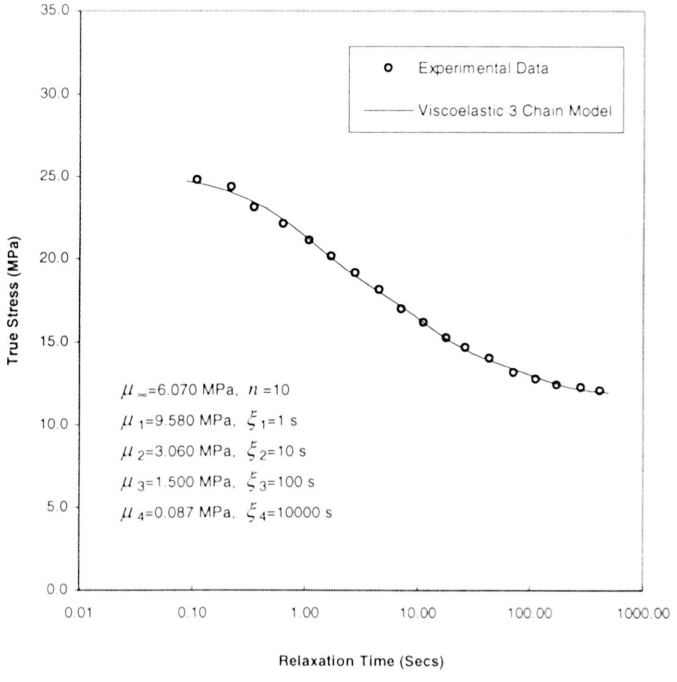


Figure 7.2 : Comparison of the viscoelastic 3 chain model with the experimental data of Quigley *et al* (1995).

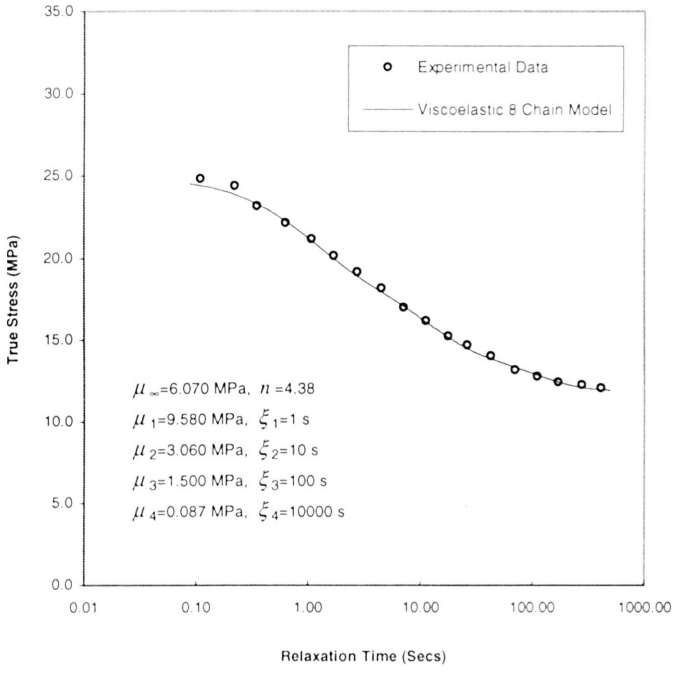


Figure 7.3 : Comparison of the viscoelastic 8 chain model with the experimental data of Quigley *et al* (1995).

We now compare the response of the three-dimensional formulations with the experimental data of Boyce and Bergström (1998). Boyce and Bergström performed a number stress relaxation tests on 15 N600 Chloroprene. Here the Mullins effect is again ignored because of the use of specimen preconditioning prior to testing. Specimens were loaded at a strain rate of -0.1 s^{-1} up to a strain of –0.6. Numerical tests were performed using a single C3D8I element. The time independent material constants (μ_∞, K, n) are taken to be the same as those given by the authors. The time dependent constants were obtained using the same approach as that employed in the previous section, which is discussed in detail in Chapter 9. Comparisons of the experimental data with the predictions of the viscoelastic forms of the 3 and 8 chain models are given in Figure 7.4 and 7.5. Both demonstrate close agreement between the predicted rate of stress relaxation and the experimental data.

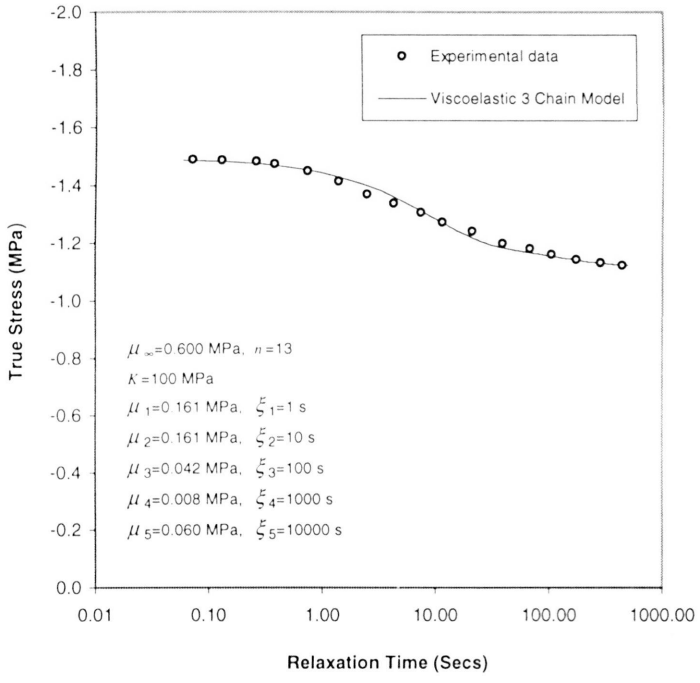


Figure 7.4 : Comparison of the viscoelastic 3 chain model with the experimental data of Boyce and Bergström (1998).

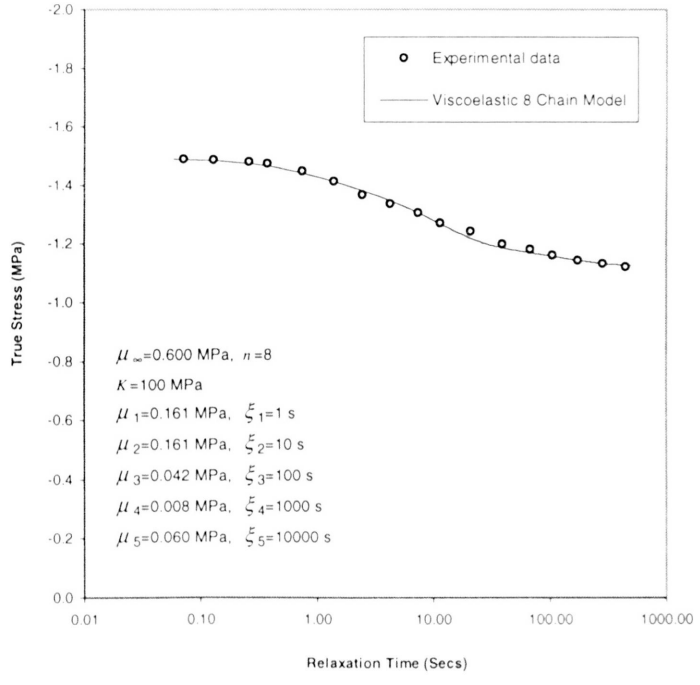


Figure 7.5 : Comparison of the viscoelastic 8 chain model with the experimental data of Boyce and Bergström (1998).

7.7 Final Remarks

In this chapter viscoelastic damage models based on the 3 and 8 chain non-Gaussian network models have been developed to describe the time dependent behaviour of filled elastomers. As in the previous chapter, discussions were initially limited to the development of constitutive relations suitable for the analysis of plane stress problems, where the incompressibility constraint was employed to eliminate the arbitrary hydrostatic stress, which arises in the analysis of volume preserving materials. Later consideration was also given to the development of relations suitable for the analysis of three-dimensional problems, by the introduction of a degree of material compressibility. A comparison of published experimental data and the response of the viscoelastic damage models indicate that the constitutive formulations provide a good description of time dependent response of elastomeric materials.

Chapter 8

8. Experimental Studies

8.1 Introduction

Whilst there is great deal of experimental data available in published literature on the mechanical behaviour of elastomeric materials, much comes from studies conducted to examine only one aspect of the materials behaviour, *i.e.* studies on the large strain behaviour of elastomers are normally only concerned with determining the elastic response and completely ignore damage and rate effects. However in order to calibrate the viscoelastic damage model presented in the previous chapter and fully assess its ability to reproduce the mechanical behaviour of elastomeric materials, experimental data from a wider set of tests is required than is available in published literature. To this end a series of experiments was performed to investigate the mechanical behaviour of two widely used elastomers. In order to determine the approximate long-term or equilibrium response of these materials interrupted loading tests were performed in uniaxial tension and compression. Stress relaxation tests (tensile and compressive) and constant velocity tests (tensile only) were also performed to study the time dependent behaviour. In addition strain softening effects were examined by repeating the above tests on a number of specimens subjected to mechanical preconditioning.

8.1.1 Materials Studied

In this project the mechanical properties of two elastomers filled with carbon black were examined. The first a lightly filled polyurethane material was supplied by the 3M company and the second a lightly filled neoprene material was obtained from RS. The polyurethane material was supplied in the form of two liquid precursors. These precursors were mixed according to the manufacturer's instructions and moulded into sheet form to enable test specimens to be cut out. Sheets 3mm thick (for tension tests) and 8mm thick (for compression tests) were produced in a purpose built sheet mould, consisting of a pair of rigid steel plates separated by appropriate sized spacers. The liquid polyurethane was prevented from bonding to the surface of the mould by inserting thin sheets of Teflon between the uncured polymer and the mould walls. The polyurethane was allowed to cure for 7 days before specimens were cut from the sheet. The neoprene material was supplied in sheet form in 2 thicknesses, 1.5 mm (for tension tests) and 6 mm (for compression tests).

8.1.2 Interrupted Uniaxial Tensile Tests

To determine the elastic or equilibrium response of these materials in tension a number of interrupted uniaxial tensile tests were performed. This test method differs from a standard uniaxial tensile test in that the specimens are strained incrementally and allowed to relax after each increment in strain. The specimen geometry employed in these tests was taken from the ASTM 412 standard for the uniaxial tensile testing of elastomeric materials, and is given in Figure 8.1. Although dumb-bell specimens like that illustrated in Figure 8.1 are more difficult to grip than conventional ring specimens, they offer the distinct advantage that the stress and strain in the central portion of the test piece is uniform. In accordance with the preferred method of fabrication described in the above standard, specimens were pressed from the sheets of polyurethane and neoprene using a steel die. Tests were performed at room temperature on an Instron model 4411 testing machine. To avoid difficulties associated with specimen slippage, a problem often encountered when testing rubberlike materials, a pair of 'Hounsfield' type grips were employed. These grips use two 6 mm pins, one passed through each end of the specimen to secure the test piece and prevent slippage. Failure in the region around the pins was prevented by the use of bonded metal end-tabs. For dumb-bell type specimens a simple exact relationship to

relate the distance between the grips to the elongation of the material in the narrow section of the test piece is unavailable. It is therefore necessary to follow the movement of marks placed on surface of the specimen to measure accurately the strain in this region. To this end, a gauge length of 25 mm was marked on each specimen using 'Snowflake' multipurpose correction fluid. Specimens were loaded at a constant crosshead velocity of 6 mm/s to a specific displacement and held for 1 hour, after which time the rate of change of stress was observed to be small. The load and gauge length (determined with aid of a vernier calliper) at the end of this period were then measured in order to obtain the appropriate values of stress and strain. To study the effect which prior tensile straining had on the elastic response of the materials examined here, a number of specimens were preconditioned by cyclic loading to one of three stretches 2, 2.5, 3. The preconditioned specimens were subject to 10 load cycles between zero load and the maximum specified stretch at a crosshead velocity of 6 mm/s. To ensure that the specimens were preconditioned up to accurately defined maximum strain, the preconditioning process was controlled by means of an optical extensometer. The preconditioned specimens were allowed to relax for a period of 24 hours before testing. Figures 8.2 and 8.3 show the results of the interrupted tensile tests performed on the virgin and preconditioned specimens of polyurethane and neoprene.

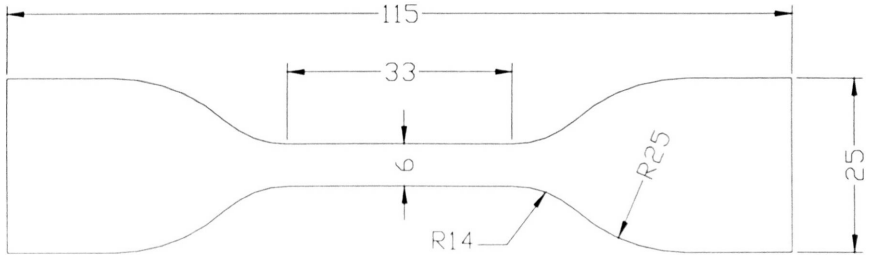


Figure 8.1 : Dumb-bell test piece. All dimensions in mm.

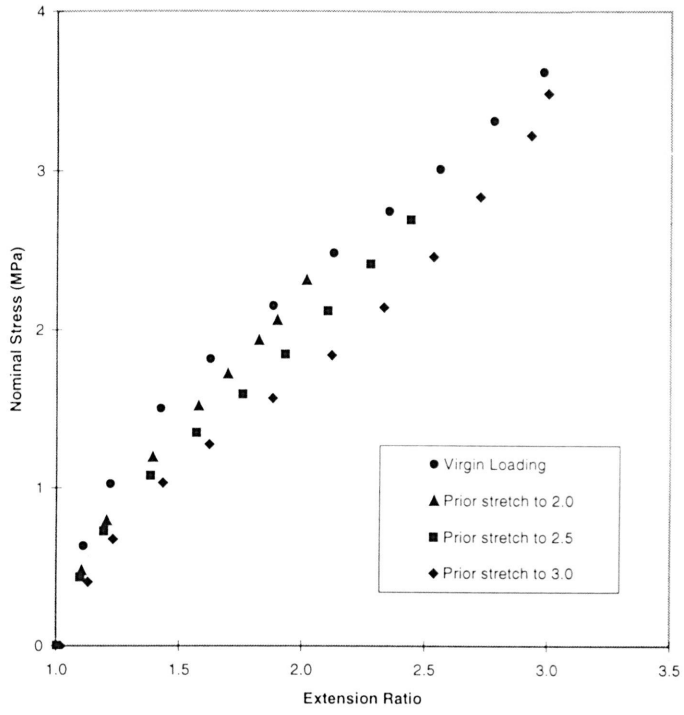


Figure 8.2 : Interrupted uniaxial tensile tests on polyurethane.

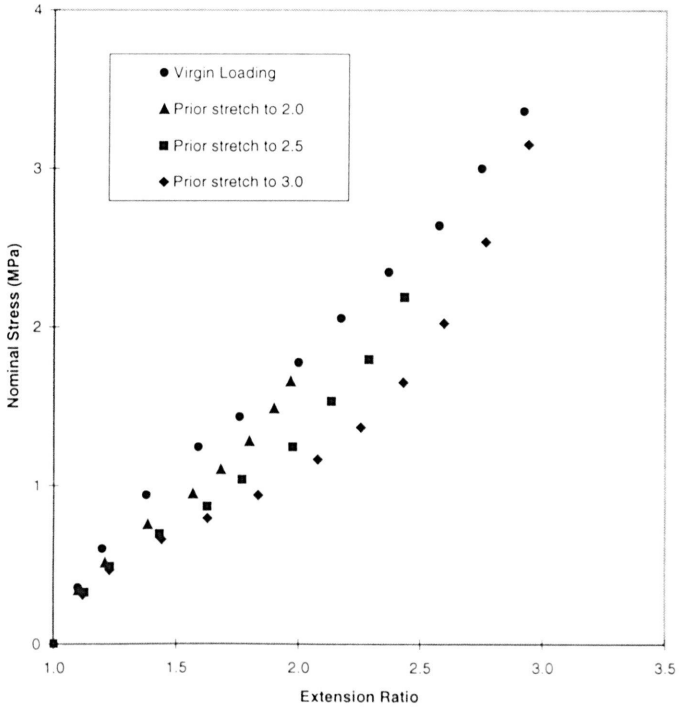


Figure 8.3 : Interrupted uniaxial tensile tests on neoprene.

It is readily apparent from the results of the interrupted uniaxial tensile tests that in tension both the polyurethane and neoprene materials exhibit a significant degree of strain induced softening or Mullins effect, the magnitude of which increases with the size of the maximum stretch employed in the preconditioning procedure.

8.1.3 Interrupted Uniaxial Compression Tests

To determine the equilibrium response of the elastomers in compression a number of interrupted uniaxial compression tests were performed. These tests were conducted at room temperature using cylindrical specimens. A circular die was used to cut out specimens of polyurethane 20 mm in diameter and 8 mm high, and neoprene specimens 20 mm in diameter and 6 mm high. The specimens were cut out using a rotating action in order to produce flat sided test pieces. Specimens were compressed between hardened steel compression plates on an Instron model 4411. Liberal lubrication was applied on the specimen surfaces in contact with the plates to ensure uniform deformation; a MoS_2 based paste made by Rocol proved sufficient for this purpose. The specimens were loaded at a constant crosshead velocity of 0.6 mm/s to a specific predefined displacement and held for 1 hour. The load and crosshead displacement at the end of this period were then measured to give the appropriate values of stress and strain. It was possible to measure strain directly from the crosshead displacement because specimens were observed to deform uniformly, *i.e.* no barrelling occurred. The effect of prior compressive straining on the equilibrium response of the polyurethane and neoprene elastomers was also examined by studying the behaviour of specimens that had been preconditioned by cyclic loading to a stretch of 0.6. The preconditioned specimens were subject to 10 load cycles between zero load and the minimum specified stretch at a crosshead velocity of 0.6 mm/s. The preconditioned specimens were removed from between the compression plates and allowed to relax for 24 hours before testing. The results of the interrupted uniaxial compression tests performed on the virgin and preconditioned specimens of polyurethane and neoprene materials are given in Figures 8.4 and 8.5, respectively. In contrast to the interrupted loading tests performed in tension the amount of strain induced softening observed in the polyurethane and neoprene materials when deformed in compression was small.

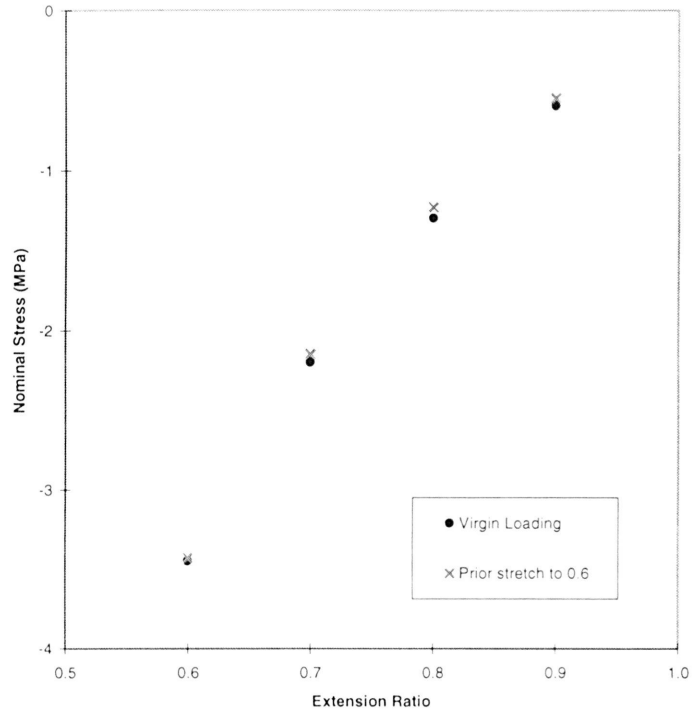


Figure 8.4 : Interrupted uniaxial compression tests on polyurethane.

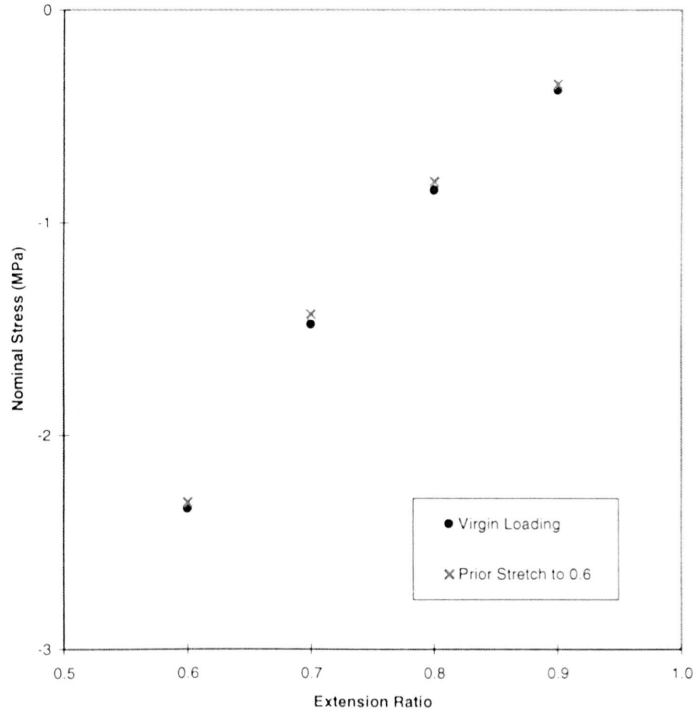


Figure 8.5 : Interrupted uniaxial compression tests on neoprene.

8.1.4 Tensile and Compressive Stress Relaxation Tests

To study further the rate dependent nature of the materials examined in this project a number of stress relaxation tests were carried out in uniaxial tension and compression. Both tensile and compressive tests were conducted at room temperature using a PC controlled Instron model 4411 testing machine, operated in stress relaxation mode. In contrast to the interrupted tests described in the previous sections, the load and crosshead displacement data was collected electronically via the PC. In order to study the influence of prior straining on subsequent stress relaxation, tests were performed in tension and compression on virgin and preconditioned specimens. Stress relaxation tests performed in tension were conducted on dumb-bell shaped specimens with the same geometry as those employed in the interrupted uniaxial tensile tests. Tests conducted in tension on virgin and preconditioned specimens were carried out at three values of stretch: 1.5, 2.0, 2.5. The specimens preconditioned in tension were subjected to 10 load cycles between zero load and the maximum specified stretch at a crosshead velocity of 6 mm/s. Specimens were tested at the maximum stretch as that employed in the preconditioning process, *i.e.* specimens preconditioned at a stretch of λ=1.5 were tested at a stretch of λ=1.5. To ensure specimens were pulled to an accurately defined maximum stretch an optical extensometer was again used to control the preconditioning process. The preconditioned specimens were allowed to relax for 24 hours before testing. Specimens were then loaded at a crosshead speed of 6 mm/s to a specified crosshead displacement and allowed to relax for 1 hour. The extension of the gauge length (initially 25 mm) at the end of this period was then measured using a vernier calliper to ensure that the desired value of strain had been attained. To capture accurately the peak stress, load data was recorded at a rate of 20 points/s for the first minute. Thereafter the data collection rate was reduced by a factor of 100. The results of the stress relaxation tests performed in uniaxial tension on the virgin and preconditioned specimens of polyurethane and neoprene are given in Figures 8.06-8.09. For both materials, the peak stresses recorded during the relaxation tests carried out on virgin specimens were higher than those conducted on preconditioned specimens. It was also observed that for both virgin and preconditioned specimens the stresses approached similar long-term or equilibrium values of stress.

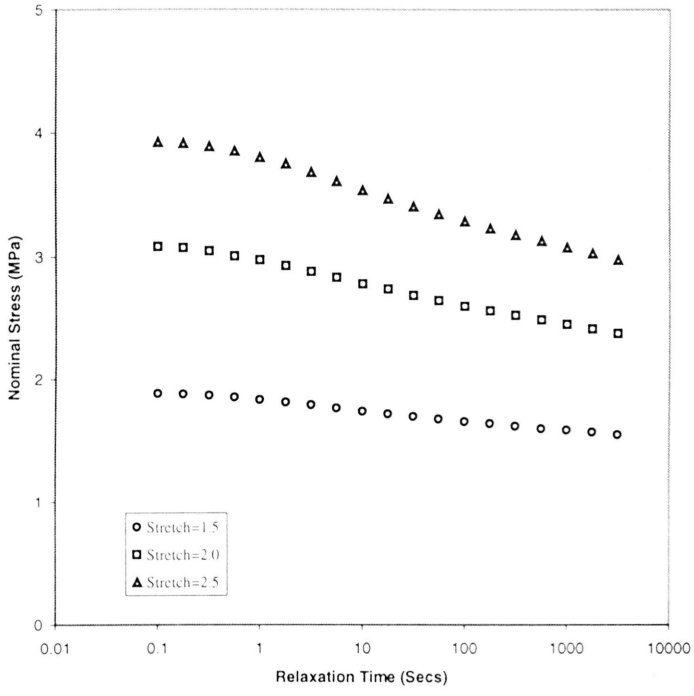


Figure 8.6 : Stress relaxation tests conducted in uniaxial tension on virgin specimens of polyurethane.

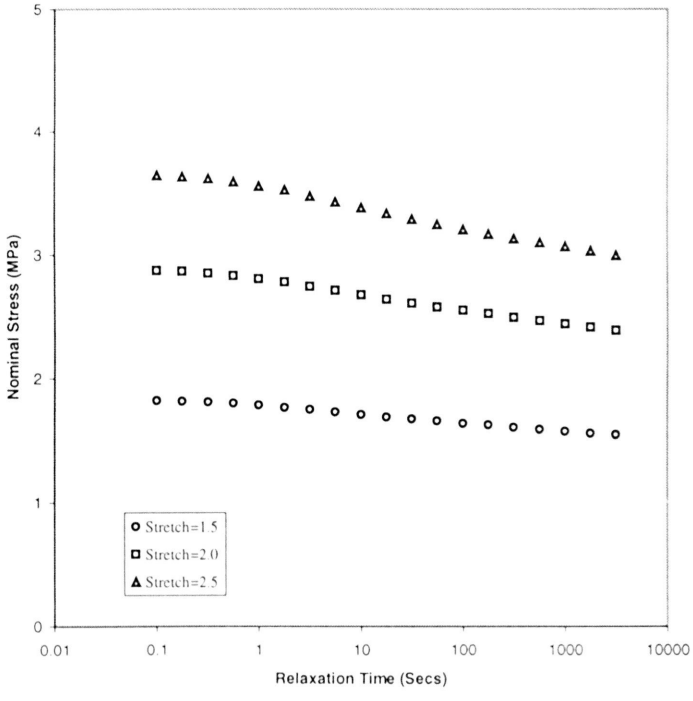


Figure 8.7 : Stress relaxation tests conducted in uniaxial tension on preconditioned specimens polyurethane.

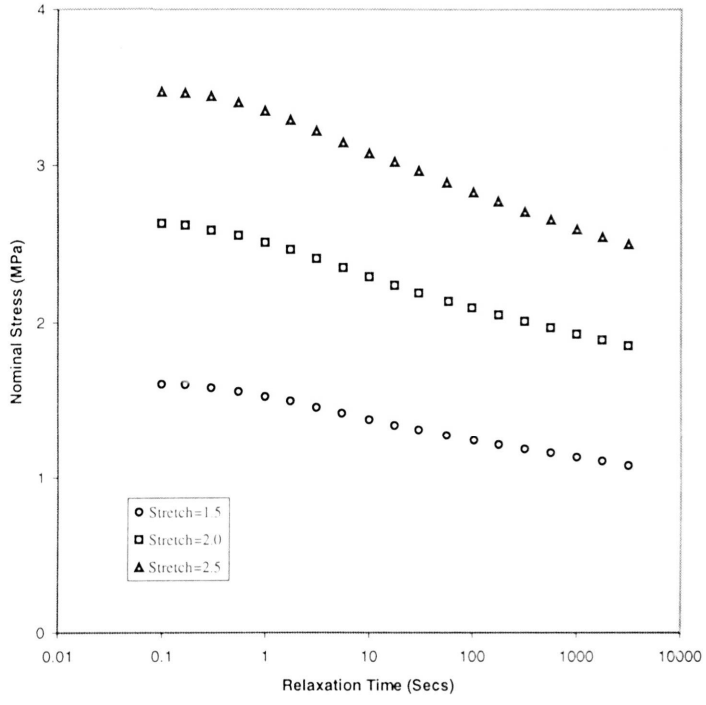


Figure 8.8 : Stress relaxation tests conducted in uniaxial tension on virgin specimens of neoprene.

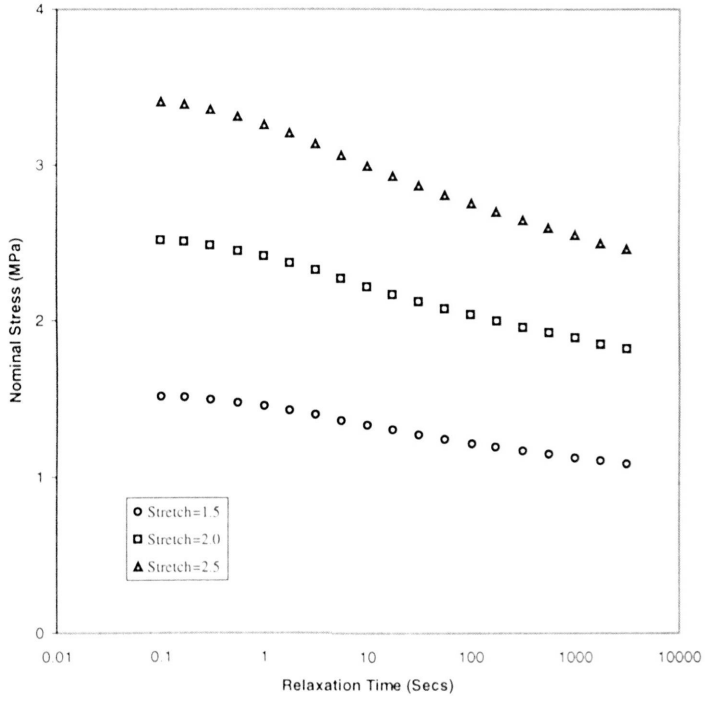


Figure 8.9 : Stress relaxation tests conducted in uniaxial tension on preconditioned specimens of neoprene.

Stress relaxation tests performed in compression were conducted on cylindrical specimens with the same dimensions as those employed in the interrupted uniaxial compression tests. Four values of stretch were considered 0.6, 0.7, 0.8, 0.9. Preconditioned specimens were subjected to 10 load cycles between zero load and the minimum specified stretch at a crosshead velocity of 0.6 mm/s and then allowed to relax for 24 hours before testing. As in the tensile test specimens the same minimum stretch as that used in the preconditioning process was used in the compression tests. In the stress relaxation tests performed in compression specimens were loaded at a crosshead speed of 0.6 mm/s to a specified stretch and allowed to relax for 1 hour. The data collection rate over this period was the same as that employed in the stress relaxation tests conducted in tension. The results are given in Figures 8.10-8.13. In common with the stress relaxation tests conducted in tension the peak stresses recorded during the compression tests on virgin specimens were higher than those conducted on preconditioned specimens. In addition the stresses in the virgin and preconditioned specimens were again observed to approach similar long-term values of stress.

To examine the influence of strain and deformation mode on the stress relaxation behaviour of these materials it is useful to inspect the normalised relaxation data. Following a similar approach to that of Quigley (1995) the stresses were normalised by subtracting the long-term stress at the end of the relaxation experiment from all previous stresses, for a given strain. This difference was then divided by the range of the experimental data, or the maximum viscoelastic stress, so that

$$\sigma_{norm} = \frac{\sigma(\lambda,t) - \sigma(\lambda,\infty)}{\sigma(\lambda,0) - \sigma(\lambda,\infty)}. \tag{8.1}$$

When t=0, $\sigma_{norm} = 1$ and the viscoelastic stress is at its peak value. As $t \to \infty$, $\sigma_{norm} \to 0$, and the viscoelastic stresses become negligible.

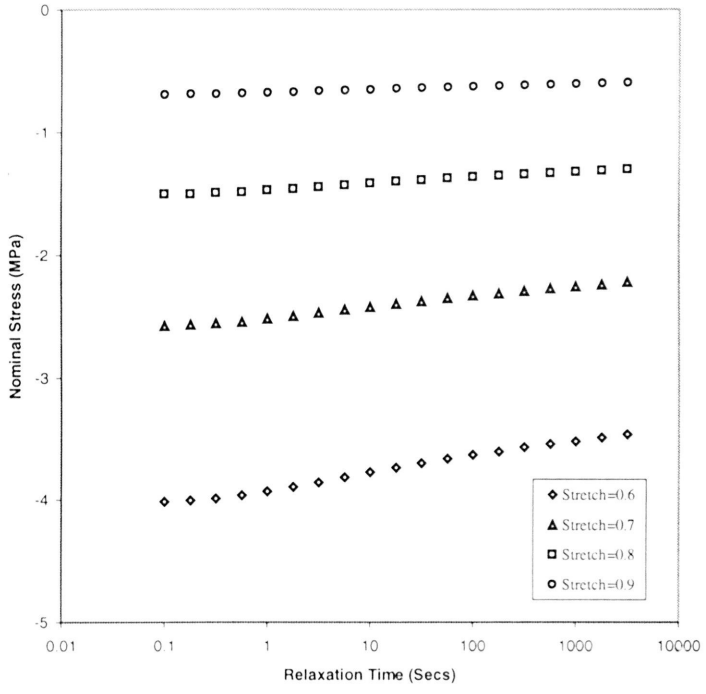


Figure 8.10 : Stress relaxation tests conducted in compression on virgin specimens of polyurethane.

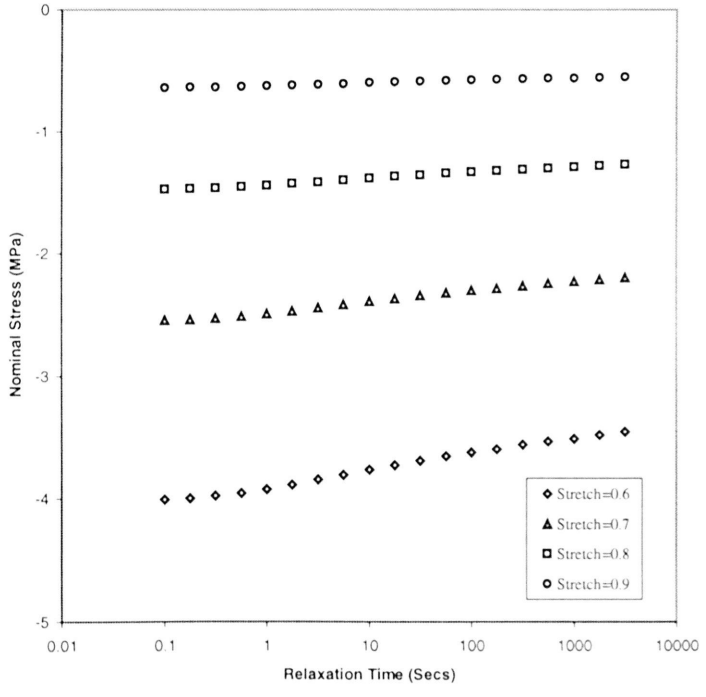


Figure 8.11 : Stress relaxation tests conducted in compression on preconditioned specimens of polyurethane.

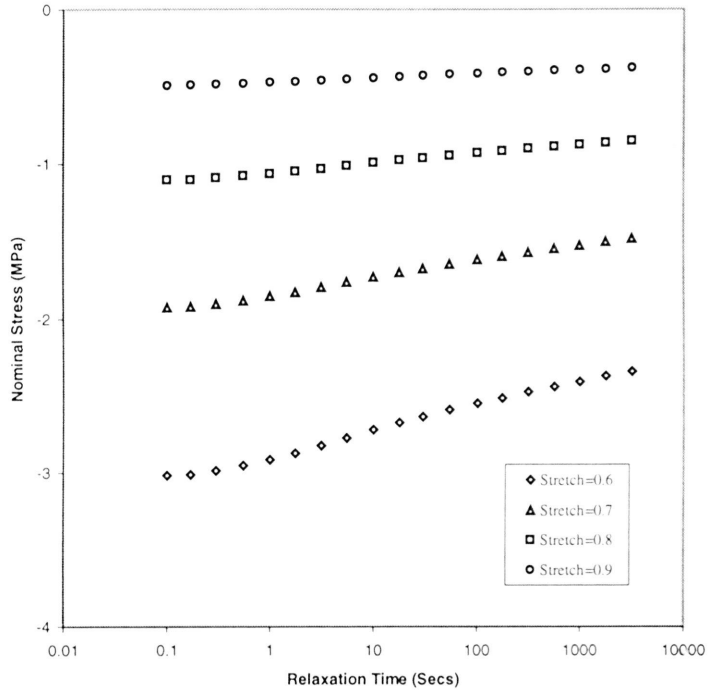


Figure 8.12 : Stress relaxation tests conducted in compression on virgin specimens of neoprene.

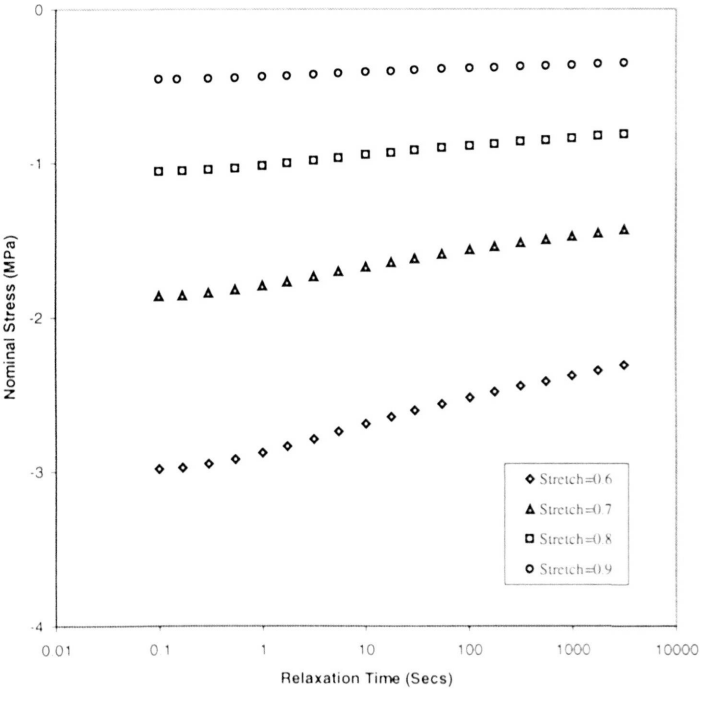


Figure 8.13 : Stress relaxation tests conducted in compression on preconditioned specimens of neoprene.

The normalised stress relaxation curves for the virgin and preconditioned specimens of polyurethane and neoprene tested in tension and compression are given in Figure 8.14-8.17. Normalising the results in this way demonstrates that the data from the tension and compression tests at each level of strain fall onto a single curve, signifying that the time dependent behaviour can be separated from the strain dependent behaviour. In addition it is apparent that the data from the virgin and preconditioned specimens fall on the same curve, indicating that the normalised relaxation behaviour is independent of the preconditioning procedure. Similar observations have also been made by Sullivan and Demery (1982) in experiments conducted on carbon black filled natural rubber. In their study, stress relaxation was found to be independent of both the mode of deformation (pure shear versus uniaxial extension) and the amount of deformation for $\lambda \leq 2$. Contrasting results have also reported by Sullivan and Mazich (1989) for natural rubber gum vulcanisates, where the relaxation spectrum was dependent on the mode of deformation at large strains.

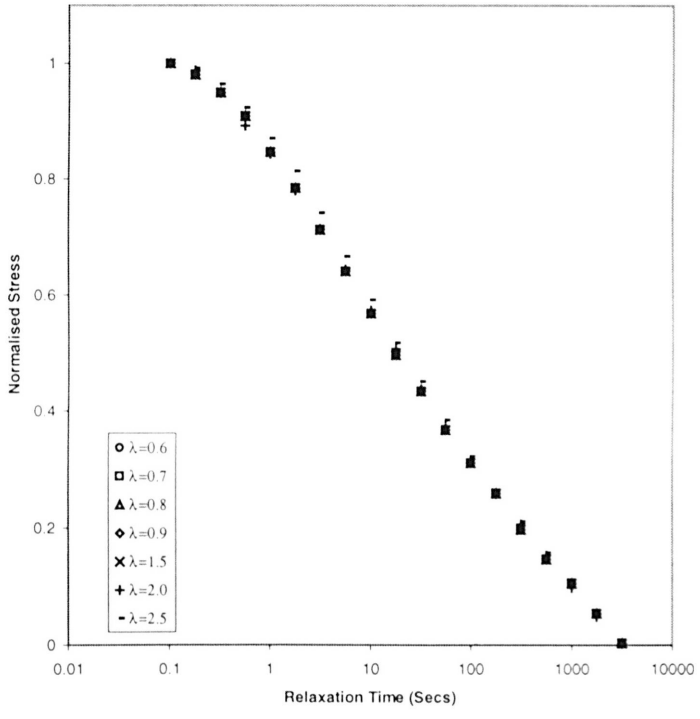


Figure 8.14 : Normalised stress relaxation data for virgin specimens of polyurethane.

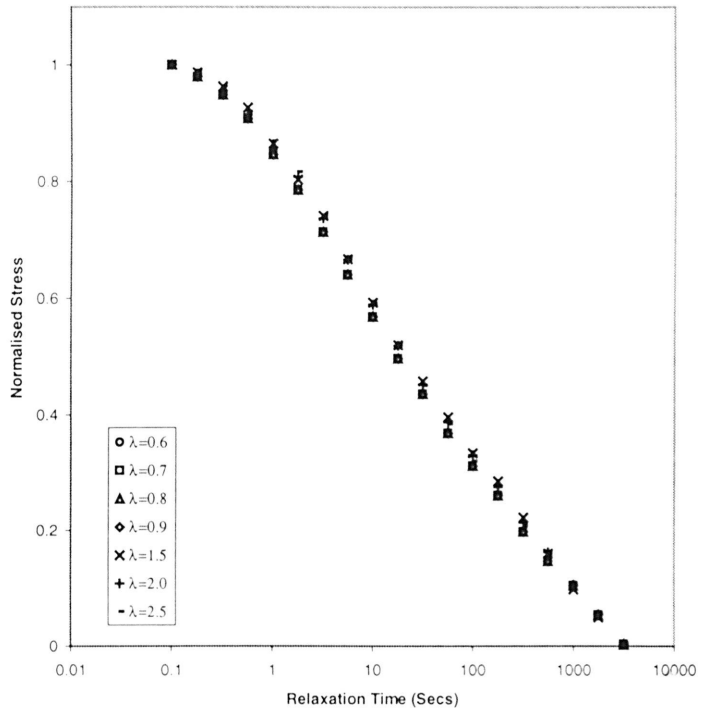


Figure 8.15 : Normalised stress relaxation data for preconditioned specimens of polyurethane.

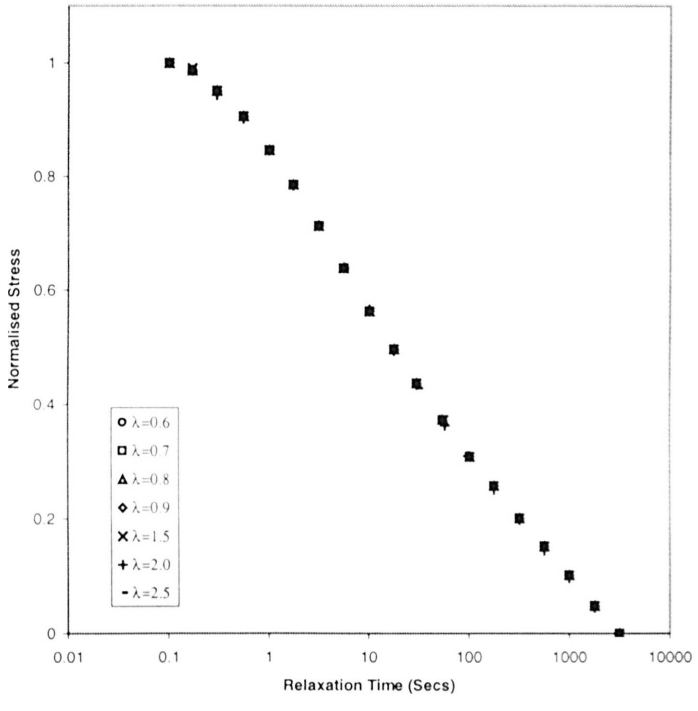


Figure 8.16 : Normalised stress relaxation data for virgin specimens of neoprene.

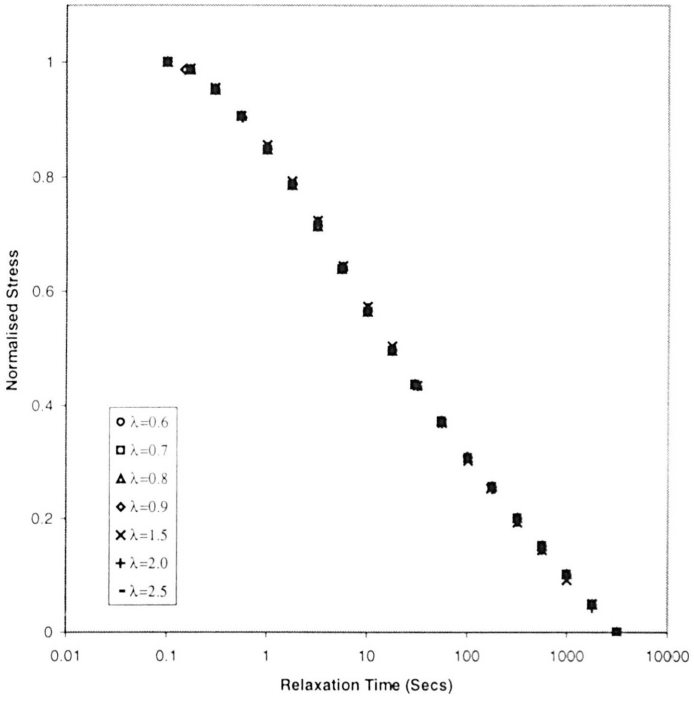


Figure 8.17 : Normalised stress relaxation data for preconditioned specimens of neoprene.

8.1.5 Constant Velocity Uniaxial Tensile Tests

To further study the rate dependent nature of the elastomers under investigation a series of constant velocity uniaxial tensile tests were conducted at room temperature. In common with the previous tests the influence of prior straining was examined by conducting tests on virgin and preconditioned specimens. Tests were conducted on specimens with the same geometry as that given in Figure 8.1 using a PC controlled Instron 4301 testing machine with an Instron optical extensometer attached. The use of an extensometer to measure the elongation of the gauge length was necessary because as mentioned previously no simple exact relationship exists between crosshead displacement and the strain in this region of the specimen. Note it was possible to measure strains using a vernier calliper in the interrupted tensile tests because the crosshead remained stationary while readings were taken. The optical extensometer employed in these tests shown in Figure 8.18, uses two photoelectric sensing devices to follow automatically by means of a servo mechanism, contrastingly coloured gauge length markers placed on the surface of the test piece. The separation of these auto

followers is measured via a displacement transducer and the resulting electrical signal fed to the attached PC.

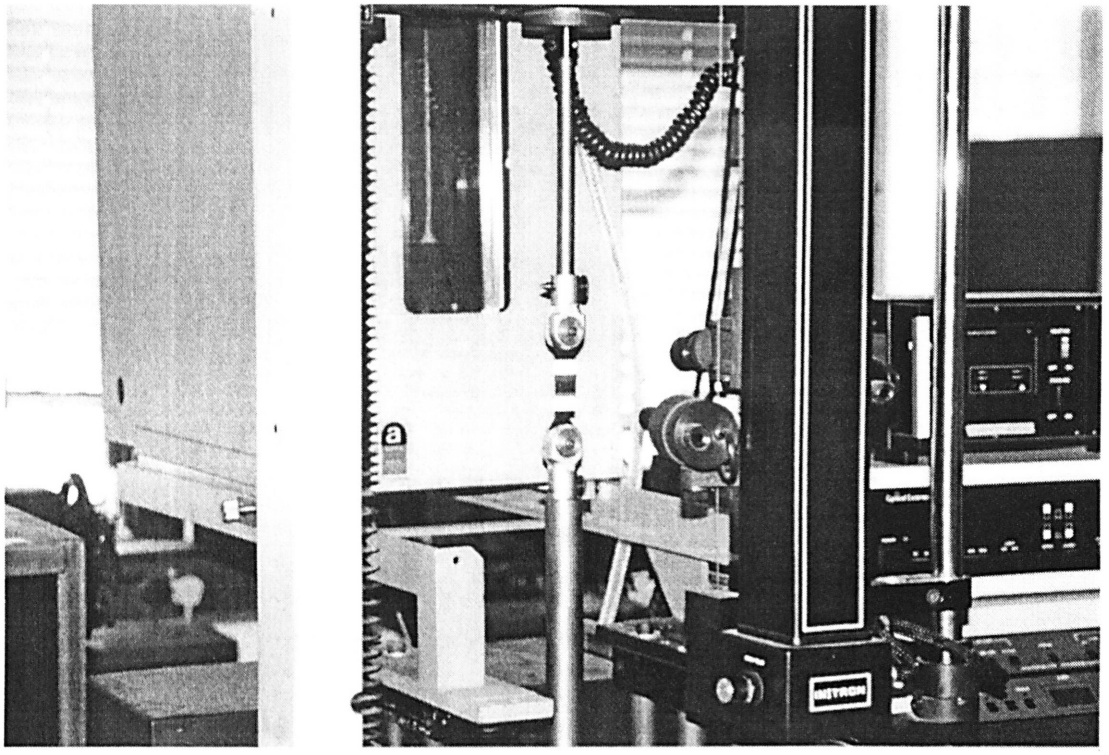


Figure 8.18 : Instron 4301 testing machine with optical extensometer attached.

The preconditioned specimens used in these tests were subjected to 10 load cycles between zero load and a maximum stretch in the gauge length of λ=3, at a crosshead velocity of 6mm/s. The specimens were then removed from the grips and allowed to relax for 24 hours before testing. The virgin and preconditioned specimens were tested at crosshead velocities of 0.006, 0.06, 0.6 and 6 mm/s up to a maximum stretch in the gauge length of λ=3. The results of the constant velocity uniaxial tensile tests performed on the virgin and preconditioned specimens of polyurethane and neoprene are given in Figures 8.19-8.22. These figures illustrate that in tests on conducted on virgin and preconditioned specimens both elastomers exhibit pronounced rate dependence. The reduction in the stiffness of these materials brought about by prior tensile straining (the Mullins effect) is also readily apparent.

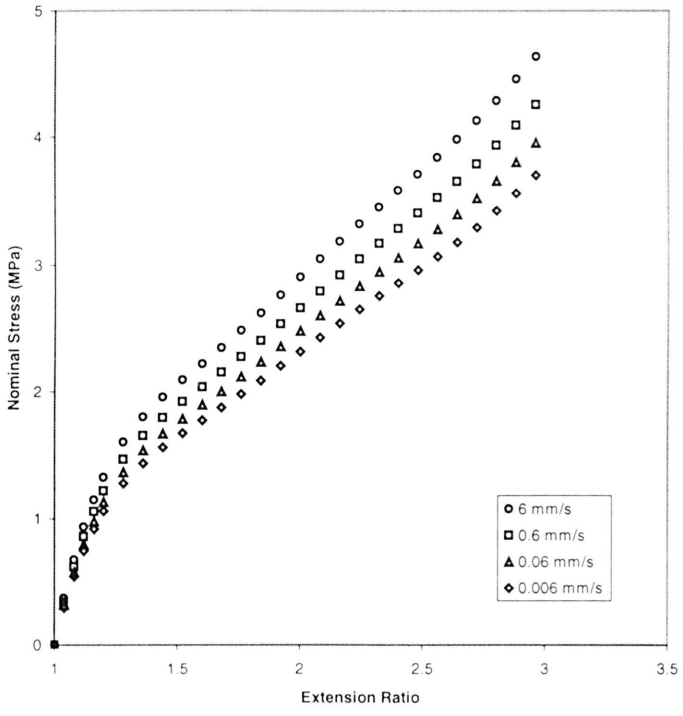


Figure 8.19 : Constant velocity tensile tests performed on virgin specimens of polyurethane.

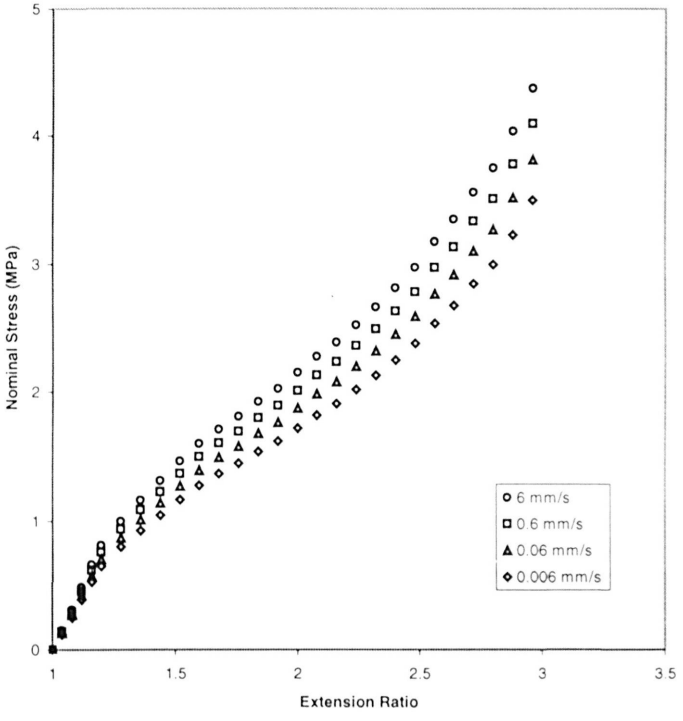


Figure 8.20 : Constant velocity tensile tests performed on preconditioned specimens of polyurethane.

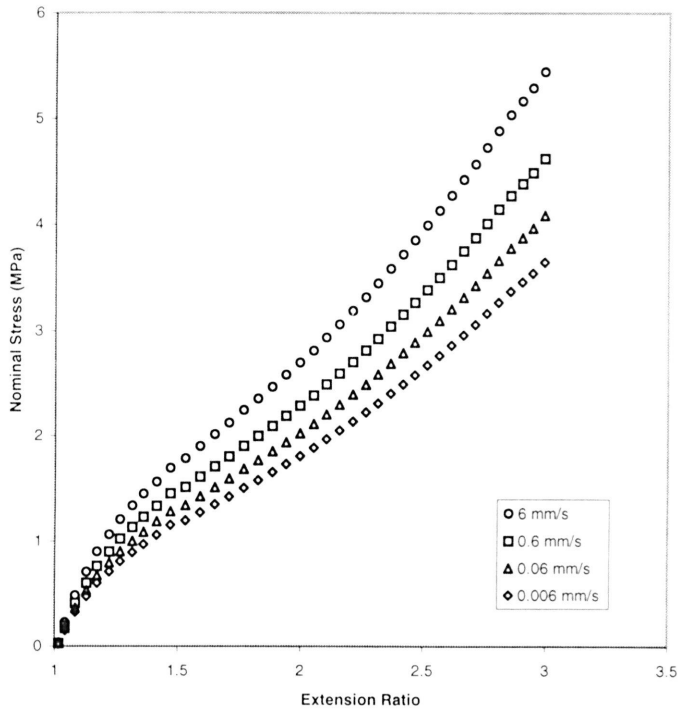


Figure 8.4 : Constant velocity tensile tests performed on virgin specimens of neoprene.

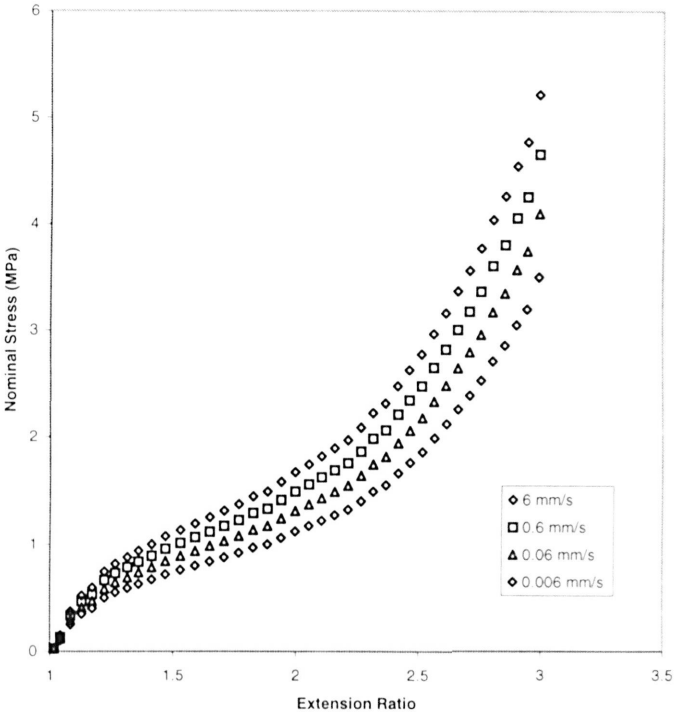


Figure 8.5 : Constant velocity tensile tests performed on preconditioned specimens of neoprene.

8.2 Final Remarks

In this chapter the mechanical properties of elastomeric compounds of polyurethane and neoprene (both lightly filled with carbon black) were investigated. The approximate long-term or equilibrium response of these materials, established via a series of interrupted tension and compression tests demonstrated that both materials exhibited a form of strain induced softening referred to as the Mullins effect. In common with experimental studies of Holt (1932) and Mullins (1948) the amount of softening was observed to increase with the magnitude of the maximum previously applied stretch. To study the time dependent response of these materials a number of stress relaxation tests were also conducted. Examination of the relaxation data from these tests revealed the normalised rate of stress relaxation to be independent of the strain and the mode of deformation (uniaxial tension versus uniaxial compression) over a wide range of strains, in agreement with the previous work of Sullivan and Demery (1982) on natural rubber. In addition stress relaxation tests performed on preconditioned specimens showed the normalised rate of relaxation to be independent of prior deformation in uniaxial tension and compression.

Chapter 9

9. Comparison with Experimental Data

9.1 Introduction

In the preceding chapters a simple constitutive model was developed to describe the mechanical behaviour of filled elastomers. The model extends the non-Gaussian network theories of James and Guth (1943) and Arruda and Boyce (1993) to account for the effects of strain softening, by the incorporation of a simple isotropic damage mechanism into the constitutive formulation. Time dependent effects are also introduced by employing a theoretical framework for finite strain viscoelasticity. In this chapter the response of the proposed model is compared with the results of a series of experiments performed on polyurethane and neoprene. The elastic response of the model is compared with a number of interrupted loading tests performed to establish the long-term or equilibrium response of these materials. The time dependent response is compared with stress relaxation and constant velocity tests performed to study the viscoelastic behaviour. A new approach is also presented to determine the time dependent constants for the proposed model, which take the form of the Prony series. The approach accounts for the stress relaxation that occurs during the loading-up phase of a typical relaxation test, and as a result provides for a more accurate description of the viscoelastic behaviour of elastomeric materials.

9.1.1 Determination of the Time Independent Material Constants

The time independent material constants for the proposed model (μ_∞, n, d_α and η_α), were obtained from the experimental data collected during the interrupted tensile tests performed on the virgin and preconditioned specimens of polyurethane and neoprene. Using the solver function in Microsoft Excel a least squares fit procedure was employed to minimise the difference between the experimental data and the response of the uniaxial version of the elastic damage model. The time independent material constants for the polyurethane and neoprene materials are given in Table 9.1and 9.2. Comparisons of the interrupted uniaxial tensile test data with predictions from the 8 chain version of elastic damage model are shown in Figure 9.1 and 9.2. Bearing in mind that the elastic behaviour of the 8 chain damage model is governed by only 4 constants, agreement between the model and the experimental data is good. Using the constants below, the response 3 chain version of the model in uniaxial extension would be identical to that of the 8 chain model.

Long-term shear modulus	μ_∞ = 1.56 MPa	
Number of rigid links	n = 23.6	(3 chain model)
	n = 8.4	(8 chain model)
Maximum damage parameter	d_α^∞ = 0.48	
Damage saturation parameter	η_α = 2.69	

Table 9.1 : Time independent material constants for polyurethane.

Long-term shear modulus	μ_∞ = 0.91 MPa	
Number of rigid links	n = 12.4	(3 chain model)
	n = 4.4	(8 chain model)
Maximum damage parameter	d_α^∞ = 0.67	
Damage saturation parameter	η_α = 3.82	

Table 9.2 : Time independent material constants for Neoprene.

The response of the 8 chain version of the elastic damage model is compared with the results of the interrupted compression tests conducted on the virgin and preconditioned specimens of polyurethane and neoprene, in Figure 9.3 and 9.4. Using the material constants determined from the uniaxial tension tests, the 8 chain model is observed to successfully reproduce the response of both elastomers in compression. In contrast the response 3 chain version of proposed model (not shown) falls significantly below the experimental data, with the difference between the model and data increasing with strain. Similar results have also reported by Arruda and Boyce (1993), who demonstrated the superior ability of the eight chain model to describe the state of deformation dependence displayed by rubber-like materials, in a series experiments conducted on elastomers tested in uniaxial and plane strain compression.

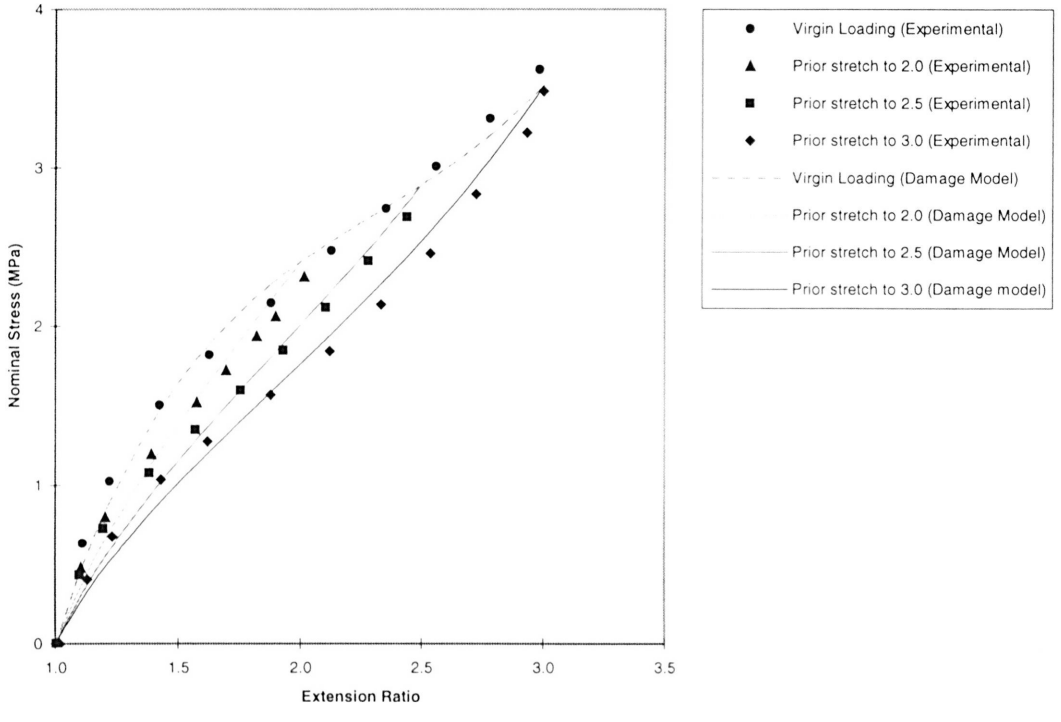


Figure 9.1 : Comparison of elastic damage model with interrupted uniaxial tensile test data for polyurethane.

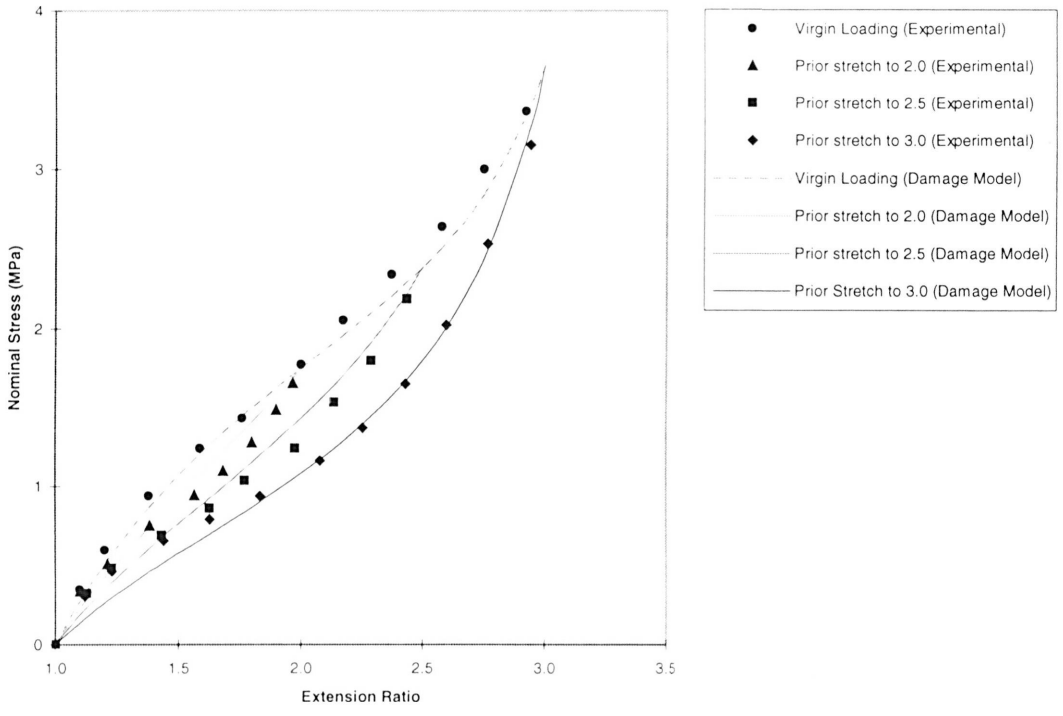


Figure 9.2 : Comparison of elastic damage model with interrupted uniaxial tensile test data for neoprene.

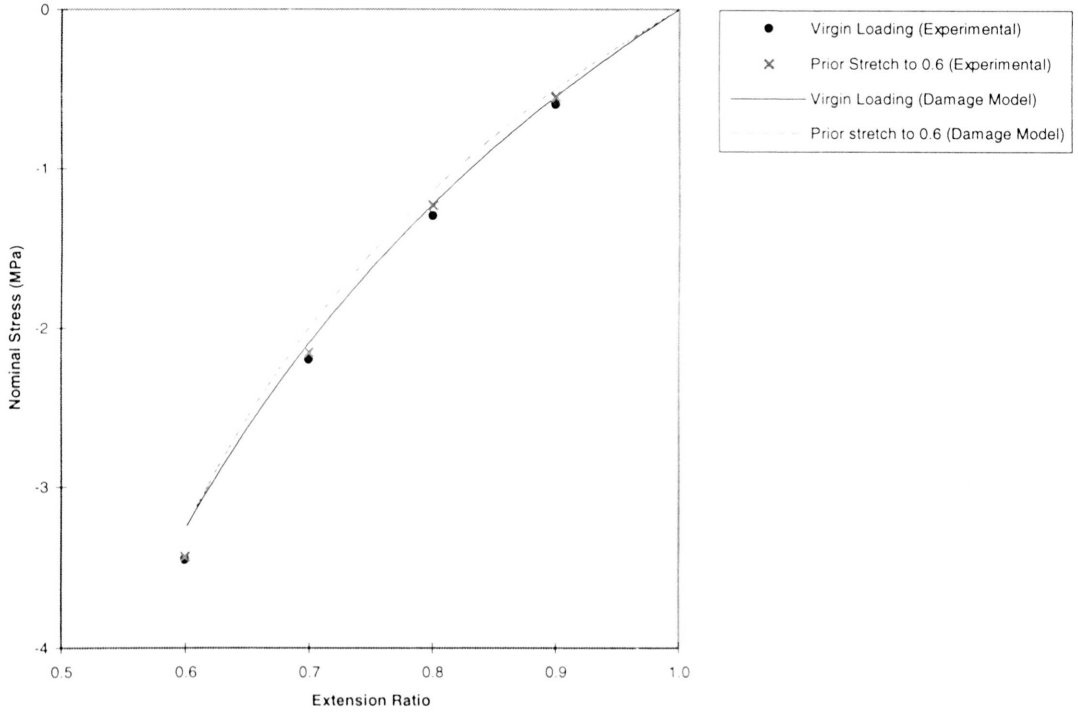


Figure 9.3 : Comparison of elastic damage model with interrupted uniaxial compression test data for polyurethane.

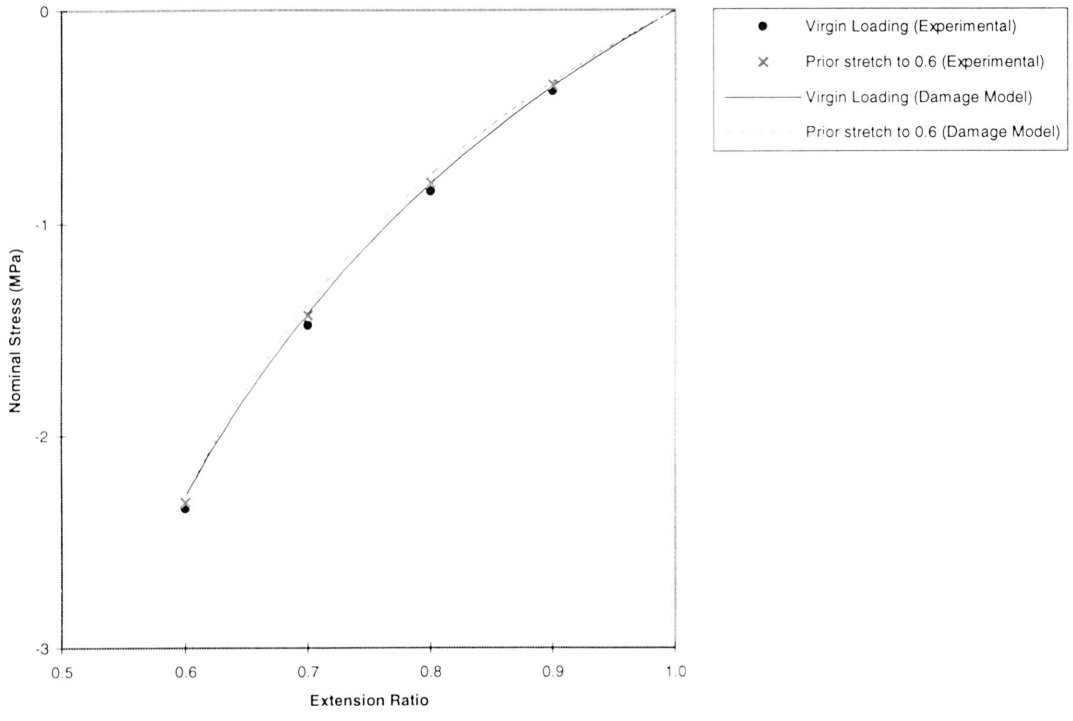


Figure 9.4 : Comparison of elastic damage model with interrupted uniaxial compression test data for neoprene.

9.1.2 Determination of the Time Dependent Material Constants

The time dependent material constants for the proposed model take the form of a Prony series. The standard approach employed to determine the Prony series (from stress relaxation data) such as that offered by the finite element program ABAQUS, significantly underpredicts the value of the relaxation moduli with the shortest relaxation times, and leads to a poor representation of the viscoelastic behaviour of rubber-like materials. This problem stems from the assumption inherent in the standard approach that specimens are loaded instantaneously during relaxation tests, a condition that is rarely fulfilled in practice. Indeed a review of the stress relaxation data available in published literature reveals that the loading phase of a typical stress relaxation test varies between a period of 5-30 seconds. To avoid this problem a new approach was developed to determine the values of the Prony series that offers the significant advantage of being able to account for the stress relaxation that occurs during the loading phase of a relaxation test. In common with the collocation and regression methods described by Quigley (1995) a set of relaxation times were first

chosen such that a single value of ξ_j falls within each decade of time. Here $\xi_j=3.6\times10^N$, N=-1, 0, ...3 were chosen. Using the solver function in Microsoft Excel a least fit procedure was then performed between the stress relaxation data obtained from the virgin specimens at values of stretch of λ=1.5 and the relaxation behaviour predicted by the equation for stress relaxation in a generalised Maxwell element, given by

$$\sigma(t) = \sigma_\infty + \sum_{j=1}^{N} \sigma_j \exp\left\{-\frac{t}{\xi_j}\right\} \tag{9.1}$$

Here σ_∞ represents the stress in the lone spring element and σ_j the initial stress in each of the N Maxwell elements. A 2 step ABAQUS input file was then written to simulate the relaxation tests. The first step simulated the real time loading up of the specimen while the second step simulated the subsequent stress relaxation. The relaxation moduli employed in the input file were varied until the stress in each Maxwell element (represented by the internal stress variables in the viscoelastic damage model) at the end of the first step were identical to those obtained from the least squares fit procedure in Excel. The experimental stress relaxation data was compared with that predicted in the second step of the analysis. The specimen geometry was modelled using the finite element mesh illustrated in Figure 9.5. The mesh consists of 200 8-noded reduced integration plane stress elements, because of the symmetry only one quarter of the specimen was analysed. The terms in the Prony series calculated by employing this approach are given in Table 9.3 and 9.4. The response of the 8 chain version viscoelastic damage model is compared with the experimental data from the relaxation tests performed in tension on virgin specimens of polyurethane and neoprene in Figure 9.6 and 9.7. The model shows close agreement with the relaxation data collected at a stretch of λ=1.5, as would be expected since this data was employed in the calibration procedure. At the higher values stretch the stresses predicted by the model during the first 30 seconds are lower than those observed experimentally, at longer times agreement between the model and data remains good. The underprediction of the peak stresses in relaxation tests performed on virgin specimens is mainly attributed to the proportion of the viscous behaviour increasing with strain. This observation is reinforced by the comparing the

response of the viscoelastic damage model with the results stress relaxation tests performed on the preconditioned specimens of polyurethane and neoprene, shown in Figure 9.8 and 9.9, where the proportion of the viscous behaviour remained approximately constant with increasing strain. The difference between the peak stress predicted by the model and the experimental data is considerable smaller at the higher stretch levels than that predicted for the virgin specimens.

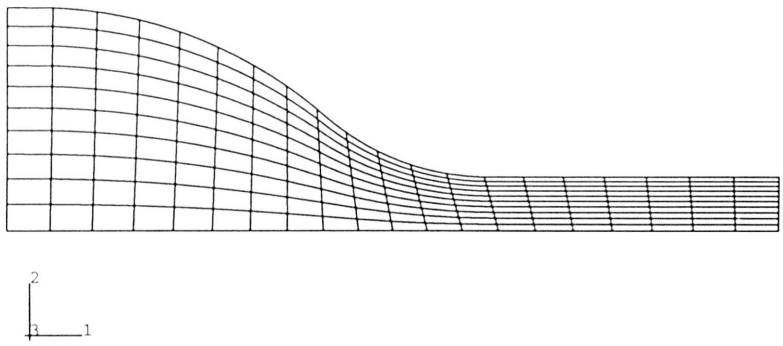


Figure 9.5 : Finite element mesh of tensile test specimen.

The response of the 8 chain version of the viscoelastic damage model is compared with the stress relaxation tests performed in compression on the virgin specimens of polyurethane and neoprene in Figures 9.10 and 9.11. Because the compression specimens deformed uniformly during tests the geometry was modelled using a single CPS4 4-noded plane stress element. Using the constants obtained from relaxation tests conducted in tension the 8 chain model shows close agreement with the experimental data for both elastomers. Indeed the difference between the peak stresses predicted by the model and those observed experimentally is smaller than in the relaxation tests performed in tension. The response of the 8 chain model is also compared with the relaxation data from the preconditioned specimens in Figures 9.12 and 9.13. Here the model again shows close agreement with the experimental data.

Term	Relaxation Modulus (MPa)	Relaxation Time (Secs)
1	0.695	3.6×10^{-1}
2	0.198	3.6×10^{0}
3	0.127	3.6×10^{1}
4	0.034	3.6×10^{2}
5	0.157	3.6×10^{3}
∞	1.560	∞

Table 9.3 : Five term Prony series for polyurethane.

Term	Relaxation Modulus (MPa)	Relaxation Time (Secs)
1	1.388	3.6×10^{-1}
2	0.303	3.6×10^{0}
3	0.130	3.6×10^{1}
4	0.106	3.6×10^{2}
5	0.081	3.6×10^{3}
∞	0.910	∞

Table 9.4 : Five term Prony series for neoprene.

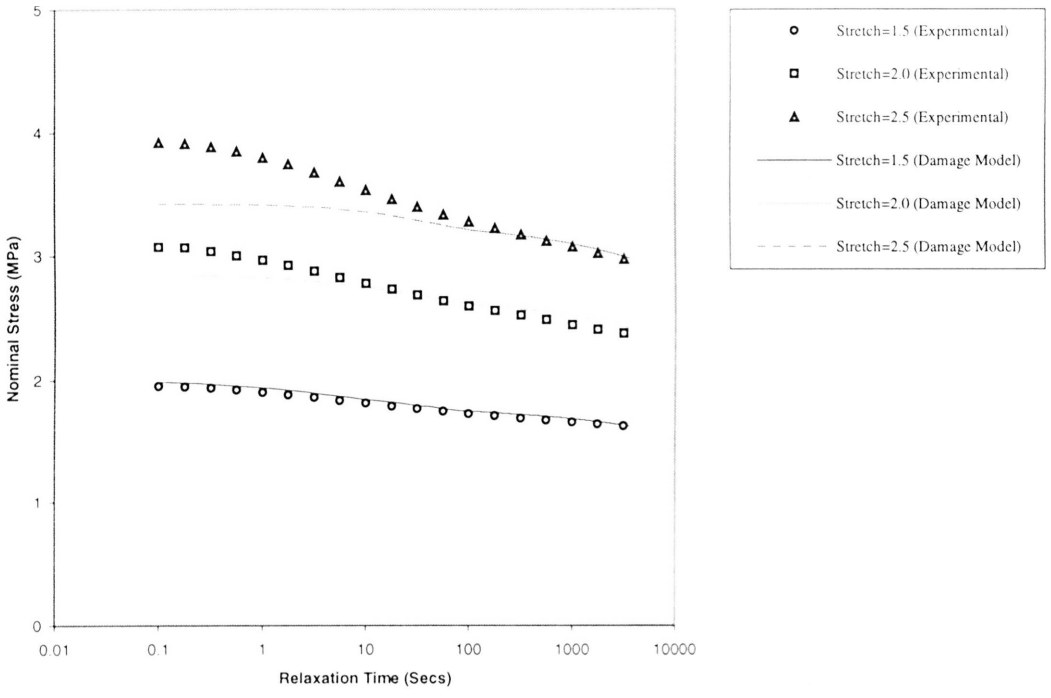


Figure 9.6 : Comparison of viscoelastic damage model with stress relaxation tests conducted in tension on virgin specimens of polyurethane.

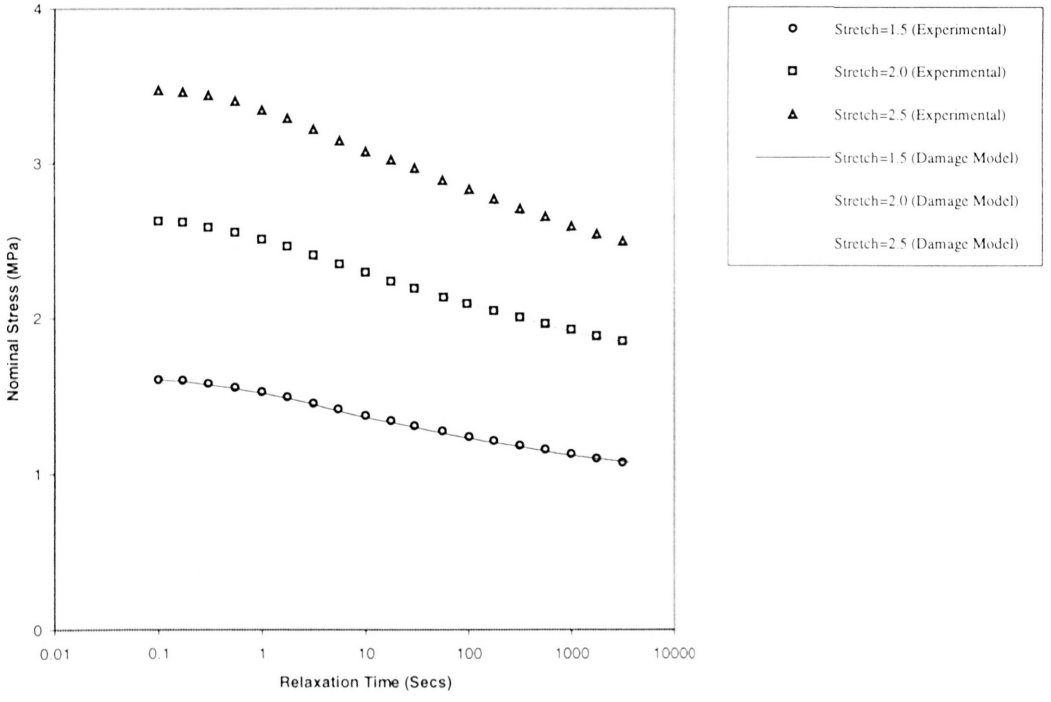


Figure 9.7 Comparison of viscoelastic damage model with stress relaxation tests conducted in tension on virgin specimens of neoprene.

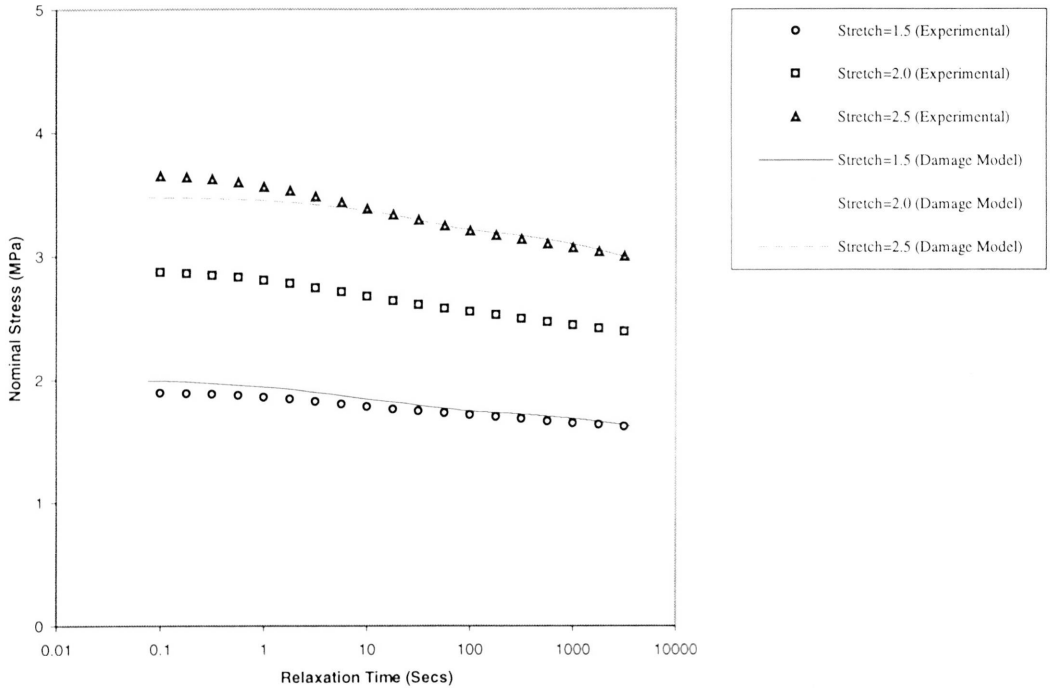


Figure 9.8 : Comparison of viscoelastic damage model with stress relaxation tests conducted in tension on preconditioned specimens of polyurethane.

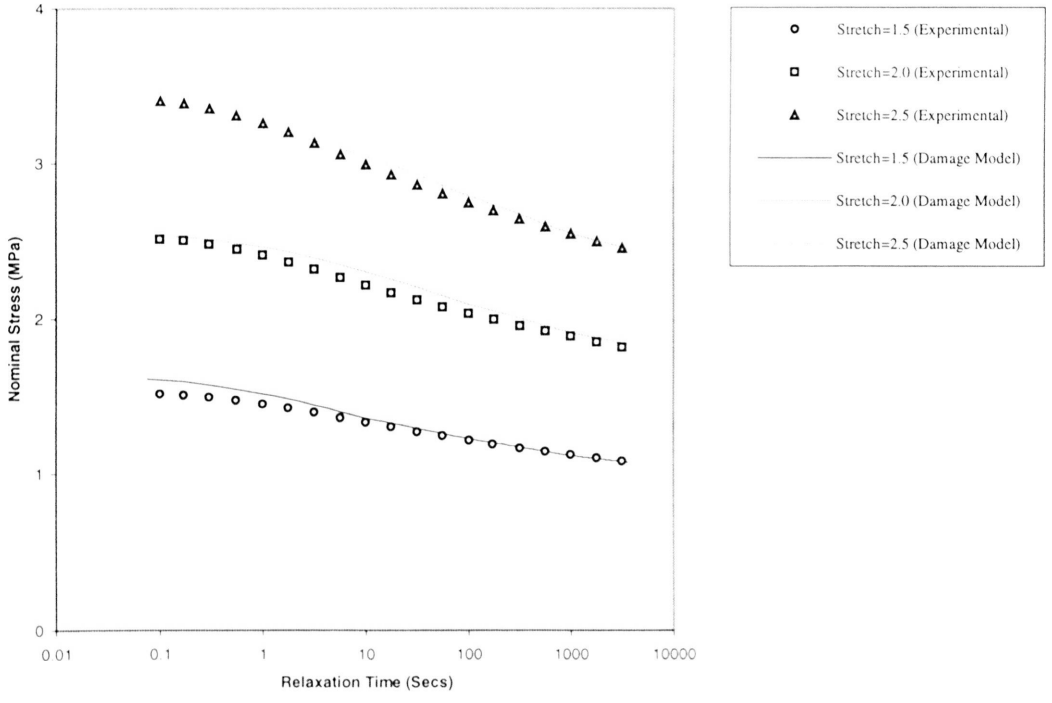


Figure 9.9 : Comparison of viscoelastic damage model with stress relaxation tests conducted in tension on preconditioned specimens of neoprene.

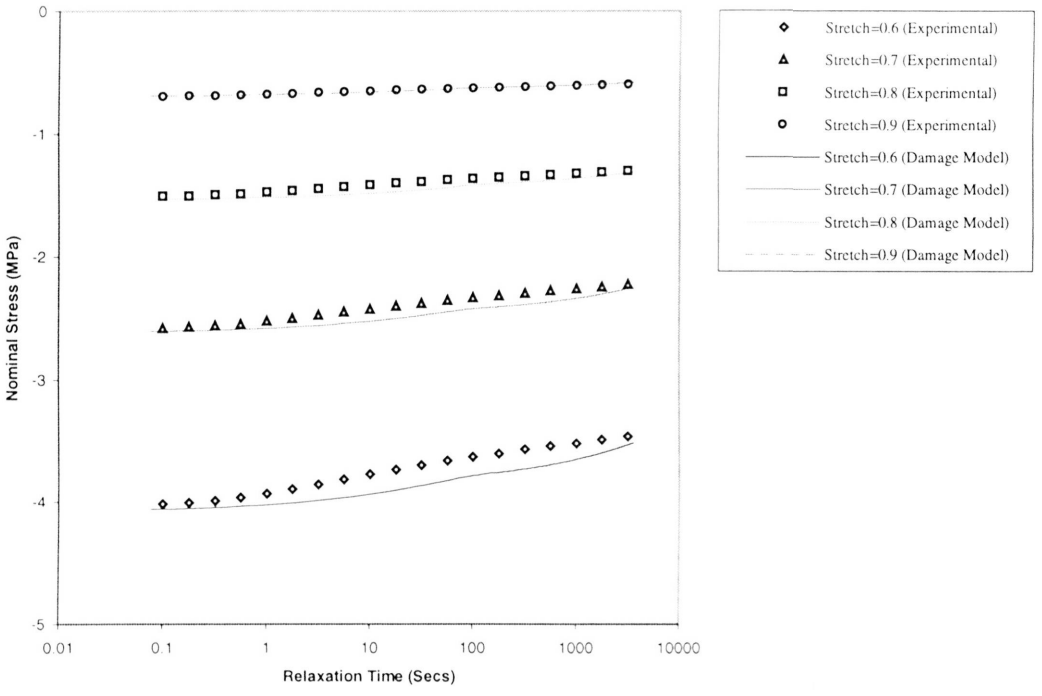


Figure 9.10 : Comparison of viscoelastic damage model with stress relaxation tests conducted in compression on virgin specimens of polyurethane.

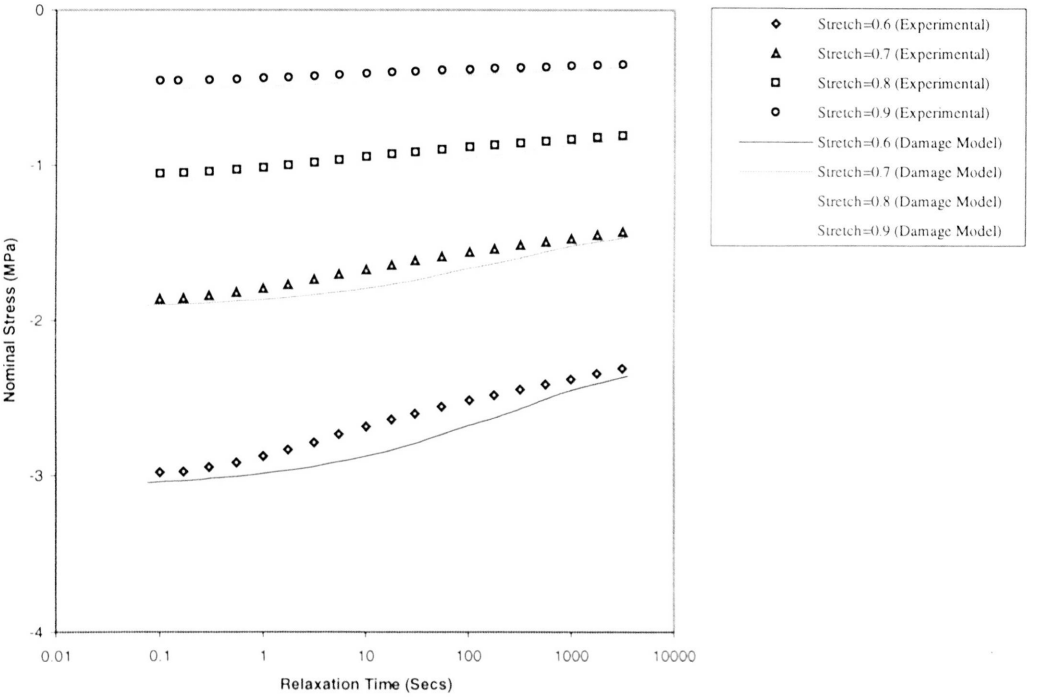


Figure 9.11 Comparison of viscoelastic damage model with stress relaxation tests conducted in compression on virgin specimens of neoprene.

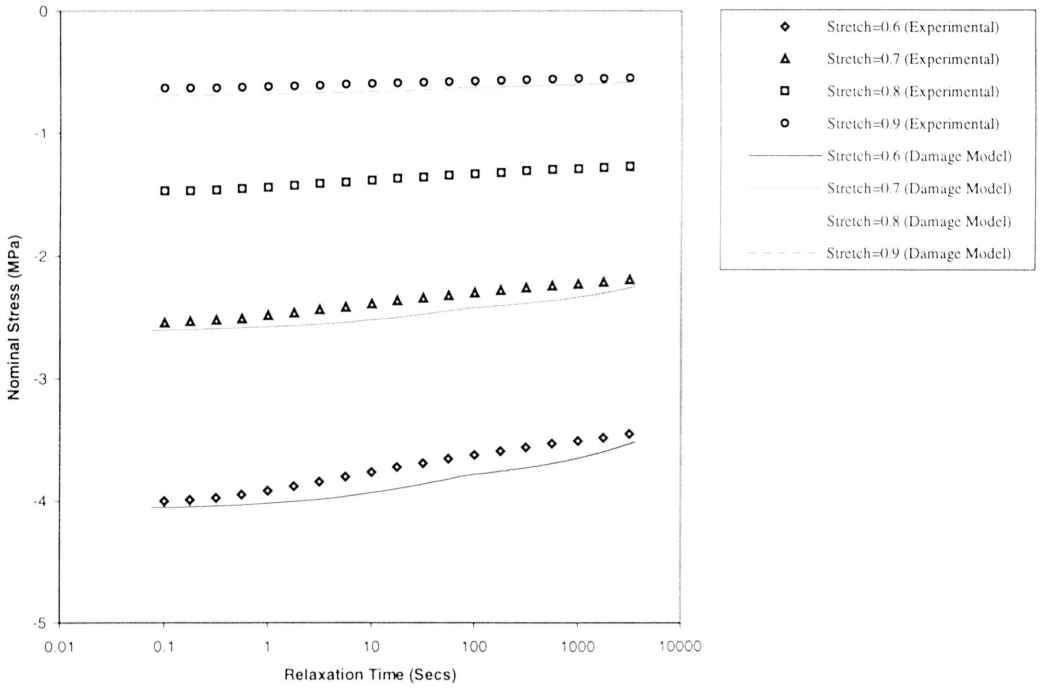


Figure 9.12 : Comparison of viscoelastic damage model with stress relaxation tests conducted in compression on preconditioned specimens of polyurethane.

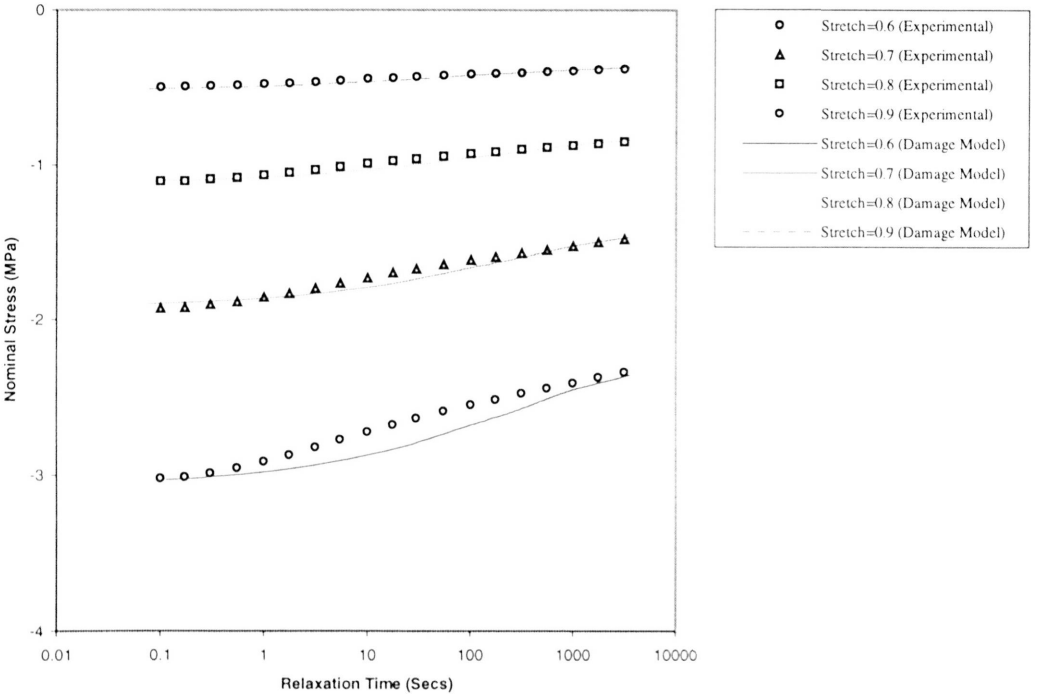


Figure 9.13 : Comparison of viscoelastic damage model with stress relaxation tests conducted in compression on preconditioned specimens of neoprene.

9.1.3 Comparison with Constant Velocity Uniaxial Tensile tests

The ability of the viscoelastic damage model to reproduce the results of the constant velocity tensile tests will now be examined. The specimen geometry is modelled using a mesh identical to that illustrated in Figure 9.5. The response of the proposed model is compared with the experimental data collected in the tests conducted on virgin specimens of polyurethane and neoprene in Figure 9.14 and 9.15 (again only the response of the 8 chain model is shown). The model is observed to be successful in describing the rate dependence of both elastomers at low extensions, but progressively underpredicts the stresses as the extension is increased above a stretch of λ=2. The underprediction of the observed stresses at higher extensions is again mainly attributed to the viscous response of the virgin material increasing with strain. A comparison of the viscoelastic damage model with the experimental data from the preconditioned specimens of polyurethane and neoprene, given in Figures 9.16 and 9.17, demonstrates that the proposed model provides a good description of the rate dependent response of both materials, even at large extensions. The model is observed to be more successful at describing the rate dependent behaviour of preconditioned material, because the preconditioning process effectively reduces the dependence of the magnitude of the viscous response on strain.

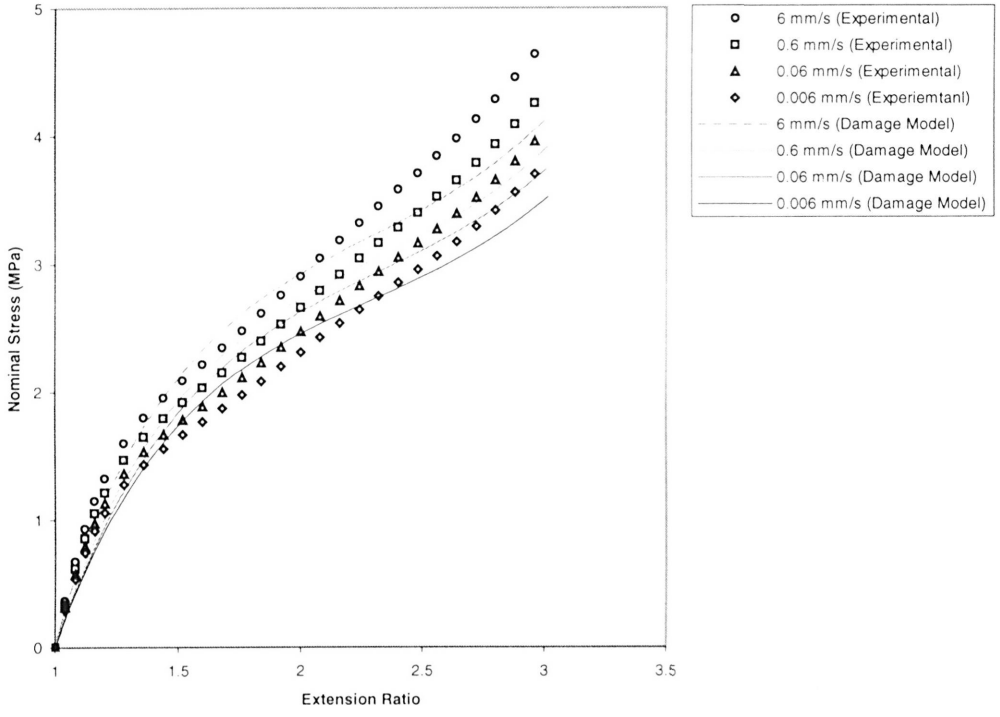


Figure 9.14 : Comparison of the constant velocity uniaxial tensile test data for virgin specimens of polyurethane with predictions of viscoelastic damage model.

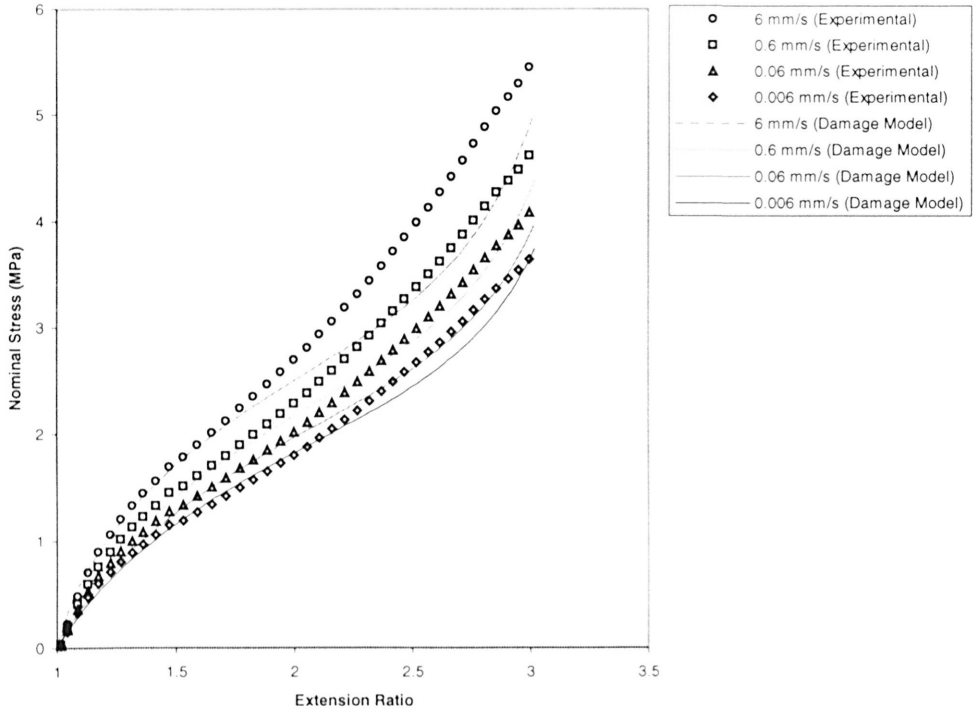


Figure 9.15 : Comparison of the constant velocity uniaxial tensile test data for virgin specimens of neoprene with predictions of viscoelastic damage model.

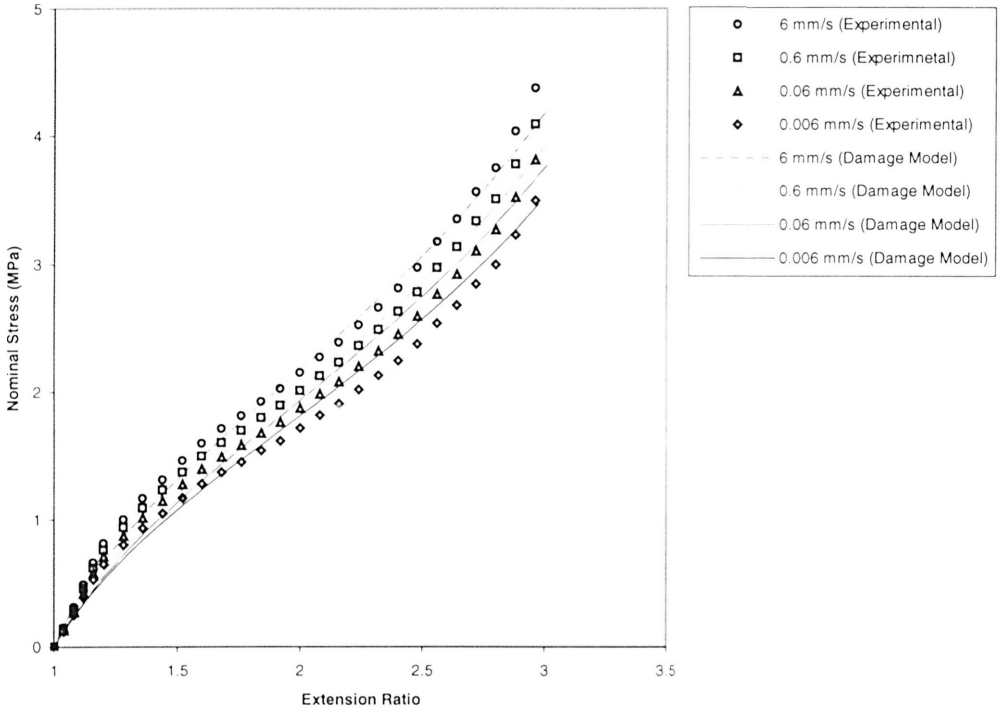


Figure 9.16 : Comparison of the constant velocity uniaxial tensile test data for preconditioned specimens of polyurethane with predictions of viscoelastic damage model.

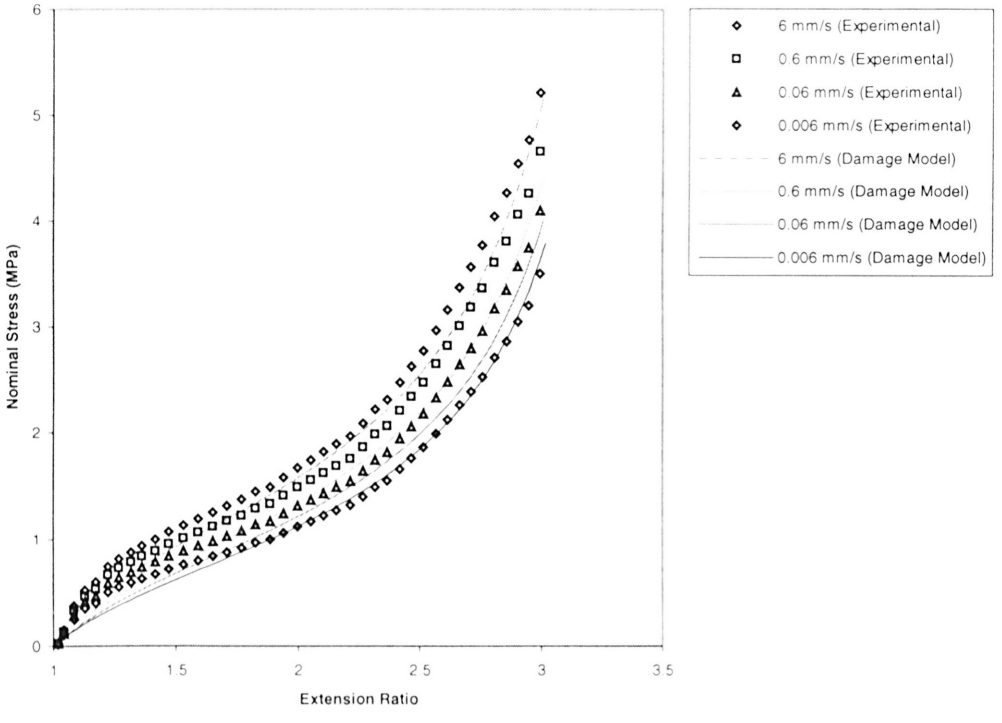


Figure 9.17 : Comparison of the constant velocity uniaxial tensile test data for preconditioned specimens of neoprene with predictions of viscoelastic damage model.

9.2 Final Remarks

In this chapter the response of simple constitutive model developed by the author to describe the mechanical behaviour of filled elastomers was compared with the results of series of experiments performed on polyurethane and neoprene. The approximate equilibrium response of these materials was established in the previous chapter in a number of interrupted loading tests performed on virgin and preconditioned specimens. The time independent material constants for the proposed model were obtained from the results of the interrupted loading tests conducted in tension. A comparison of the response of the proposed model with the experimental data from the interrupted loading tests showed that while both the 3 and 8 chain versions of the model provided a good description of the mechanical behaviour in tension, only the 8 chain version of the model was also able to describe the response in compression.

The ability of the proposed model to describe the rate dependent behaviour of rubber-like materials was also examined, using the results from a series of stress relaxation tests conducted on polyurethane and neoprene. The time dependent constants for the model, which take the form of a Prony series were determined using the relaxation data from the tests conducted on virgin specimens at a stretch λ=1.5. To enhance the ability of the model to describe the stress relaxation behaviour of elastomers, a new approach was developed to determine the values of the Prony series. The approach accounts for the stress relaxation that occurs during the loading-up phase of a typical relaxation test, and so provides a more accurate description of the viscoelastic behaviour. Comparisons between the model and the experimental data revealed that the stress relaxation was described more successfully in preconditioned specimens than in the virgin specimens. This was attributed to the fact the proportion of the viscous response remained constant in the relaxation tests performed on preconditioned specimens but increased with strain in the tests on virgin specimens. The response of the proposed model was also compared with the results of a number of constant velocity uniaxial tensile tests performed on polyurethane and neoprene. The model was again observed to reproduce the response of the preconditioned specimens more closely than that of the virgin specimens, this was again attributed to the magnitude of the viscous response remaining constant in the tests conducted on preconditioned specimens.

Chapter 10

10. Conclusions and Future Work

10.1 Conclusions

A new approach has been developed to implement a family of non-Gaussian network models into the commercial finite element program ABAQUS. In contrast with traditional methods of implementation which rely on a series approximation of the inverse Langevin function, the new approach employs a simple iterative procedure to determine the exact value of the inverse Langevin function and its derivative. This in turn permits the derivation of exact expressions for the principal stresses and principal components of the tangent modulus, the values of which may be rotated to the base directions of the active coordinate system using a standard coordinate transformation. Following this approach two of the most well known non-Gaussian theories, the 3 chain model of James and Guth (1943) and the 8 chain model of Arruda and Boyce (1993) have been implemented into ABAQUS using the user defined material subroutine facility known as UMAT. Constitutive equations were derived for the analysis of plane stress, plane strain, axisymmetric and three-dimensional problems.

Using continuum damage mechanics, the 3 and 8 chain models were also extended to account for the strain induced softening by the introduction of an isotropic damage mechanism into the constitutive formulations. To further enhance the ability of the non-Gaussian network theories to describe mechanical behaviour of filled elastomers, viscoelastic models based on the 3 and 8 chain models were also developed. A Prony series was used to represent the time dependent effects, which were introduced into the constitutive formulations by employing a theoretical framework for finite strain viscoelasticity.

A comparison of the equilibrium response of the modified network models with interrupted loading tests performed on polyurethane and neoprene, showed the modified 8 chain model to be superior in its description of the long-term behaviour of these materials.

The ability of the modified network models to describe the time dependent behaviour of filled elastomers was also examined in a series of stress relaxation tests performed on polyurethane and neoprene. Comparisons between the modified network models and the relaxation data demonstrated that the models were more successful at describing stress relaxation in preconditioned specimens than in virgin specimens. This was attributed to the fact that the proportion of the viscous response remained constant in the relaxation tests performed on preconditioned specimens but increased with strain in the tests on virgin specimens. Similar observations were made with regard to a number of constant velocity uniaxial tensile tests that were also performed.

A new approach was also presented to determine the values of the Prony series that accounts for the stress relaxation that occurs during the loading-up phase of a typical stress relaxation test. The approach leads to a more accurate description of the viscoelastic behaviour of rubber-like materials and may be used to determine the time dependent constants for any viscoelastic model that employs the Prony series.

10.2 Future Work

Interrupted loading tests performed on polyurethane and neoprene have shown that material constants for the 8 chain model obtained by comparison with uniaxial data are also successful at describing the response of these materials in compression. In future

work it would be worthwhile to investigate the ability of these constants describe the material response in other deformation states e.g. biaxial extension.

The development of free volume based models to describe "yield-like" behaviour of solid polymers is currently an active field of study. In the work of O'Dowd and Knauss (1995) the yield-like behaviour of PMMA has been reproduced using a model (limited to homogeneous deformation states) incorporating only two important ideas, molecular orientation and the effect of volumetric strain on material behaviour (described via free volume concepts). This approach is unlike the material description of developed by Boyce *et al* (1988) which introduces an explicit "yield point". In this regard the extension of the viscoelastic models developed in this work to include free volume effects would be useful in permitting an investigation of non-homogeneous deformation states, using the finite element method.

References

ABAQUS theory manual V.5.6, Hibbit, Karlson and Sorensen, Inc., Providence, R.I., USA, 1996.

Allport, J.M., Day, A.J., "Statistical mechanics material model for the constitutive modelling of elastomeric compounds", *Proceedings of the Institute of Mechanical Engineers, Part C: Journal of Mechanical Engineering Science*, Vol. 210, No. 6, 1996.

Anand, L., "A constitutive model for compressible elastomeric solids", *Computational Mechanics*, Vol. 18, No. 5, 339-355, 1996.

Arruda, E.A., Boyce, M.C., "A three dimensional constitutive model for the large stretch behaviour of rubber elastic materials", *Journal of the Mechanics and Physics of Solids*, Vol. 41, No. 2, 389-412, 1993.

Bergström, J.S., Boyce, M.C., "Constitutive modelling of the large strain time-dependent behaviour of elastomers", *Journal of the Mechanics and Physics of Solids*, Vol. 46, No. 5, 931-954, 1998.

Blanchard, A.F., Parkinson, D., "Breakage of carbon-rubber networks by applied stress", *Industrial Engineering and Chemistry*, Vol. 44, No. 4, 799-812, 1952.

Boyce, M.C., Parks, D.M., Argon, A.S., "Large inelastic deformation of glassy polymers. Part I: Rate dependent constitutive model", *Mechanics of Materials*, Vol. 7, 15-33,1988.

Blow, C.M., Hepburn, C., *Rubber Technology and Manufacturing*, Butterworth, London, England, 1982

Bridgman, P.W., "The compression of 61 substances to 25000 kg/cm^2. Determined by a new rapid method", *Proceedings of the American Academy of Arts and Sciences*, Vol. 76, 9-24, 1945.

Brown, R.P., *Physical Testing of Rubber*, Chapman & Hall, London, England, 1996.

Bueche, F., "Molecular basis for the Mullins effect", *Journal of Applied Polymer Science*, Vol. 4, No. 10, 107-114, 1960.

Bueche, F., "Mullins effect and rubber-filler interaction", *Journal of Applied Polymer Science*, Vol. 5, No. 15, 271-281, 1961.

Chadwick, P., Ogden, R.W., "On the definition of elastic moduli", *Archive for Rational Mechanics and Analysis*, Vol. 44, No. 1, 41-53, 1971a.

Chadwick, P., Ogden, R.W., "A theorem of tensor calculus and its application to isotropic elasticity", *Archive for Rational Mechanics and Analysis*, Vol. 44, No. 1, 54-68, 1971b.

Chang, W.V., Bloch, R., Tschoegl, N.W., "On the theory of the viscoelastic behaviour of soft polymers in moderately large deformations", *Rheologica Acta*, Vol. 15, No. 7/8, 367-378, 1976.

Charlton, D.J., Yang, J., "A review of methods to characterize rubber elastic behaviour for use in finite element analysis", Rubber Chemistry and Technology, Vol. 67, No. 3, 481-503, 1989.

Christensen, R.M., "A non-linear theory of viscoelasticity for application to elastomers", *Transaction of the AMSE: Journal of Applied Mechanics*, Vol. 47, No. 4, 762-768, 1980.

Cook, R.D., Malkus, D.S., Plesha, M.E., *Concepts and Applications of the Finite Element Method*, John Wiley & Sons, Chichester, England, 1989.

Crisfield, M.A., *Non-linear Finite Element Analysis of Solids and Structures Volume 2 Advanced Topics*, John Wiley & Sons, Chichester, England, 1997.

Dannenburg, E.M., "The effect of surface chemical interactions on the properties of filler-reinforced rubbers", *Rubber Chemistry and Technology*, Vol. 48, No. 3, 410-444, 1975.

Eirich, F.R., *Science and Technology of Rubber*, Academic Press, London, 1978.

Flory, P.J., Rehner, J., "Statistical mechanics of cross-linked polymer networks", *Journal of Chemical Physics*, Vol. 11, No. 11, 512-520, 1943.

Flory, P.J., "Thermodynamic relations for high elastic materials", *Transactions of the Faraday Society*, Vol. 57, 829-838, 1961.

Gent, A.N., *Engineering with Rubber*, Hanser, 1992.

Govindjee, S., Simo, J.C., "Transition from micro-mechanics to computationally efficient phenomenology: Carbon black filled rubbers incorporating Mullins effect", *Journal of the Mechanics and Physics of Solids*, Vol. 40, No. 1, 213-233, 1992.

Gruttmann, F., Taylor, R.L., "Theory and finite element formation of rubberlike membrane shells using principal stretches" *International Journal for Numerical Methods in Engineering*, Vol. 35, No. 5, 1111-1126, 1992.

Gurtin, M.E., Francis, E.C., "Simple rate-independent model for damage", *Journal of Spacecraft and Rockets*, Vol. 18, No. 3, 285-286, 1981.

Guth, E., "Theory of filler reinforcement", *Journal of Applied Physics*, Vol. 16, January, 20-25, 1945.

Harwood, J.A.C, Mullins, L., Payne, A.R., "Stress softening in natural rubber vulcanizates. Part II. Stress softening effects in pure gum and filler loaded rubbers", *Journal of Applied Polymer Science*, Vol. 9, No. 9, 3011-3021,1965.

Harwood, J.A.C, Payne, A.R., "Stress softening in natural rubber vulcanizates. Part III. Carbon black-filled vulcanizates", *Journal of Applied Polymer Science*, Vol. 10, No. 2, 315-324,1966a.

Harwood, J.A.C, Payne, A.R., "Stress softening in natural rubber vulcanizates. Part IV. Unfilled vulcanizates", *Journal of Applied Polymer Science*, Vol. 10, No. 8, 1203-1211,1966b.

Holt, W.L., "Behavior of rubber under repeated stresses", *Rubber Chemistry and Technology*, Vol. 5, No. 1, 79-89, 1932.

Holzapfel, G.A., "On large strain viscoelasticity: Continuum formulation and finite element applications to elastomeric structures", *International Journal for Numerical Methods in Engineering*, Vol. 39, No. 22, 3903-3926, 1996.

Hughes, T.J.R., *The Finite Element Method: Linear static and Dynamic Finite Element Analysis*, Prentice-Hall, London, England, 1987.

James, A.G., Green, A., Simpson, G.M., "Strain energy functions of rubber. I. Characterization of gum vulcanizates", *Journal of Applied Polymer Science*, Vol. 19, 2033-2058, 1975.

James, H.M., Guth, E., "Theory of the elastic properties of rubber", *Journal of Chemical Physics*, Vol. 11, No. 10, 455-480, 1943.

Jankovich, E., Leblanc, F., Durand, M., Bercovier, M., "A finite element method for the analysis of rubber parts experimental and analytical assessment", *Computers and Structures*, Vol. 14, No. 5/6, 385-391, 1981.

Johnson, A.R., Quigley, C.J., Mead, J.L., "Large strain viscoelastic models for rubber, Part I: Formulations", *Rubber Chemistry and Technology*, Vol. 67, No. 5, 904-917, 1994.

Jones, D.F., Treloar, L.R.G., "The properties of rubber in pure homogeneous strain", *Journal of Physics D: Applied Physics*, Vol. 8, No.11, 1285-1304, 1975.

Kachanov, L.M., *Introduction to Continuum Damage Mechanics*, Martinus Nijhoff Publishers, Dordrecht, Netherlands, 1986.

Kaliske, M., Rothert, H., "Formulation and implementation of three-dimensional viscoelasticity at small and finite strain", *Computational Mechanics*, Vol. 19, No. 2/3, 228-239, 1997.

Kaliske, M., Rothert, H., "On the finite element implementation of rubber-like materials at finite strain", *Engineering Computations*, Vol. 14, No. 2, 216-232, 1997.

Khan, A.S., Huang, S., *Continuum Theory of Plasticity*, John Wiley & Sons, Chichester, England, 1995.

Lee, B.S., Rivin, E.I., "Finite element analysis of load-deflection and creep characteristics of compressed rubber components for vibration control devices", *Journal of Mechanical Design*, Vol. 118, No. 3, 328-336, 1996.

McCrum, N.G., Buckley, C.P., Bucknall, C.B., *Principles of Polymer Engineering*, Oxford University Press, Oxford, England, 1988.

Medelia, A.I., "Effective degree of immobilisation of rubber occluded within carbon black aggregates", *Rubber Chemistry and Technology*, Vol. 45, No. 5, 1171-1194, 1972.

Miehe, C., "Discontinuous and continuous damage evolution in Ogden-type large strain elastic materials", *European Journal of Mechanics: A Solids*, Vol. 14, No. 5, 697-720, 1995.

Moita, G.F., *Non-Linear Finite Element Analysis of Continua with Emphasis on Hyperelasticity*, PhD Thesis, Department of Aeronautics, Imperial College of Science, Technology and Medicine, London, England, 1995.

Mooney, M., "A theory of large elastic deformation", *Journal of Applied Physics*, Vol. 11, September, 582-592, 1940.

Morman, K.N., "The generalised strain measure with application in nonhomogeneous deformation in rubber-like solids", *Transactions of the ASME: Journal of Applied Mechanics*, Vol. 53, No. 3, 726-728, 1986.

Morman, K.N, Pan, T.Y., "Application of finite-element analysis in the design of automotive elastomeric components", *Rubber chemistry and Technology*, Vol. 61, No. 3, 503-533, 1988.

Mullins, L., "Effect of stretching on the properties of rubber", *Rubber Chemistry and Technology*, Vol. 21, No. 2, 281-300, 1948.

Mullins, L. and Tobin, N.R., "Theoretical model for the elastic behavior of filler-reinforced vulcanized rubbers", *Rubber Chemistry and Technology*, Vol. 30, No. 2, 555-571,1957.

Mullins, L. and Tobin, N.R., "Stress softening in rubber vulcanizates. Part I. Use of a strain amplification factor to describe the elastic behavior of filler-reinforced vulcanized rubber", *Journal of Applied Polymer Science*, Vol. 9, No. 9, 2993-3009, 1965.

Needleman, A., "Inflation of spherical rubber balloons", *International Journal of Solids and Structures*, Vol. 13, No. 5, 409-421, 1977.

O'Dowd, N.P., Knauss, W.G., "Time dependent large principle deformation of polymers", *Journal of the Mechanics and Physics of Solids*, Vol. 43, No. 5, 771-792, 1995.

Obata, Y., Kawabata, S., Kawai, H., "Mechanical properties of natural rubber vulcanizates in finite deformation", *Journal of Polymer Science, Part A-2: Polymer Physics*, Vol. 8, No. 6, 903-919, 1970.

Ogden, R.W., "Large deformation isotropic elasticity - on the correlation of theory and experiment for incompressible rubberlike solids", *Proceedings of the Royal Society of London: Series A.*, Vol. 326, 565-584, 1972a.

Ogden, R.W., "Large deformation isotropic elasticity: on correlation of theory and experiment for compressible rubberlike solids", *Proceedings of the Royal Society of London, Series A*, Vol. 328, 567-583, 1972b.

Peng, S.H., Chang, W.V., "A compressible approach in finite element analysis of rubber-elastic materials", *Computers and Structures*, Vol. 62, No. 3, 573-593, 1997.

Quigley, C.J., Mead, J., Johnson, A.R., "Large strain viscoelastic constitutive models for rubber, Part II: Determination of material constants", *Rubber Chemistry and Technology*, Volume 68, No. 2, 230-247, 1995.

Reese, S., Wriggers, P., "A finite element method for stability problems in finite elasticity", *International Journal for Numerical Methods in Engineering*, Vol. 38, No. 7, 1171-1200, 1995.

Rigbi, Z., "Reinforcement of rubber by carbon black", *Advances in Polymer Science,* Vol.36, 21-68, 1980.

Rivlin, R.S., "Large elastic deformations of isotropic solids. I. Fundamental concepts", *Philosophical Transactions of the Royal Society of London: Series A*, Vol. 240, 459-490, 1948a.

Rivlin, R.S., "Large elastic deformations of isotropic solids. II. Some uniqueness theorems for pure, homogeneous deformation", *Philosophical Transactions of the Royal Society of London: Series A*, Vol. 240, 491-508, 1948b.

Rivlin, R.S., "Large elastic deformations of isotropic solids. III. Some simple problems in cylindrical polar co-ordinates", *Philosophical Transactions of the Royal Society of London: Series A*, Vol. 240, 509-525, 1948c.

Rivlin, R.S., "Large elastic deformations of isotropic solids. IV. Further development of the general theory", *Philosophical Transactions of the Royal Society of London: Series A*, Vol. 241, 379-397, 1948d.

Rivlin, R.S., "Large elastic deformations of isotropic solids. V. The problem of flexure", *Proceedings of the Royal Society of London: Series A.*, Vol. 195, 463-473, 1949a.

Rivlin, R.S., "Large elastic deformations of isotropic solids. VI. Further results in the theory of torsion, shear and flexure", *Philosophical Transactions of the Royal Society of London: Series A*, Vol. 242, 173-195, 1949b.

Rivlin, R.S., "A note on the torsion of an incompressible highly-elastic cylinder", *Proceedings of the Cambridge Philosophical Society*, Vol. 45, No. 3, 485-487, 1949c.

Rivlin, R.S., Sawyers, K.N., "The strain-energy function for elastomers", *Transactions of the Society of Rheology*, Vol. 20, No. 4, 545-577, 1976.

Simo, J.C., "On a fully three-dimensional finite-strain viscoelastic damage model: Formulation and Computation aspects", *Computer Methods in Applied Mechanics and Engineering*, Vol. 60, 153-173, 1987.

Simo, J.C., Armero, F., "Geometrically non-linear enhanced strain mixed methods and the method of incompatible modes", *International Journal for numerical methods in Engineering*, Vol. 33, No. 7, 1413-1449, 1992.

Simo, J.C., Taylor, R.L., "Quasi-incompressible finite elasticity in principle stretches. Continuum basis and numerical algorithms", *Computer Methods in Applied Mechanics and Engineering*, Vol. 85, No. 3, 273-310, 1991.

Smallwood, H.M., "Limiting law for the reinforcement of rubber", *Journal of Applied Physics*, Vol. 15, November, 758-766, 1944.

Sullivan, J.L., Demery, V.C., "The nonlinear viscoelastic behavior of carbon black-filled elastomer", *Journal of Polymer Science, Polymer Physics Edition*, Volume 20, No. 1, 2083-2101, 1982.

Sullivan, J.L., Mazich, K.A., "Nonseparable behaviour in rubber viscoelasticity", *Rubber Chemistry and Technology*, Volume 62, No. 1, 68-811, 1989.

Taylor, R.L., Pister, K.S., Goudreau, G.L., "Thermomechanical analysis of viscoelastic solids", *International Journal for Numerical Methods in Engineering*, Vol. 2, No. 1, 45-59, (1970).

Treloar, L.R.G., "Stress-strain data for vulcanised rubber under various types of deformation", *Transactions of the Faraday Society*, Vol. 40, 59-70, 1944.

Treloar, L.R.G., "The elasticity of a network of long chain molecules", *Transactions of the Faraday Society*, Vol. 42, 83-94, 1946.

Treloar, L.R.G., *The Physics of Rubber Elasticity*, Clarendon Press, Oxford, England, 1975.

Treloar, L.R.G., Riding, "A non-Gaussian theory for rubber in biaxial strain. I Mechanical Properties", *Proceedings of the Royal Society of London, Series A*, Vol. 369, 261-280,1979.

Valanis, K.C., Landel, R.F., "The strain-energy function of a hyperelastic material in terms of the extension ratios", *Journal of Applied Physics*, Vol. 38, No. 7, 2997-3003, 1967.

Vangerko, H., Treloar, L.R.G., "The inflation and extension of rubber tube for biaxial strain studies", *Journal of Physics D: Applied Physics*, Vol. 11, No. 14, 1969-1978, 1978.

Wriggers, P., Taylor, R.L., "Fully non-linear axisymmetrical membrane element for rubber-like materials", *Engineering Computations*, Vol. 7, No. 4, 303-310, 1990.

Zdunek, A.B., Bercovier, M., "Numerical evaluation of finite element methods for rubber parts", *Proceedings of the Sixth International Conference of Vehicle Structural Mechanics: American Society of Automobile Engineers*, Detroit, USA, April, 155-167, 1986.